Quantum networks with satellites: hardware, protocols and architecture

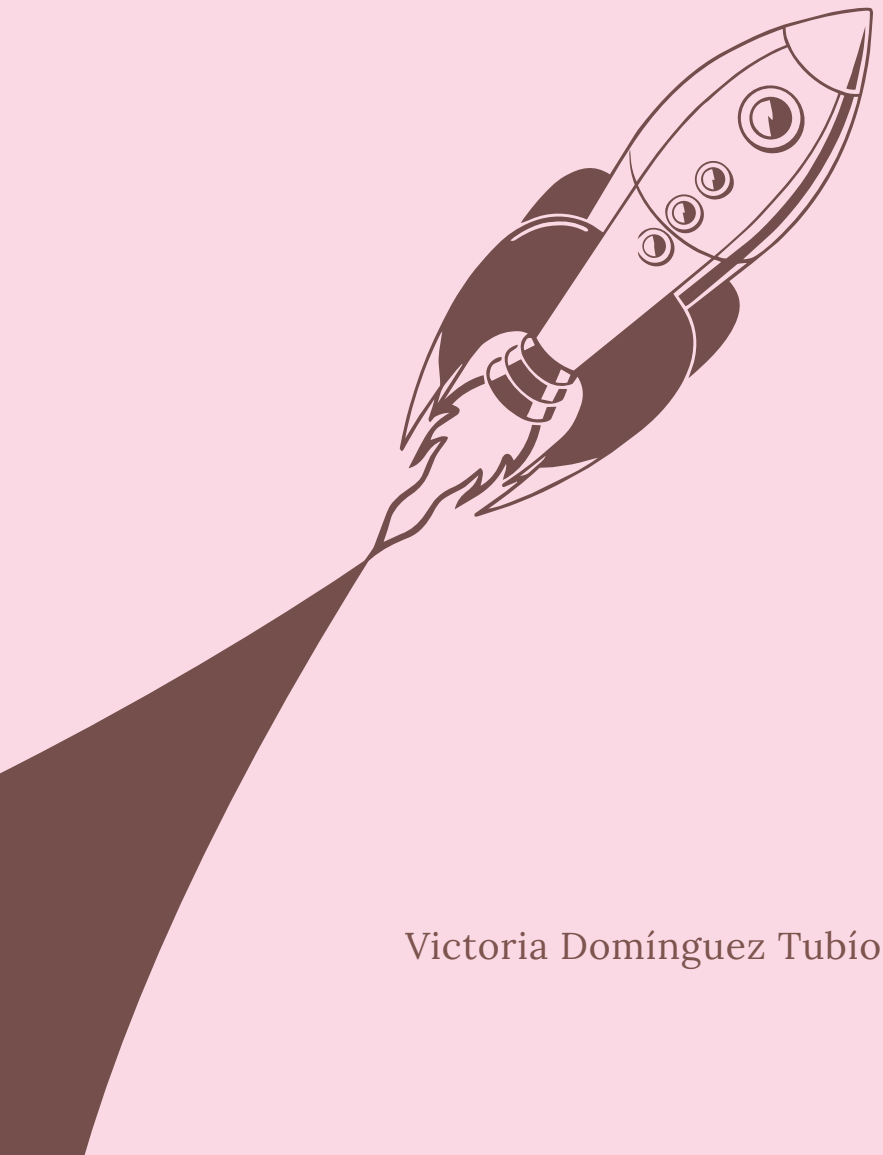

Victoria Domínguez Tubío

Quantum networks with satellites

hardware, protocols and architecture

Quantum networks with satellites

hardware, protocols and architecture

Dissertation

for the purpose of obtaining the degree of doctor
at Delft University of Technology
by the authority of the Rector Magnificus, prof. dr. ir. H. Bijl,
chair of the Board for Doctorates
to be defended publicly on
Tuesday, 7 July 2026, 12:30

by

Victoria DOMINGUEZ TUBIO

This dissertation has been approved by the promotors.

Composition of the doctoral committee:

Rector Magnificus,	chairperson
Prof. dr. S.D.C. Wehner,	Delft University of Technology, *promotor*
Dr. ir. C. Errando Herranz,	Delft University of Technology, *copromotor*
Dr. J. Borregaard,	Harvard University, *external adviser*
Independent members:	
Prof. dr. M.T. Wimmer	Delft University of Technology
Prof. dr. T. Schroeder	Humboldt Universitait, Germany
Dr. I. Dimitrova	Northeastern University, USA
Dr. R. Ishihara	Delft University of Technology
Prof. dr. G.A. Steele,	Delft University of Technology, reserve member

Keywords: Quantum optics, satellites, quantum memories, quantum networks, quantum key distribution, quantum communication.

Printed by: Gildeprint.

Cover by: Marta Crespí Campomar

To my niece, mother, grandmother and sister,
cause the future is female.

To my father and grandfather,
who taught me that kindness and empathy,
are the foundation of society.

CONTENTS

SUMMARY

The implementation of a quantum network opens up a range of new opportunities for secure communication and distributed quantum computing. To achieve this, entanglement must be distributed between remote users, using photons as carriers of quantum information. However, the probability of photon absorption in optical fibers increases exponentially with distance. To address this, quantum repeaters have been proposed, dividing the total distance into shorter segments where direct transmission is more feasible. Nevertheless, for long-distance links, satellite-assisted free-space channels offer a promising near-term alternative that avoids the complexity of quantum repeaters needed to compensate for transmission losses. The distribution of quantum keys between distant users has already been demonstrated via a single satellite link over distances of up to 7000 km. In this thesis, we focus on the development and analysis of satellite-based quantum networks.

To this end, we begin by exploring how current satellite links can be made more efficient, specifically, how to increase the amount of quantum information reaching the ground stations, avoiding the requirement of long coherent time in the quantum memories and without altering the satellite hardware. We propose the use of high-dimensional encoding, showing an improvement in the rate of entanglement compared with conventional qubit encoding.

From there, the discussion expands to a full quantum network architecture using several quantum repeaters place in space, with the aim of achieving secure liks across intercontinental distances. We propose a setup based on individually trapped atoms acting as both single-photon sources and quantum memories. Incorporating hardware imperfections and modeling transmission losses through free space and the atmosphere, we estimate the hardware performance required to achieve high-fidelity entanglement at a chosen transmission rate.

Finally, we go to a more specific example of distributing quantum key (QKD) to different cities of the Iberian Peninsula. Taking into account real-time weather conditions, atmospheric effects, and propagating losses, we analyze the feasibility of deploying current use cases of satellite-based QKD.

SAMENVATTING

De implementatie van een quantumnetwerk opent een reeks nieuwe mogelijkheden voor veilige communicatie en gedistribueerde quantumcomputing. Om dit te realiseren, moet verstrengeling worden verdeeld tussen gebruikers op afstand, waarbij fotonen worden gebruikt als dragers van quantuminformatie. De kans op absorptie van fotonen in optische vezels neemt echter exponentieel toe met de afstand. Om dit probleem aan te pakken, zijn quantumrepeaters voorgesteld, waarbij de totale afstand wordt opgedeeld in kortere segmenten waar directe transmissie haalbaarder is. Toch bieden satelliet-geassisteerde vrije-ruimtekanalen op de lange afstand een veelbelovend alternatief op korte termijn, dat de complexiteit van quantumrepeaters om transmissieverliezen te compenseren vermijdt. De distributie van quantumsleutels tussen verre gebruikers is reeds aangetoond via een enkele satellietverbinding over afstanden tot 7000 km. In deze thesis richten we ons op de ontwikkeling en analyse van satelliet-gebaseerde quantumnetwerken.

Om dit te bereiken beginnen we met het onderzoeken van hoe huidige satellietverbindingen efficiënter kunnen worden gemaakt, met name hoe de hoeveelheid quantuminformatie die de grondstations bereikt kan worden vergroot, zonder dat lange coherente tijden in quantummemories vereist zijn en zonder wijzigingen aan de satelliethardware. We stellen het gebruik van hoog-dimensionale codering voor, en tonen aan dat dit leidt tot een verbetering in de verstrengelingssnelheid vergeleken met conventionele qubitcodering.

Vervolgens breiden we de discussie uit naar een volledige quantumnetwerkarchitectuur met meerdere quantumrepeaters die zich in de ruimte bevinden, met als doel het realiseren van veilige verbindingen over intercontinentale afstanden. We stellen een opstelling voor gebaseerd op individueel gevangen atomen die zowel fungeren als enkel-fotonbronnen als quantummemories. Door hardware-imperfecties te integreren en transmissieverliezen via vrije ruimte en de atmosfeer te modelleren, schatten we de hardwareprestaties die nodig zijn om verstrengeling met hoge nauwkeurigheid te bereiken bij een gekozen transmissiesnelheid.

Tot slot gaan we in op een specifieker voorbeeld: het verdelen van quantumsleutels (QKD) naar verschillende steden op het Iberisch Schiereiland. Rekening houdend met realtime weersomstandigheden, atmosferische effecten en propagatieverliezen analyseren we de haalbaarheid van het inzetten van huidige toepassingen van satelliet-gebaseerde QKD.

1

INTRODUCTION

Quantum mechanics is the fundamental theory of physics which describes the behaviour of nature at very small scales. Being very small below the size of atoms.

At these scales, physical systems exhibit behaviour that differs significantly from what we observe in what we called the *classical world*, the world we observe and experience in our daily lifes. Notable examples of such quantum phenomena include superposition and entanglement. Superposition refers to the ability of a quantum system to exist in multiple states simultaneously. Entanglement occurs when two particles become correlated in such a way that the state of one directly influences the state of the other, even when separated by large distances. Entanglement arises when superposition is extended across multiple particles in a way that correlates them.

Quantum technologies take advantage of these properties— superposition, entanglement, and tunneling—to develop new devices and systems with capabilities that go beyond those of classical technologies. These advancements rely on the ability to isolate, manipulate, and measure individual quantum systems, and mark the beginning of what is often called the second quantum revolution [1].

Quantum computers harness the principle of superposition to tackle computational problems more efficiently. The fundamental unit of information in quantum computing is the qubit, which is similar to the classical bit used in traditional computers. However, unlike a classical bit that can only be 0 or 1, a qubit can exist in a superposition of both 0 and 1 simultaneously. This unique property allows quantum computers to explore multiple solutions at once, potentially leading to significant speedups for certain types of problems.

Quantum tunneling refers to a phenomenon where a particle crosses a barrier it would not be able to overcome according to classical physics, due to insufficient energy. For example, while a ball in classical mechanics cannot roll over a hill without enough energy, a

quantum particle has a nonzero probability of appearing on the other side. Quantum sensing leverages this effect, taking advantage of how highly sensitive tunneling probabilities are to even tiny changes in the surrounding environment.

Quantum networks use entanglement to connect distant nodes. A widely studied application is quantum key distribution (QKD), in which cryptographic keys are shared using quantum states to ensure secure communication. Because quantum information cannot be copied without being disturbed, any attempt at eavesdropping can be detected. Beyond QKD, quantum networks could enable improvements in telescope resolution [2], more precise clock synchronization [3], and secure remote access to quantum computing systems [4].

We use photons to establish entanglement between two nodes. However, photons get lost in the transmission between the nodes and the loss cannot be compensated with standard classical amplification techniques due to the quantum no-cloning theorem [5]. Instead, the total distance between the nodes is divided into segments where direct transmission is possible. To have entanglement between the nodes, entanglement swapping between the elementary nodes is carried out. These intermediaries in establishing entanglement between the nodes are quantum repeaters.

In fiber-based quantum repeater systems, photon loss increases exponentially with distance. This means that covering just a few hundred kilometers already requires several repeaters, and connecting across continents would need hundreds. On top of that, intercontinental links usually involve crossing oceans, which makes installing and maintaining fiber infrastructure even more challenging.

A promising alternative is to use satellite-assisted free-space optical links, where transmission decreases polynomially with distance. QKD has already been demonstrated with a single satellite link [6–8], where photons are sent from the satellite to the ground stations in what is known as a downlink setup. The distances achieved to distribute key are up to 7000 km [7]. In that case, the satellite is a trusted node, meaning that the information is decoded, classically stored and encoded until it is sent to the ground station. The disadvantage of such a scheme is that it is not quantum-resistant to eavesdroppers. An already proven alternative is the use of entangled photon sources, where entangled photons are sent to the ground stations [9]. In this case, the link does not depend on storing the information classically, therefore keeping its quantum properties. The disadvantage of such a link is that the maximum distance at which two ground stations can be located is within the line of sight of the satellite.

One solution to establish entanglement between two ground stations at larger distances, is the use of quantum repeaters in space. Several recent works have demonstrated the advantages of using quantum

repeaters in space to establish entanglement across distances of several hundred kilometers [10–12]. However, these works often assume the availability of on-demand entangled photon-pair sources, a capability that remains a significant technological challenge [13]. A promising candidate for such sources is solid-state semiconductor quantum dots, which require cryogenic temperatures to operate reliably [14]. Similarly, many leading quantum memory platforms, such as defect centers in diamond [15] or rare-earth-doped crystals [16], also rely on cryogenic environments, presenting substantial cost challenges for implementation in space-based systems.

Additionally, it is worth noting that QKD represents only one application of quantum networks. To enable broader functionalities, such as quantum state teleportation and distributed quantum computation, quantum memories must be employed to store and manipulate entanglement. In these scenarios, multiple photonic qubit pairs are distributed sequentially [17] or in parallel [18, 19], and successful entangled pairs must be held in a register of quantum memories until all required links are established. This requirement imposes stringent demands on the coherence time of the memories, which scales inversely with the transmission probability of the photonic link [20].

This thesis focuses on the development and analysis of satellite-based quantum networks. It begins by exploring how current satellite links can be made more efficient, specifically, how to increase the amount of quantum information reaching the ground stations, avoiding the requirement of long coherent times in the quantum memories and without altering the satellite hardware. From there, the discussion expands to a full quantum network architecture using several quantum repeaters placed in space, with the aim of achieving secure links across intercontinental distances. A proposed hardware setup based on laser-cooled atoms [21–23], which avoids the use of cryogenic technology, is introduced, and its feasibility is assessed by analyzing the impact of hardware imperfections and atmospheric losses. Finally, we go to a more specific example of distributing quantum key (QKD) to different cities of the Iberian Peninsula and study possible current use cases.

The thesis is then divided as follows: in Chapter 2 we give an introduction to satellite-based quantum networks explaining their main architectures, showing the state of the art, and introducing satellite-based quantum repeaters. In Chapter 3, we investigate entanglement distribution using high-dimensional photonic encoding via a single satellite link, assuming a satellite with specifications similar to the Micius satellite [8]. Based on the qudit entanglement protocols proposed in [20, 24], we consider the use of 2^m-dimensional time-bin encoded qudits generated by a spontaneous parametric down-conversion (SPDC) source. These qudits are then mapped onto m qubits stored in m

independent quantum memories. This strategy only requires updates at the ground stations compared to standard qubit protocols. We evaluate and compare the entanglement generation rate and fidelity for both qubit and qudit schemes at varying inter-ground station distances.

In Chapter 4, we extend our investigation to a space-based quantum repeater architecture. We propose a setup based on individually trapped atoms acting as both single-photon sources and quantum memories. Incorporating hardware imperfections and modeling transmission losses through free space and the atmosphere, we estimate the hardware performance—both in terms of quantum components and satellite capabilities—required to achieve high-fidelity entanglement at a chosen transmission rate.

Chapter 5 returns to the application of QKD, where we simulate a single-satellite link distributing secure keys across various cities in the Iberian Peninsula. Taking into account real-time weather conditions, atmospheric effects, and propagation losses, we analyze the feasibility of deploying current use cases of satellite-based QKD.

REFERENCES

[1] J. P. Dowling and G. J. Milburn. “Quantum technology: the second quantum revolution”. In: *Philosophical Transactions of the Royal Society of London. Series A: Mathematical, Physical and Engineering Sciences* 361.1809 (2003), pp. 1655–1674. doi: 10.1098/rsta.2003.1227. url: https://royalsocietypublishing.org/doi/10.1098/rsta.2003.1227.

[2] D. Gottesman, T. Jennewein, and S. Croke. “Longer-Baseline Telescopes Using Quantum Repeaters”. In: *Phys. Rev. Lett.* 109 (7 Aug. 2012), p. 070503. doi: 10.1103/PhysRevLett.109.070503. url: https://link.aps.org/doi/10.1103/PhysRevLett.109.070503.

[3] P. Kómár, E. M. Kessler, M. Bishof, L. Jiang, A. S. Sørensen, J. Ye, and M. D. Lukin. “A quantum network of clocks”. In: *Nature Physics* 10.8 (June 2014), pp. 582–587. issn: 1745-2481. doi: 10.1038/nphys3000. url: http://dx.doi.org/10.1038/nphys3000.

[4] A. Broadbent, J. Fitzsimons, and E. Kashefi. “Universal Blind Quantum Computation”. In: *2009 50th Annual IEEE Symposium on Foundations of Computer Science*. IEEE, Oct. 2009, pp. 517–526. doi: 10.1109/focs.2009.36. url: http://dx.doi.org/10.1109/FOCS.2009.36.

[5] W. K. Wootters and W. H. Zurek. “A single quantum cannot be cloned”. In: *Nature* 299.5886 (1982), pp. 802–803. doi: 10.1038/299802a0. url: https://doi.org/10.1038/299802a0.

[6] J. Yin, Y. Cao, Y.-H. Li, J.-G. Ren, S.-K. Liao, L. Zhang, W.-Q. Cai, W.-Y. Liu, B. Li, H. Dai, M. Li, Y.-M. Huang, L. Deng, L. Li, Q. Zhang, N.-L. Liu, Y.-A. Chen, C.-Y. Lu, R. Shu, C.-Z. Peng, J.-Y. Wang, and J.-W. Pan. “Satellite-to-Ground Entanglement-Based Quantum Key Distribution”. In: *Phys. Rev. Lett.* 119 (20 Nov. 2017), p. 200501. doi: 10.1103/PhysRevLett.119.200501. url: https://link.aps.org/doi/10.1103/PhysRevLett.119.200501.

[7] S.-K. Liao, W.-Q. Cai, J. Handsteiner, B. Liu, J. Yin, L. Zhang, D. Rauch, M. Fink, J.-G. Ren, W.-Y. Liu, Y. Li, Q. Shen, Y. Cao, F.-Z. Li, J.-F. Wang, Y.-M. Huang, L. Deng, T. Xi, L. Ma, T. Hu, L. Li, N.-L. Liu, F. Koidl, P. Wang, Y.-A. Chen, X.-B. Wang, M. Steindorfer, G. Kirchner, C.-Y. Lu, R. Shu, R. Ursin, T. Scheidl, C.-Z. Peng, J.-Y. Wang, A. Zeilinger, and J.-W. Pan. "Satellite-Relayed Intercontinental Quantum Network". In: *Phys. Rev. Lett.* 120 (3 Jan. 2018), p. 030501. doi: 10.1103/PhysRevLett.120.030501. url: https://link.aps.org/doi/10.1103/PhysRevLett.120.030501.

[8] S.-K. Liao, W.-Q. Cai, W.-Y. Liu, L. Zhang, Y. Li, J.-G. Ren, J. Yin, Q. Shen, Y. Cao, Z.-P. Li, F.-Z. Li, X.-W. Chen, L.-H. Sun, J.-J. Jia, J.-C. Wu, X.-J. Jiang, J.-F. Wang, Y.-M. Huang, Q. Wang, Y.-L. Zhou, L. Deng, T. Xi, L. Ma, T. Hu, Q. Zhang, Y.-A. Chen, N.-L. Liu, X.-B. Wang, Z.-C. Zhu, C.-Y. Lu, R. Shu, C.-Z. Peng, J.-Y. Wang, and J.-W. Pan. "Satellite-to-ground quantum key distribution". In: *Nature* 549.7670 (Sept. 2017). Number: 7670 Publisher: Nature Publishing Group, pp. 43–47. issn: 1476-4687. doi: 10.1038/nature23655. url: https://www.nature.com/articles/nature23655 (visited on 08/14/2023).

[9] J. Yin, Y.-H. Li, S.-K. Liao, M. Yang, Y. Cao, L. Zhang, J.-G. Ren, W.-Q. Cai, W.-Y. Liu, S.-L. Li, R. Shu, Y.-M. Huang, L. Deng, L. Li, Q. Zhang, N.-L. Liu, Y.-A. Chen, C.-Y. Lu, X.-B. Wang, F. Xu, J.-Y. Wang, C.-Z. Peng, A. K. Ekert, and J.-W. Pan. "Entanglement-based secure quantum cryptography over 1,120 kilometres". In: *Nature* 582.7813 (June 2020). Number: 7813 Publisher: Nature Publishing Group, pp. 501–505. issn: 1476-4687. doi: 10.1038/s41586-020-2401-y. url: https://www.nature.com/articles/s41586-020-2401-y (visited on 08/14/2023).

[10] J. Wallnöfer, F. Hahn, M. Gündoğan, J. S. Sidhu, F. Wiesner, N. Walk, J. Eisert, and J. Wolters. "Simulating quantum repeater strategies for multiple satellites". In: *Communications Physics* 5.1 (June 2022). doi: 10.1038/s42005-022-00945-9. url: https://doi.org/10.1038%2Fs42005-022-00945-9.

[11] C. Liorni, H. Kampermann, and D. Bruß. "Quantum repeaters in space". In: *New Journal of Physics* 23.5 (May 2021), p. 053021. doi: 10.1088/1367-2630/abfa63. url: https://doi.org/10.1088%2F1367-2630%2Fabfa63.

[12] D. L. Bakker, Y. Jong, B. P. F. Dirks, and G. C. Amaral. "A Best-Path Approach to the Design of a Hybrid Space–Ground Quantum Network with Dynamic Constraints". In: *Photonics* 11.3 (2024). issn: 2304-6732. doi: 10.3390/photonics11030268. url: https://www.mdpi.com/2304-6732/11/3/268.

[13] A. Anwar, C. Perumangatt, A. Villar, A. Lohrmann, and A. Ling. “Development of compact entangled photon-pair sources for satellites”. In: *Applied Physics Letters* 121.22 (Nov. 2022), p. 220503. issn: 0003-6951. doi: 10.1063/5.0109702. eprint: https://pubs.aip.org/aip/apl/article-pdf/doi/10.1063/5.0109702/16485971/220503_1_online.pdf. url: https://doi.org/10.1063/5.0109702.

[14] C. Schimpf, M. Reindl, F. Basso Basset, K. D. Jöns, R. Trotta, and A. Rastelli. “Quantum dots as potential sources of strongly entangled photons: Perspectives and challenges for applications in quantum networks”. In: *Applied Physics Letters* 118.10 (Mar. 2021), p. 100502. issn: 0003-6951. doi: 10.1063/5.0038729. eprint: https://pubs.aip.org/aip/apl/article-pdf/doi/10.1063/5.0038729/14544746/100502_1_online.pdf. url: https://doi.org/10.1063/5.0038729.

[15] M. Pompili, S. L. N. Hermans, S. Baier, H. K. C. Beukers, P. C. Humphreys, R. N. Schouten, R. F. L. Vermeulen, M. J. Tiggelman, L. dos Santos Martins, B. Dirkse, S. Wehner, and R. Hanson. “Realization of a multinode quantum network of remote solid-state qubits”. In: *Science* 372.6539 (2021), pp. 259–264. doi: 10.1126/science.abg1919. eprint: https://www.science.org/doi/pdf/10.1126/science.abg1919. url: https://www.science.org/doi/abs/10.1126/science.abg1919.

[16] D. Lago-Rivera, J. V. Rakonjac, S. Grandi, and H. d. Riedmatten. “Long distance multiplexed quantum teleportation from a telecom photon to a solid-state qubit”. In: *Nature Communications* 14.1 (2023), p. 1889. doi: 10.1038/s41467-023-37518-5. url: https://doi.org/10.1038/s41467-023-37518-5.

[17] N. Kalb, A. A. Reiserer, P. C. Humphreys, J. J. Bakermans, S. J. Kamerling, N. H. Nickerson, S. C. Benjamin, D. J. Twitchen, M. Markham, and R. Hanson. “Entanglement distillation between solid-state quantum network nodes”. In: *Science* 356.6341 (June 2017), pp. 928–932. issn: 10959203. doi: 10.1126/science.aan0070. url: https://www.science.org/doi/10.1126/science.aan0070.

[18] L. Jiang, J. M. Taylor, K. Nemoto, W. J. Munro, R. Van Meter, and M. D. Lukin. “Quantum repeater with encoding”. In: *Physical Review A* 79.3 (2009). issn: 1050-2947. doi: 10.1103/physreva.79.032325.

[19] W. J. Munro, K. Azuma, K. Tamaki, and K. Nemoto. *Inside Quantum Repeaters*. May 2015. doi: 10.1109/JSTQE.2015.2392076.

[20] Y. Zheng, H. Sharma, and J. Borregaard. "Entanglement Distribution with Minimal Memory Requirements Using Time-Bin Photonic Qudits". In: *PRX Quantum* 3.4 (2022). issn: 26913399. doi: 10.1103/PRXQuantum.3.040319.

[21] J. McKeever, A. Boca, A. D. Boozer, R. Miller, J. R. Buck, A. Kuzmich, and H. J. Kimble. "Deterministic Generation of Single Photons from One Atom Trapped in a Cavity". In: *Science* 303.5666 (2004), pp. 1992–1994. doi: 10.1126/science.1095232. eprint: https://www.science.org/doi/pdf/10.1126/science.1095232. url: https://www.science.org/doi/abs/10.1126/science.1095232.

[22] D. Bluvstein, H. Levine, G. Semeghini, T. T. Wang, S. Ebadi, M. Kalinowski, A. Keesling, N. Maskara, H. Pichler, M. Greiner, V. Vuletić, and M. D. Lukin. "A quantum processor based on coherent transport of entangled atom arrays". In: *Nature* 604.7906 (Apr. 2022), pp. 451–456. doi: 10.1038/s41586-022-04592-6. url: https://doi.org/10.1038%2Fs41586-022-04592-6.

[23] A. W. Young, W. J. Eckner, W. R. Milner, D. Kedar, M. A. Norcia, E. Oelker, N. Schine, J. Ye, and A. M. Kaufman. "Half-minute-scale atomic coherence and high relative stability in a tweezer clock". In: *Nature* 588.7838 (Dec. 2020), pp. 408–413. doi: 10.1038/s41586-020-3009-y. url: https://doi.org/10.1038%2Fs41586-020-3009-y.

[24] Z. Xie, Y. Liu, X. Mo, T. Li, and Z. Li. "Quantum entanglement creation for distant quantum memories via time-bin multiplexing". In: *Physical Review A* 104.6 (Dec. 2021), p. 062409. issn: 24699934. doi: 10.1103/PhysRevA.104.062409. url: https://journals.aps.org/pra/abstract/10.1103/PhysRevA.104.062409.

2

SATELLITE-ASSISTED LONG DISTANCE ENTANGLEMENT

In this chapter, we introduce the building blocks of a satellite-based quantum network. We begin by introducing a single satellite link, and then we transition to quantum repeaters in space to cover intercontinental distances.

2.1. SINGLE-SATELLITE LINK

A quantum link can be established using a single satellite. The simplest example of a quantum network of this kind involves a satellite and two ground stations that we want to entangle. In such a configuration, two main architectures are possible: either photons are transmitted from the satellite to the ground stations, known as a downlink setup, shown in Fig.2.1(a), or from the ground stations to the satellite, referred to as an uplink setup, depicted in Fig.2.1(b). Downlink configurations have been demonstrated to be more resilient to atmospheric attenuation and beam divergence effects, resulting in lower channel losses [1, 2]. The reasoning behind this is that in the uplink scenario, photons go through the atmosphere in their first kilometres, having a bigger initial divergence when they go through free space than in the downlink setup. For this reason, all the projects discussed in this thesis consider downlink schemes.

In a downlink setup, photons are emitted from the satellite to the ground stations. This implies that the satellite must carry an onboard photon source, which can either emit entangled photon pairs and send one photon to each ground station, or emit individual photons separately to each station. This approach assumes that the satellite operates as a trusted node, meaning that quantum information is measured onboard, stored classically, and then re-encoded and sent to the second ground

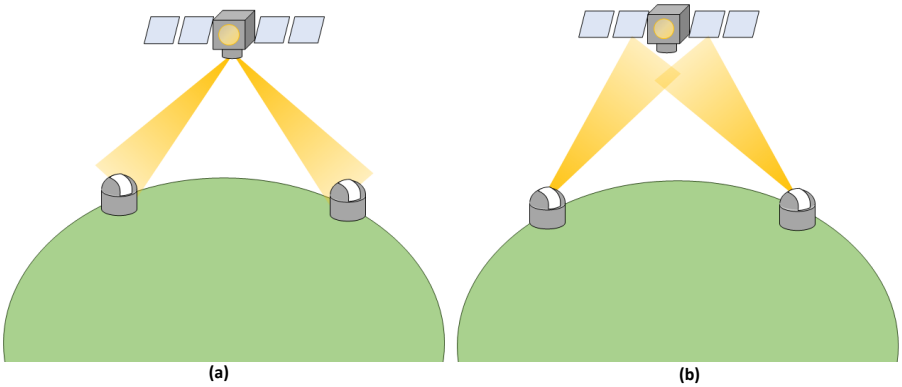

Figure 2.1: **Satellite-based architectures(a)Downlink setup**. In this scheme, photons are sent from the satellite to the ground stations.**(b)Uplink setup**. Photons are sent from the ground stations to the satellite. In this type of architecture, divergence effects are more significant.

station. This breaks the end-to-end quantum link, making the connection no longer fully quantum and more vulnerable to eavesdropping. In the case of entangled photon pairs, a quantum link is established directly between the two ground stations, and both stations must be within the line of sight of the satellite. The higher the satellite's orbit, the longer the distance between the ground stations that can be reached. However, this increased reach comes at the cost of higher photon losses, as photons must travel longer distances through the atmosphere. In the latter case, where single photons are sent independently to each ground station, the physical separation between the two stations can exceed the line-of-sight limits imposed by the satellite's altitude.

The altitude of a satellite determines its classification into one of three orbital regimes. Low-Earth orbit (LEO) satellites operate at altitudes ranging from approximately 160 km to 2,000 km. Medium-Earth orbit (MEO) satellites are positioned between 2,000 km and 35,786 km. Geostationary Earth orbit (GEO) satellites maintain an altitude of approximately 35,786 km. GEO satellites have the same angular speed as Earth's rotation and therefore appear stationary relative to a point on Earth's surface, providing continuous coverage of a fixed region. However, their high altitude leads to substantial channel losses, making satellite-to-ground quantum communication especially challenging at such heights. In contrast, LEO satellites complete approximately 12 to 16 orbits per day, taking between 1.5 and 2 hours to circle the Earth. As a result, the communication window, defined as the period

during which the satellite is visible from a given ground station, is limited to several minutes per orbit. Given that losses are minimized in LEO configurations, this thesis focuses exclusively on quantum network architectures based on LEO satellites.

An additional consideration in satellite-based quantum networks is the geographical placement of ground stations, such that the orbital inclination of the satellite chosen is the most suitable to allow for the best coverage. The orbital inclination significantly affects the duration and frequency of communication windows. Common orbital types include equatorial orbits, which follow a 0° inclination and orbit along Earth's equator, and polar orbits, which pass over or near the Earth's poles and provide full global coverage over time as the Earth rotates beneath them. A special category of polar orbits is the sun-synchronous orbit, which crosses each latitude at the same local solar time on each pass. Low-inclination orbits are also used, especially when coverage is focused on specific regions.

Single-satellite quantum links are already in use. In 2016, China launched the first quantum satellite, *Micius* [3–6]. This satellite, placed in a sun-synchronous LEO orbit at an altitude of approximately 500 km, is equipped with two transmitter telescopes of apertures 18 cm and 30 cm, as well as a spontaneous parametric down-conversion (SPDC) source. Several proof-of-concept demonstrations were conducted using Micius. These include satellite-to-ground decoy-state quantum key distribution (QKD)[7], trusted-node QKD between Vienna and Beijing[4], which are separated by over 7,000 km, and entanglement-based QKD over distances of up to 1,200 km, in which the satellite acted as a source of entangled photon pairs[5, 6].

More recently, in 2022, China launched the Jinan-1 satellite, a small LEO satellite that successfully demonstrated trusted-node QKD between China and South Africa[8].

Several missions aiming to demonstrate or expand satellite-based quantum networks are currently under development. The Canadian Space Agency (CSA) is planning to launch the Quantum Encryption and Science Satellite (QEYSSat) in 2026, a microsatellite designed to demonstrate an uplink quantum link [9]. In parallel, the European Space Agency (ESA), in collaboration with the European Commission and several commercial space companies in Europe, plans to launch a LEO satellite by the end of 2025 or early 2026 to demonstrate QKD feasibility [10]. Additionally, Thales Alenia Space and Hispasat are developing what is expected to be the first QKD-enabled GEO satellite [11].

Quantum key distribution (QKD) is just one application of quantum networks. To fully realize a quantum network between two ground stations, quantum memories are required to store and manipulate entanglement, enabling more advanced functionalities such as quantum state teleportation and distributed quantum computing. Establishing

entanglement between ground stations across intercontinental distances remains challenging. One possibility is to use GEO satellites, which suffer from significant losses due to their altitude and lack of global coverage. Another approach is to use satellites as trusted nodes, at the cost of breaking quantum security. A third, and more promising, approach involves the deployment of quantum repeaters in space, which would require satellites equipped with quantum memories. This latter approach is explored in Chapter 4 of this thesis, where we propose and analyze a specific architecture for satellite-based quantum repeaters.

2.2. QUANTUM REPEATERS IN SPACE

When the separation between two ground stations becomes too large for direct photon transmission to be feasible, the total distance is divided into smaller segments known as elementary links, as shown in Fig.2.2. These are defined as distances over which direct quantum communication is possible. In the context of satellite-based networks, elementary links typically correspond to the distances between adjacent satellites or between the end-satellites and the ground stations.

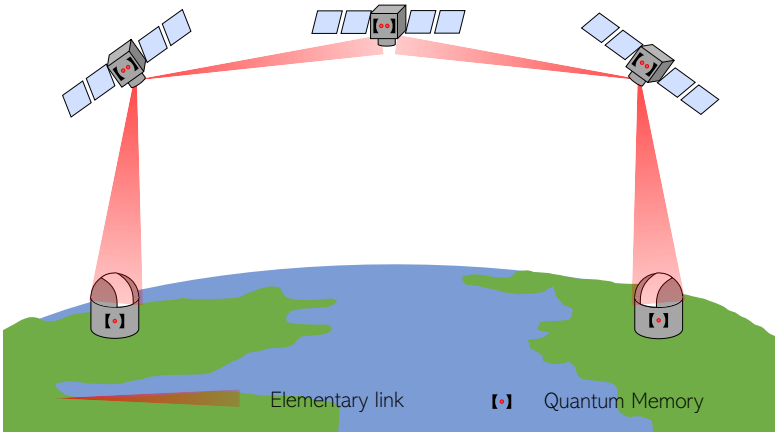

Figure 2.2: **Satellite-based quantum repeaters** In this scheme each satellite is equipped with a quantum memory, meaning that the entanglement swapping is performed in each of them. The elementary links are the distance between adjacent satellites and between the end-satellites and the ground stations.

Once entanglement has been successfully established across one of these elementary links, it is stored in quantum memories located at the endpoints of the link, either on the satellites or at the ground stations,

until entanglement is similarly established in all the other elementary links composing the full network path.

Quantum memories are physical systems capable of storing quantum states while maintaining their coherence, i.e., the preservation of their quantum properties. These memories allow for the retrieval of the stored quantum information at a later time, playing a crucial role in significantly enhancing the overall rate of entanglement generation [12, 13].

Several physical platforms can serve as quantum memories, including defect centers in diamond [14], rare-earth-ion-doped crystals [15–17], and cold atoms [18–20]. Cold atoms are particularly advantageous for satellite-based quantum memories because they do not require expensive cryogenic systems and allow for the individual trapping of hundreds of atoms. In contrast, both defect centers and rare-earth-ion-doped crystals rely on cryogenic technology to operate effectively [15]. Nevertheless, rare-earth-ion-doped crystals are well-suited for ground-based applications due to their long storage times—up to one hour [17]—and their ability to operate at telecom wavelengths (1550 nm) [16], which are compatible with fiber-optic communication.

However, retaining quantum states for extended durations leads to decoherence, meaning the quantum properties gradually deteriorate due to interactions with the environment [21–23]. This results in a decline in the fidelity, or quality, of the stored entangled states. To mitigate this effect, a technique involving a *cut-off time* is employed: if a quantum state remains stored in memory beyond a predefined duration (chosen to be shorter than the memory's coherence time), it is discarded [24, 25]. This approach introduces a trade-off between the entanglement generation rate and the achievable fidelity. In Chapter 3, we implement such a cut-off time in our system to ensure high-fidelity entanglement.

Moreover, equipping each repeater station and final node with multiple quantum memories enables the storage of several quantum states simultaneously. By sending photons in different time bins to distinct memories, we can further enhance the entanglement generation rate, a technique known as *multiplexing*.

Once entanglement has been successfully established and stored across all elementary links, the stored states are retrieved from the quantum memories, and adjacent links are connected through a process known as Bell State Measurement (BSM), thereby extending entanglement across the entire network.

2.2.1. BELL STATE MEASUREMENT

The state of a qubit, the fundamental unit of quantum information, can be described as:

$$|\psi\rangle = \alpha|0\rangle + \beta|1\rangle, \tag{2.1}$$

where $|0\rangle$ and $|1\rangle$ are vectors, and α and β are complex coefficients that satisfy the normalization condition $|\alpha|^2 + |\beta|^2 = 1$. When both α and β are non-zero, the qubit is said to be in a superposition. The qubit can be encoded using different degrees of freedom such as its polarization, horizontal $|H\rangle$ and vertical $|V\rangle$, or its time of emission, early $|e\rangle$ and late $|l\rangle$.

Extending this to two qubits, their joint state can be any normalized superposition of the four computational basis states: $|0\rangle \otimes |0\rangle$, $|0\rangle \otimes |1\rangle$, $|1\rangle \otimes |0\rangle$, and $|1\rangle \otimes |1\rangle$. Within this framework, we define the Bell states [26, 27] as:

$$|\phi_{ij}\rangle = (X^i Z^j \otimes \mathbb{I}_2)\frac{1}{\sqrt{2}}(|00\rangle + |11\rangle), \tag{2.2}$$

where X and Z are the Pauli operators given by $X = |0\rangle\langle 1| + |1\rangle\langle 0|$ and $Z = |0\rangle\langle 0| - |1\rangle\langle 1|$, and $\mathbb{I}_2$ is the identity operator in the two-dimensional Hilbert space. The Bell states defined in Eq. (2.2) are maximally entangled states, meaning that they cannot be decomposed into a product of two independent single-qubit states:

$$|\phi\rangle_{ij} \neq |\psi\rangle_A \otimes |\psi\rangle_B. \tag{2.3}$$

Additionally, Bell states are maximally entangled states, implying that if one the qubits is lost, we will not have information about the other one either.

To link two elementary segments in a quantum network, we perform a Bell State Measurement (BSM), which projects a two-qubit state onto the Bell basis (for a formal introduction to quantum measurements, see [26]). Suppose qubits 1 and 2 are in the entangled state $|\phi_{ij}\rangle_{1,2}$, and qubits 3 and 4 in $|\phi_{kl}\rangle_{3,4}$. Performing a BSM on qubits 2 and 3 and obtaining the outcome $|\phi_{nm}\rangle$ results in the entangled state:

$$\frac{(|\phi_{nm}\rangle\langle\phi_{nm}|)_{2,3}|\phi_{i,j}\rangle_{1,2}|\phi_{k,l}\rangle_{3,4}}{|(|\phi_{nm}\rangle\langle\phi_{nm}|)_{2,3}|\phi_{i,j}\rangle_{1,2}|\phi_{k,l}\rangle_{3,4}|} = |\phi_{i\oplus k\oplus n, j\oplus l\oplus m}\rangle_{1,4}|\phi_{k,m}\rangle_{2,3}. \tag{2.4}$$

After the measurement, qubits 2 and 3 are projected into the state $|\phi_{k,m}\rangle$, consistent with the BSM outcome, while qubits 1 and 4, which were initially unentangled and may be spatially separated, are now entangled. This process, known as entanglement swapping, has been demonstrated in multiple experimental setups using diverse physical platforms [28–30].

In linear optics, BSMs are performed with a beam splitter (BS) and photon detectors in the output modes, and it has a 50% probability of

success. It can only detect the states $|\Psi^{\pm}\rangle = 1/\sqrt{2}\,(|01\rangle + |10\rangle)$, as it requires the detection of both modes after the beam splitter. The states $|\Phi^{\pm}\rangle = 1/\sqrt{2}\,(|00\rangle + |11\rangle)$ cannot be detected, since both photons exit in the same mode, revealing their individual state [31].

Therefore, to establish entanglement between two ground stations separated by intercontinental distances, several approaches exist. One option is to deploy quantum repeaters in optical fibers, which may require hundreds of repeater nodes and face geographical challenges, such as laying infrastructure under oceans. Another possibility is to utilize geostationary (GEO) satellites, though this introduces substantial transmission losses due to the high altitude. A more promising alternative is to use a network of low-Earth orbit (LEO) satellites in combination with a smaller number of quantum repeaters. Realizing this strategy necessitates the availability of quantum memories in space.

REFERENCES

[1] L. C. Andrews and R. L. Phillips. *Laser Beam Propagation Through Random Media*. 1000 20th Street, Bellingham, WA 98227-0010 USA: SPIE, Sept. 2005. isbn: 978-0-8194-5948-0. doi: 10.1117/3.626196. url: http://link.aip.org/link/doi/10.1117/3.626196 (visited on 06/07/2022).

[2] M. Gündoğan, J. S. Sidhu, V. Henderson, L. Mazzarella, J. Wolters, D. K. L. Oi, and M. Krutzik. "Proposal for space-borne quantum memories for global quantum networking". In: *npj Quantum Information* 7.1 (2021), p. 128. doi: 10.1038/s41534-021-00460-9. url: https://doi.org/10.1038/s41534-021-00460-9.

[3] J. Yin, Y. Cao, Y.-H. Li, J.-G. Ren, S.-K. Liao, L. Zhang, W.-Q. Cai, W.-Y. Liu, B. Li, H. Dai, M. Li, Y.-M. Huang, L. Deng, L. Li, Q. Zhang, N.-L. Liu, Y.-A. Chen, C.-Y. Lu, R. Shu, C.-Z. Peng, J.-Y. Wang, and J.-W. Pan. "Satellite-to-Ground Entanglement-Based Quantum Key Distribution". In: *Phys. Rev. Lett.* 119 (20 Nov. 2017), p. 200501. doi: 10.1103/PhysRevLett.119.200501. url: https://link.aps.org/doi/10.1103/PhysRevLett.119.200501.

[4] S.-K. Liao, W.-Q. Cai, J. Handsteiner, B. Liu, J. Yin, L. Zhang, D. Rauch, M. Fink, J.-G. Ren, W.-Y. Liu, Y. Li, Q. Shen, Y. Cao, F.-Z. Li, J.-F. Wang, Y.-M. Huang, L. Deng, T. Xi, L. Ma, T. Hu, L. Li, N.-L. Liu, F. Koidl, P. Wang, Y.-A. Chen, X.-B. Wang, M. Steindorfer, G. Kirchner, C.-Y. Lu, R. Shu, R. Ursin, T. Scheidl, C.-Z. Peng, J.-Y. Wang, A. Zeilinger, and J.-W. Pan. "Satellite-Relayed Intercontinental Quantum Network". In: *Phys. Rev. Lett.* 120 (3 Jan. 2018), p. 030501. doi: 10.1103/PhysRevLett.120.030501. url: https://link.aps.org/doi/10.1103/PhysRevLett.120.030501.

[5] J. Yin, Y.-H. Li, S.-K. Liao, M. Yang, Y. Cao, L. Zhang, J.-G. Ren, W.-Q. Cai, W.-Y. Liu, S.-L. Li, R. Shu, Y.-M. Huang, L. Deng, L. Li, Q. Zhang, N.-L. Liu, Y.-A. Chen, C.-Y. Lu, X.-B. Wang, F. Xu, J.-Y. Wang, C.-Z. Peng, A. K. Ekert, and J.-W. Pan. "Entanglement-based secure quantum cryptography over 1,120 kilometres". In: *Nature* 582.7813 (June 2020). Number: 7813 Publisher: Nature Publishing Group, pp. 501–505. issn: 1476-4687. doi: 10.1038/s41586-020-2401-y. url: https:

//www.nature.com/articles/s41586-020-2401-y (visited on 08/14/2023).

[6] J. Yin, Y. Cao, Y. H. Li, S. K. Liao, L. Zhang, J. G. Ren, W. Q. Cai, W. Y. Liu, B. Li, H. Dai, G. B. Li, Q. M. Lu, Y. H. Gong, Y. Xu, S. L. Li, F. Z. Li, Y. Y. Yin, Z. Q. Jiang, M. Li, J. J. Jia, G. Ren, D. He, Y. L. Zhou, X. X. Zhang, N. Wang, X. Chang, Z. C. Zhu, N. L. Liu, Y. A. Chen, C. Y. Lu, R. Shu, C. Z. Peng, J. Y. Wang, and J. W. Pan. "Satellite-based entanglement distribution over 1200 kilometers". In: *Science* 356.6343 (2017), pp. 1140–1144. issn: 10959203. doi: 10.1126/science.aan3211.

[7] S.-K. Liao, W.-Q. Cai, W.-Y. Liu, L. Zhang, Y. Li, J.-G. Ren, J. Yin, Q. Shen, Y. Cao, Z.-P. Li, *et al.* "Satellite-to-ground quantum key distribution". In: *Nature* 549.7670 (2017), pp. 43–47. doi: 10.1038/nature23655.

[8] Xinhua. *Chinese-led team achieves world's first 10,000-km quantum-secured communication*. Ed. by Huaxia. Xinhua News Agency. 2025. url: %5Curl%7Bhttps://english.news.cn/20250320/%20b2d639fd9eb94da295b0668e92279248/%20c.html%7D.

[9] Canadian Space Agency. *Quantum Encryption and Science Satellite (QEYSSat)*. Government of Canada. 2025. url: https://www.asc-csa.gc.ca/eng/satellites/qeyssat.asp.

[10] European Space Agency. *Eagle-1*. European Space Agency. 2025. url: https://www.esa.int/Applications/Connectivity_and_Secure_Communications/Eagle-1.

[11] Thales Alenia Space. *Thales Alenia Space and Hispasat start the development of the world's first quantum key distribution system capacity from geostationary orbit*. Accessed: 2025-04-25. Thales Alenia Space. 2025. url: https://www.thalesaleniaspace.com/en/press-releases/thales-alenia-space-and-hispasat-start-development-worlds-first-quantum-key.

[12] K. Azuma, S. E. Economou, D. Elkouss, P. Hilaire, L. Jiang, H.-K. Lo, and I. Tzitrin. "Quantum repeaters: From quantum networks to the quantum internet". In: *Reviews of Modern Physics* 95.4 (Dec. 2023). issn: 1539-0756. doi: 10.1103/revmodphys.95.045006. url: http://dx.doi.org/10.1103/RevModPhys.95.045006.

[13] W. J. Munro, K. Azuma, K. Tamaki, and K. Nemoto. "Inside Quantum Repeaters". In: *IEEE Journal of Selected Topics in Quantum Electronics* 21.3 (2015), pp. 78–90. doi: 10.1109/JSTQE.2015.2392076.

[14] M. Pompili, S. L. N. Hermans, S. Baier, H. K. C. Beukers, P. C. Humphreys, R. N. Schouten, R. F. L. Vermeulen, M. J. Tiggelman, L. dos Santos Martins, B. Dirkse, S. Wehner, and R. Hanson. "Realization of a multinode quantum network of remote solid-state qubits". In: *Science* 372.6539 (2021), pp. 259–264. doi: 10.1126/science.abg1919. eprint: https://www.science.org/doi/pdf/10.1126/science.abg1919. url: https://www.science.org/doi/abs/10.1126/science.abg1919.

[15] D. Lago-Rivera, J. V. Rakonjac, S. Grandi, and H. d. Riedmatten. "Long distance multiplexed quantum teleportation from a telecom photon to a solid-state qubit". In: *Nature Communications* 14.1 (2023), p. 1889. doi: 10.1038/s41467-023-37518-5. url: https://doi.org/10.1038/s41467-023-37518-5.

[16] D. Lago-Rivera, S. Grandi, J. V. Rakonjac, A. Seri, and H. de Riedmatten. "Telecom-heralded entanglement between multimode solid-state quantum memories". In: *Nature* 594.7861 (June 2021), pp. 37–40. doi: 10.1038/s41586-021-03481-8.

[17] Y. Ma, Y.-Z. Ma, Z.-Q. Zhou, C.-F. Li, and G.-C. Guo. "One-hour coherent optical storage in an atomic frequency comb memory". In: *Nature Communications* 12 (Apr. 2021), p. 2381. doi: 10.1038/s41467-021-22706-y.

[18] J. McKeever, A. Boca, A. D. Boozer, R. Miller, J. R. Buck, A. Kuzmich, and H. J. Kimble. "Deterministic Generation of Single Photons from One Atom Trapped in a Cavity". In: *Science* 303.5666 (2004), pp. 1992–1994. doi: 10.1126/science.1095232. eprint: https://www.science.org/doi/pdf/10.1126/science.1095232. url: https://www.science.org/doi/abs/10.1126/science.1095232.

[19] D. Bluvstein, H. Levine, G. Semeghini, T. T. Wang, S. Ebadi, M. Kalinowski, A. Keesling, N. Maskara, H. Pichler, M. Greiner, V. Vuletić, and M. D. Lukin. "A quantum processor based on coherent transport of entangled atom arrays". In: *Nature* 604.7906 (2022), pp. 451–456. doi: 10.1038/s41586-022-04592-6. url: https://doi.org/10.1038/s41586-022-04592-6.

[20] A. W. Young, W. J. Eckner, W. R. Milner, D. Kedar, M. A. Norcia, E. Oelker, N. Schine, J. Ye, and A. M. Kaufman. "Half-minute-scale atomic coherence and high relative stability in a tweezer clock". In: *Nature* 588.7838 (Dec. 2020), pp. 408–413. doi: 10.1038/s41586-020-3009-y. url: https://doi.org/10.1038%2Fs41586-020-3009-y.

[21] V. Krutyanskiy, M. Canteri, M. Meraner, J. Bate, V. Krcmarsky, J. Schupp, N. Sangouard, and B. P. Lanyon. “Telecom-Wavelength Quantum Repeater Node Based on a Trapped-Ion Processor”. In: *Physical Review Letters* 130.21 (May 2023). issn: 1079-7114. doi: 10.1103/physrevlett.130.213601. url: http://dx.doi.org/10.1103/PhysRevLett.130.213601.

[22] M. H. Abobeih, J. Cramer, M. A. Bakker, N. Kalb, M. Markham, D. J. Twitchen, and T. H. Taminiau. “One-second coherence for a single electron spin coupled to a multi-qubit nuclear-spin environment”. In: *Nature Communications* 9 (2018), p. 2552. doi: 10.1038/s41467-018-04916-z. url: https://doi.org/10.1038/s41467-018-04916-z.

[23] C. E. Bradley, S. W. de Bone, P. F. W. Möller, S. Baier, M. J. Degen, S. J. H. Loenen, H. P. Bartling, M. Markham, D. J. Twitchen, R. Hanson, D. Elkouss, and T. H. Taminiau. “Robust quantum-network memory based on spin qubits in isotopically engineered diamond”. In: *npj Quantum Information* 8.1 (2022), p. 122. doi: 10.1038/s41534-022-00637-w. url: https://doi.org/10.1038/s41534-022-00637-w.

[24] B. Li, T. Coopmans, and D. Elkouss. “Efficient Optimization of Cut-offs in Quantum Repeater Chains”. In: *2020 IEEE International Conference on Quantum Computing and Engineering (QCE)*. 2020, pp. 158–168. doi: 10.1109/QCE49297.2020.00029.

[25] F. Rozpędek, K. Goodenough, J. Ribeiro, N. Kalb, V. C. Vivoli, A. Reiserer, R. Hanson, S. Wehner, and D. Elkouss. “Parameter regimes for a single sequential quantum repeater”. In: *Quantum Science and Technology* 3.3 (Apr. 2018), p. 034002. issn: 2058-9565. doi: 10.1088/2058-9565/aab31b. url: http://dx.doi.org/10.1088/2058-9565/aab31b.

[26] M. A. Nielsen and I. L. Chuang. *Quantum Computation and Quantum Information: 10th Anniversary Edition*. 10th. New York, USA: Cambridge University Press, 2011. isbn: 9781107002173.

[27] S. Khatri and M. M. Wilde. “Principles of Quantum Communication Theory: A Modern Approach”. In: *arXiv preprint arXiv:2011.04672* (2020). arXiv: 2011.04672 [quant-ph]. url: https://arxiv.org/abs/2011.04672.

[28] M. Pompili, S. L. N. Hermans, S. Baier, H. K. Beukers, P. C. Humphreys, R. N. Schouten, R. F. L. Vermeulen, M. J. Tiggelman, L. dos Santos Martins, B. Dirkse, and et al. “Realization of a multinode quantum network of remote solid-state qubits”. In: *Science* 372.6539 (2021), pp. 259–264. doi: 10.1126/science.abg1919.

[29] M. K. Bhaskar, R. Riedinger, B. Machielse, D. S. Levonian, C. T. Nguyen, E. N. Knall, H. Park, D. Englund, M. Lončar, D. D. Sukachev, and et al. “Experimental demonstration of memory-enhanced quantum communication”. In: *Nature* 580 (2020), pp. 60–64. doi: 10.1038/s41586-020-2103-5.

[30] F. B. Basset, M. B. Rota, C. Schimpf, D. Tedeschi, K. D. Zeuner, S. C. D. Silva, M. Reindl, V. Zwiller, K. D. Jöns, A. Rastelli, and et al. “Entanglement swapping with photons generated on demand by a quantum dot”. In: *Physical Review Letters* 123.16 (2019), p. 160501. doi: 10.1103/PhysRevLett.123.160501.

[31] H. K. Beukers, M. Pasini, H. Choi, D. Englund, R. Hanson, and J. Borregaard. “Remote-Entanglement Protocols for Stationary Qubits with Photonic Interfaces”. In: *PRX Quantum* 5 (1 Mar. 2024), p. 010202. doi: 10.1103/PRXQuantum.5.010202. url: https://link.aps.org/doi/10.1103/PRXQuantum.5.010202.

3

SATELLITE-ASSISTED ENTANGLEMENT DISTRIBUTION WITH HIGH-DIMENSIONAL PHOTONIC ENCODING

V. Domínguez Tubío, M.C. Dijksman, J. Borregaard

Satellite-assisted entanglement distribution is a promising approach for realizing long-range quantum networking. However, the limited coherence time of existing quantum memories makes it challenging to obtain multiple event-ready entangled pairs between ground stations since one pair decoheres before the successful distribution of another. We demonstrate how this can be circumvented by pairing existing satellite-compatible spontaneous parametric down conversion (SPDC) sources with qudit-compatible quantum memories on ground. By operating the SPDC source as a source of time-bin encoded photonic qudits, simultaneous distribution of multiple entangled pairs between the ground stations can be achieved at a significantly higher rate than if the SPDC sources was operated as a source of photonic qubits. We find that for achievable coherence times of several seconds and demonstrated satellite performances from the Micius satellite, the qudit operation leads to several orders of magnitude faster distribution

This chapter is based on the prepint arXiv:2505.16751

rates than the qubit-based operation when more than one event-ready high-quality (Bell pair fidelity ≥ 0.95) entangled pair is desired. To ensure high-quality entanglement distribution, we consider multiplexed quantum memory operation storage and, in the qubit case, we also consider storage cutoff times.

3.1. INTRODUCTION

Encoding information into quantum systems leads to fundamentally new capabilities for data processing and transmission [1]. Quantum key distribution (QKD) [2, 3] and blind quantum computing [4, 5] can enable information-theoretic security in communication and cloud quantum computing provided that entanglement can be established between the communicating parties. The standard approach for entanglement distribution involves sending photons through optical fibres. However, for long-distance links, satellite-assisted free space links is a promising near-term approach that circumvents the need of complex quantum repeaters to compensate transmission loss [6–11]. For example, QKD has already been demonstrated with the Micius satellite as a trusted node for distances ranging from 500 to 700 km [12, 13]. In a more advanced approach, entanglement-based QKD was achieved without relying on a trusted node, spanning distances of up to 1,200 km [14], which is well outside the reach of any current fibre-based approach.

To unlock the full potential of entanglement-based quantum networking, the distribution of multiple high-quality entangled pairs will be necessary. This allows for combating noise and imperfections through entanglement purification [15, 16] as well as more advanced applications such as distributed or blind quantum computing [17, 18]. In conventional photonic qubit-based approaches, multiple photonic qubit pairs are distributed sequentially [19] or in parallel [20, 21] and rely on a register of quantum memories to store the successful pairs until all required entangled pairs are distributed. This puts daunting requirements on the coherence time of the quantum memories, which will be proportional to the inverse of the transmission probability of the photonic link [22]. To address this challenge, it has been proposed to use high-dimensional photonic qudit encoding to simultaneously entangle multiple pairs [22, 23]. However, the compatibility of such protocols with realistic satellite-based entanglement sources, as well as their comparison with other qubit-compatible techniques like temporal multiplexing [24–26] and storage-time cutoffs [27, 28], remains largely unexplored.

In this work, we propose a promising scheme for long-distance entanglement distribution where a satellite-based SPDC source is operated as an approximate source of photonic qudits to entangle two ground-based quantum memory registers. The qudit operation of the SPDC sources does not require any significant upgrade of the quantum hardware on the satellite, which we assume have similar characteristics as the Micius satellite [14]. Qudit compatible quantum memories are required for the ground nodes, which can be realized with existing hardware based on cavity-coupled diamond color centers or atomic qubits [22, 29–31].

We compare the performance of the SPDC qudit operation with the

standard qubit operation considering multiplexed memory operation in both cases and storage cutoff times for the qubit one. For the former, we assume the quantum memories can store more qubit pairs than required, which, in some cases, can result in an effectively higher distribution rate. For the latter, we assume that an entangled pair is discarded if it has been stored longer than a certain cut-off time since the quality of the entanglement will have degraded too much from decoherence. By operating with a qudit dimension that corresponds to the desired number of event-ready entangled pairs, the memories only need to store the entangled pairs for the duration of classical communication between two ground stations. This leads to several orders of magnitude faster distribution rates for high-fidelity entanglement distribution (Bell pair fidelity ≥ 0.90) over distances ranging from hundreds to over a thousand kilometers compared to the qubit operation for similar parameters of the source, quantum memories, and satellite-link. Our results demonstrate the practical advantage of high-dimensional photonic encoding for long-range entanglement distribution with existing satellite-based quantum hardware and near-term ground-based quantum memories.

3.2. MODEL

We consider a downlink setup where photons are sent from the satellite to the ground stations, as sketched in Fig. 5.1. The goal is to establish m event-ready high-fidelity entangled pairs between two ground stations meaning that at a certain point in time, we have m entangled pairs simultaneously available. We consider two distinct modes of operation.

In the first qubit mode of operation, shown in Fig. 5.1(a), approximate entangled photonic qubit pairs are generated from an SPDC source and transmitted to the ground stations. The photonic qubits are assumed to be encoded in the time-bin basis consisting of an early or late time bin. Upon successful arrival at their respective nodes, the photons are stored in time-bin compatible quantum memories in a heralded manner. This can e.g. be achieved through spin-dependent reflection of cavity-coupled diamond defect centers or atomic quantum memories as we will detail below. We will consider cases where the number of available memory modes is equal or higher than the required number of entangled pairs. Furthermore, we include the possibility of operating with a cutoff time such that pairs that have been stored for too long and correspondingly been subject to too much decoherence will be discarded.

In the second qudit mode of operation, depicted in Fig.5.1(b), the SPDC source generates approximate entangled photonic qudit pairs encoded in a high-dimensional time-bin basis. We note that this merely corresponds to viewing the consecutive emission of 2^{m-1} approximate qubit pairs as an approximate 2^m dimensional qudit as we detail below.

Thus, the operation of the SPDC source is in many ways exactly the same as in the qubit mode of operation. The ground-based memories will, however, need to store high-dimensional qudit states of dimension 2^m in a heralded manner. Similarly to the qubit case, multiple cavity-coupled diamond defect centers or atomic qubits can be used to achieve this. Once successfully heralded, a photonic qudit pair generates m Bell pairs between the ground stations simultaneously. We will always consider the case where the qudit dimension matches the desired number of Bell pairs. For this reason, we do not consider cutoff strategies for the qudit mode of operation but still include the possibility of having more memory modes than the required number of Bell pairs to increase the distribution rate through multiplexing.

3.2.1. ENTANGLED PHOTON PAIR SOURCE

We consider an SPDC source as our probabilistic source of entangled photonic pairs. A pump laser is used to drive a nonlinear optical crystal to emit time-correlated signal and idler photon pairs with a certain probability [14, 32, 33]. To generate time-bin encoded states, we consider a pulsed operation corresponding to well-defined time bins of length τ_{rep}. Two consecutive pulses generates an approximate time-bin qubit pair and, in general, 2^m consecutive pulses generates an approximate 2^m-dimensional entangled qudit pair of the form:

$$\begin{aligned} |\Psi\rangle_{\text{A,B}} &= \bigotimes_{l=0}^{2^m-1} \sqrt{1-\lambda^2} \sum_{n=0}^{\infty} \lambda^n |n_l, n_l\rangle_{A,B} \\ &\approx (1-\lambda^2)^{2^{m-1}} \big[|0,0\rangle_{A,B} + \lambda \sum_{l=0}^{2^m 1} |1_l, 1_l\rangle_{A,B} + \\ &+ \lambda^2 \sum_{l=0}^{2^m-1} \sum_{j\geq l}^{2^m-1} |1_l 1_j, 1_l 1_j\rangle_{A,B} + O(\lambda^3) \big], \end{aligned} \tag{3.1}$$

where the subscripts A and B correspond to two different spatial modes directed toward the ground stations of Alice and Bob respectively, and the subscripts l, j enumerate the time bins that contain photons. In other words, the state $1_l 1_j, 1_l 1_{j_{A,B}}$ denotes a state with photon pairs (in spatial mode A and B) in the l'th and j'th timebin. The desired term in Eq. (3.1) is $\sum_{l=0}^{2^m 1} |1_l, 1_l\rangle_{A,B}$, which corresponds to a (not normalized) maximally entangled qudit pair of dimension 2^m.

We assume the source operates in a weak-pump regime, where the squeezing parameter is much less than one ($\lambda \ll 1$). Lowering the squeezing parameter decreases the probability of emitting a photon pair, yet improves the fidelity by reducing multi-photon events ($\propto \lambda^2$).

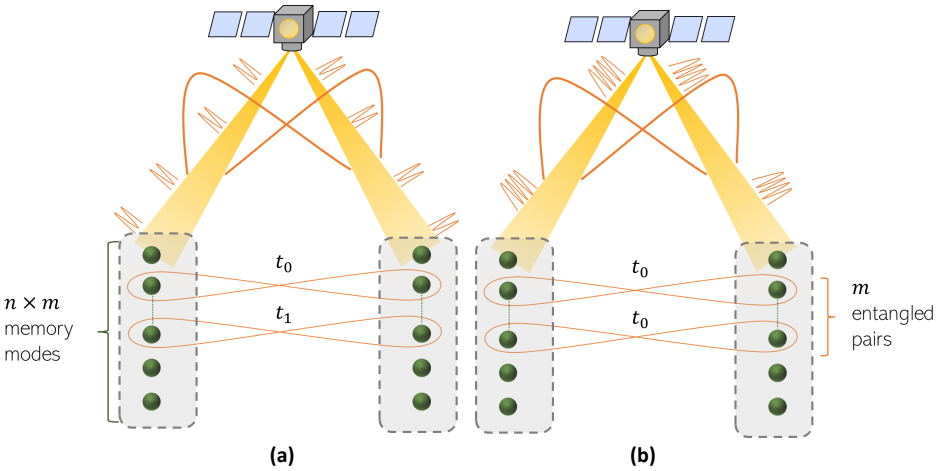

Figure 3.1: **Experimental setup.** We consider a down-link scenario where the entangled photons are transmitted from the satellite to the ground stations. We also consider multiplexing, where we have more memory modes, $n \times m$ than pairs we want to entangle. Here m is the desired number of pairs and n is the multiplexing factor. **(a) Qubit mode of operation.** The source fires entangled photons encoded in a two-dimensional time-bin encoding. If both photons arrive successfully at their ground stations, they are stored in the quantum memories, depicted as the first successful pair at t_0. The other successful pair arrives at a later time, t_1. **(b) Qudit mode of operation.** The source fires entangled photons in a 2^m-dimensional time-bin encoding. When one pair of entangled photons arrives successfully at both ground stations, we simultaneously obtain the desired number of Bell pairs.

In other words, there is a trade-off between the rate and the fidelity of entanglement which depends on the dimension of the entangled pair.

3.2.2. PHOTON TRANSMISSION

Photon loss during transmission to the two ground stations will change the received state from the one emitted by the SPDC source. We model this by passing the state in Eq. (3.1) through fictitious beam splitters in each spatial mode where one output mode of the beam splitters corresponds to the loss while the other is the transmitted mode. As we detail below, we assume that the storage of the received photons in the quantum memories is heralded by the detection of the photon. Any loss and inefficiency in the memory storage process can be directly included in the effective transmission probability, p_T, of the fictitious beam splitter together with the the free space transmission probability. The free space transmission probability is derived using the model in Ref. [34], which includes divergence, atmospheric absorption and pointing jitter. Additionally, we model false detections assuming that there is a probability p_{dark} that a detector clicks despite no photon was received. We assume that this results in a stored state with zero fidelity with the desired entangled Bell pairs to have a lower bound on the Bell pair fidelity.

3.2.3. QUANTUM MEMORY OPERATION

Upon arrival at the ground stations, the incoming photonic state is mapped to a (multi-)qubit state in the qubit registers of the ground stations. We assume the availability of qubit-photon controlled gates, which makes the transformation

$$|\text{vac}\rangle_{\text{ph}}|0\rangle \rightarrow |\text{vac}\rangle_{\text{ph}}|0\rangle, \qquad |1\rangle_{\text{ph}}|0\rangle \rightarrow |1\rangle_{\text{ph}}|1\rangle, \tag{3.2}$$

where $|\text{vac}\rangle_{\text{ph}}$ ($|1\rangle_{\text{ph}}$) denotes the absence (presence) of a photon in a particular mode. Such gates can be implemented with existing hardware of cavity-coupled diamond color centers [29, 30] or atomic qubits [31, 35] and can be used to store 2^m dimensional photonic qudits in m qubits in a heralded manner with the protocol of Ref. [22]. Here, we sketch the main steps of this protocol and note that it also works for photonic qubits ($m = 1$).

To simplify the explanation, we consider only the desired component of the photon state in Eq. (3.1):

$$|\Psi\rangle = \frac{1}{\sqrt{2^m}} \sum_{l=0}^{2^m-1} |l\rangle_{A,ph}|l\rangle_{B,ph}. \tag{3.3}$$

At both Alice and Bobs side, the corresponding qudit interacts with m cavity-coupled qubit memories. Which of the m qubit memories

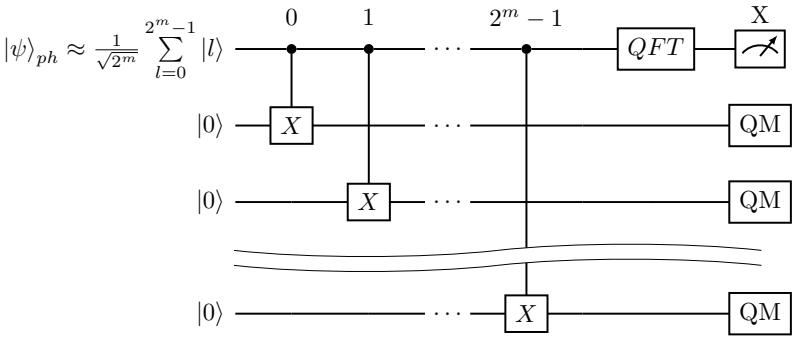

Figure 3.2: **Qudit state mapping to multi-qubit states.** Quantum circuit illustrating the qudit memory protocol at the ground stations. The control nodes represent optical switches that route the incoming time-bin pulses to the corresponding quantum memories based on the binary encoding of the time-bin. At the memories, a qubit-photon controlled note gate is performed which entangles the qubit state of the memories with the photon. After the interaction, the incoming photon is measured in the Fourier basis, which heralds the successful simultaneous storage of multiple Bell pairs.

that the photon interacts with depends on the specific time-bin and is controlled by photonic switching. The switching is programmed according to the binary representation of the time-bins (see Fig. 3.2). Consequently, the decimal time-bin encoding of the 2^m-dimensional qudits in Eq. (3.3) will be transformed into the corresponding binary encoding in m qubits. A 2^m-dimensional qudit state represented by $|l\rangle$ ($l = 0, 1, \ldots, 2^m - 1$) can be changed to binary encoding by the following conversion: $[l]_{10} = [l_{m-1} \cdots l_k \cdots l_1 l_0]_2$ ($l_i \in \{0, 1\}$) [22]. For example, the number 5_{10} is mapped to 101_2 in binary encoding.

The m-qubit register is initialized in the $|0\rangle^{\otimes m}$ state, and the incoming photon flips the qubits corresponding to its binary-encoded state. If $l_i = 1$ the ith qubit of the register will flip from $|0\rangle$ to $|1\rangle$. If $l_i = 0$ the qubit remains in state $|0\rangle$. After interaction at both ground stations, the resulting state of the qudit and qubit memory registers is:

$$|\psi\rangle = \frac{1}{\sqrt{2^m}} \sum_{l=0}^{2^m-1} |l\rangle_{A,ph} |l\rangle_{B,ph} |l_2\rangle_A |l_2\rangle_B, \tag{3.4}$$

where $|l_2\rangle$ represents the state of the multi-qubit register in binary encoding. The successful storage of the qudit information in the qubit registers is completed by detecting the photonic modes in a generalized X-basis such that the information about which time-bin the photons were in is erased. Such a measurement can be implemented by applying local quantum Fourier transforms (QFT) to the photonic modes at the ground stations, which can be implemented with optical delay lines, beam splitters and phase shifters as outlined in Refs. [22, 36]. It corresponds to projecting the photonic modes onto basis states of the form

$$|X_k\rangle = \frac{1}{\sqrt{2^m}} \sum_{l=0}^{2^m-1} e^{2i\pi lk/2^m} |l\rangle, \tag{3.5}$$

where $k \in \{0, 1, \ldots, 2^m - 1\}$. The measurement also heralds the successful transfer of the qudit information to the qubit register i.e. that a photon was received. Up to local phases determined by the measurement outcomes at Bob and Alice, the qubit register state following detection will be:

$$|\psi\rangle = \frac{1}{\sqrt{2}} (|0, 0\rangle_{A,B} + |1, 1\rangle_{A,B})^{\otimes m}. \tag{3.6}$$

To confirm the success of both sides, the measurement outcomes must be communicated between Alice and Bob. During this time, referred to as the heralding time, τ_h, the stored qubits experience decoherence. Additionally, in the qubit case, when more than one event-ready entangled pair is desired, the already entangled pairs need to wait until all desired pairs have been successfully entangled

during which they also suffer from decoherence. We model this as a depolarizing channel where the quantum state decays to a mixed state over time (t), with a decoherence probability of $1-\exp(-t/\tau_{coh})$. Here, τ_{coh} is the coherence time of the memories.

Besides the limited decoherence time of the qubit registers, additional errors such as photon loss and imperfect spin-photon gates will also affect the performance of the qubit registers. The photon loss can be directly absorbed into the overall photon transmission probability as previously described. Imperfect spin-photon gates and photonic switching affect the quality of the generated Bell pairs in a non-trivial way, which is treated in detail in Ref. [36]. In particular, the qudit encoding can result in correlated errors between the Bell pairs, which is a clear distinction between the qubit and the qudit mode of operation considered here. As shown in Ref. [36], the effect of such correlated errors depends on the application; purification schemes are able to effectively target such correlated errors while quantum error correction codes are less effective. Since the focus of this work is to study the effect of limited coherence time of the qubit registers as well as the approximate entangled pair source, we will assume that these are the dominant errors and neglect the effect of other imperfections in the qubit register storage in our further analysis. This will allow us to provide general, hardware-agnostic bounds on the performance of both the qubit and qudit operation of a satellite-based SPDC source for long-distance entanglement distribution.

3.3. PERFORMANCE

To compute the rate of entanglement distribution, we need to estimate the rate of photons successfully mapped to the qubit registers at the ground stations in both the qubit and qudit mode of operation. However, for the following analysis, the qubit mode of operation can be viewed as a special example of a 2-dimensional qudit.

The length of a photonic time-bin is set by the repetition rate of the pump laser, r_{rep}. Consequently, an approximate qudit pair of the form in Eq. (3.1) is emitted at a rate of $r_{\text{rep}}/2^m$. If a detector clicks at a ground station, which ideally heralds a successful storage, the receiver will close the access to the qubits involved and send a (classical) heralding signal to the other ground station. If no signal has been received from the other ground station after the heralding time τ_h has elapsed (time of communication between the ground stations), the qubits will be immediately reset in order to receive photons again. Additionally, if a heralding signal for the corresponding qubits at the other ground station is received within the communication time, the qubits will also be immediately reset. A successful entanglement will only happen when the qubit pairs are available in both ground stations and heralding

clicks are simultaneously recorded so that the ground stations both receive a heralding signal at the same time. Thus, the probability of successful entanglement distribution is given by $p_{\text{ent}} = p_{\text{suc}}\pi_{(0,0)}$, where p_{suc} denotes the probability that a single qudit pair is successfully transmitted and mapped onto the qubit registers, assuming the qubits are available, and $\pi_{(0,0)}$ represents the probability that the qubits are indeed available. We calculate the latter probability using a Markov chain [37].

To increase the entanglement distribution rate, we consider a multiplexing scheme, where there are more available quantum memories than the desired number of entangled pairs. In particular, if m entangled pairs are desired, we define a multiplexing parameter $n \in \{0, 1, \dots\}$ that specifies that mn qubit memories are available at each ground station. We will count one entanglement generation attempt as attempting all mn qubit memories sequentially. Thus, the time of one attempt is $\tau_c = 2mn/r_{\text{rep}}$ ($\tau_c = 2^m n/r_{\text{rep}}$) for the qubit (qudit) mode of operation. Additionally, we are in the limit $p_{\text{suc}} \ll 1$ and we will therefore consider a slightly sub-optimal protocol where we only allow for a single heralding click per attempt. In other words, we discard events with more than a single heralding click per attempt. However, as we detail below, the probability of multiple heralding clicks is very low for practically relevant parameters meaning that including such events would not significantly increase the rate.

We estimate the average rate of the entanglement distribution from the average number of attempts, $\langle A \rangle$ to obtain the desired number of event-ready entangled pairs:

$$R = \frac{1}{\langle A \rangle \tau}. \tag{3.7}$$

To calculate $\langle A \rangle$, it is useful to define the parameters D and N to keep track of the many possible combinations of obtaining m entangled pairs across multiple attempts. In the qubit (qudit) mode of operation $D = mn$ ($D = n$) and $N = m$ ($N = 1$). Since we have at most one heralding click per attempt, the average number of attempts to get m entangled pairs can be estimated as:

$$\begin{aligned}\langle A \rangle = \frac{D!}{(D-N)!\, p_{\text{approx}}} p_{ent}^N \sum_{i_1=0}^{\infty} \cdots \sum_{i_N > i_{N-1}}^{\infty} \big(i_1 + 1 + \\ + \sum_{k=2}^{N} (i_k - i_{k-1})\big)(1-p_{ent})^{(D-N+1)i_N + D - N + \sum_{k=1}^{N-1} i_k} = \\ = N + \sum_{k=1}^{N} \frac{(1-p_{ent})^{D+1-k}}{1-(1-p_{ent})^{D+1-k}}.\end{aligned} \tag{3.8}$$

This expression is valid both in the qubit and qudit mode of operation with the suitable choices of D and N. It captures that in each attempt i_j, we go through all the available memories. As the probability of entanglement is small, we discard the events in which more than one pair is entangled in a single attempt. To account for all possible combinations where there are no simultaneous successes, we sum over these combinations with condition $i_k > i_{k-1}$ to ensure that each pair needs a different number of attempts. The term $1-p_{\text{approx}}$ is the probability of obtaining m_t entangled pairs with more than one heralding click per attempt. This can be calculated as:

$$p_{\text{approx}} = \frac{D!}{(D-N)!} p_{\text{ent}}^{N} (1-p_{\text{ent}})^{ND-\left[(N-1)^2+2\right]} \sum_{i_1=0}^{\infty} \cdots \sum_{i_N=0}^{\infty} (1-p_{ent})^{\sum_{k=1}^{N}(D+1-k)}. \tag{3.9}$$

In our simulations, we keep $1-p_{\text{approx}} < 1\%$, which ensures that we do not significantly reduce the rate by discarding events with multiple heralding clicks in one attempt.

To compute the average fidelity of the entangled pairs, we take into account the effects of decoherence during the waiting period for all pairs to become successfully entangled.

$$\begin{aligned}\langle F(t)\rangle = \frac{D!}{N\cdot(D-N)!\,p_{\text{approx}}} p_{ent}^{N} (1-p_{ent})^{ND-\left((N-1)^2+2\right)} \\ \sum_{i_1=0}^{\infty} \cdots \sum_{i_N=0}^{\infty} \Big[(1-p_{ent})^{\sum_{k=1}^{N}(D+1-k)i_k} \\ \big(F(\tau_h) + F(\tau_h + (i_N+1)\tau_c) + \cdots \\ + F(\tau_h + \tau_c \sum_{j=2}^{N}(i_j+1))\big)\Big],\end{aligned} \tag{3.10}$$

where $F(t)$ is the fidelity of a pair after a storage time t. The detailed expression for $F(t)$ can be found in Appendix 3.5.1, which also includes infidelities from higher-order photon terms and dark counts. Note that we assume a worst-case scenario where these events result in states with fidelity of zero with the desired Bell states. The ordering used in Eq. (3.10) means that the i_N'th pair is the last pair that gets entangled and consequently, it only decoheres for the heralding time τ_h. On the other hand, the first pair (i_1) has to wait the longest, namely for $\tau_h + \tau_c \sum_{k=2}^{N} i_k$, where i_k is the number of entanglement attempts needed for the k^{th} pair to be successfully entangled.

The previous expressions for the average rate and fidelity of the entangled pairs (Eqs. (3.8),(3.10)), do not operate with a cut-off time.

In the qubit scheme, we add a cut-off time to the memories to ensure a certain target fidelity of the entangled pairs. We consider a strategy where once the first pair has been entangled, it will be stored in the quantum memory the chosen cut-off time, and the rest of the pairs we want to entangle must be successfully entangled within that time. To account for that in our expression of the rate and the fidelity, the sums over the attempts that occur after the first successfully entangled pair will be bounded by the cut-off time. The updated expressions including this can be found in the Appendix 4.4.1 for the case of $m = 2$.

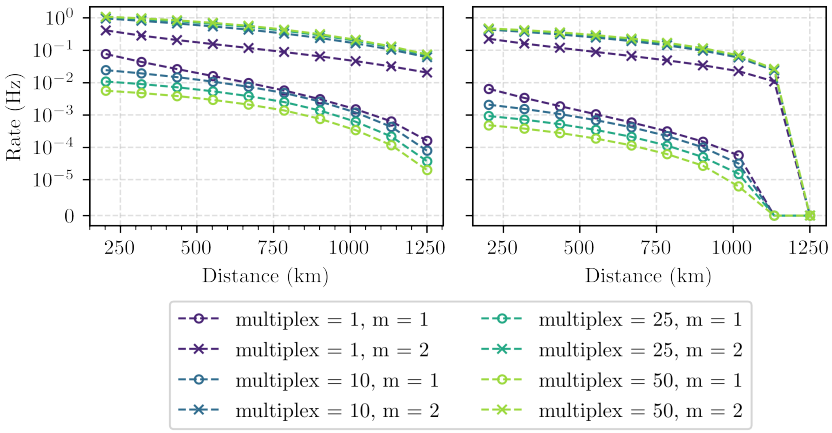

Figure 3.3: Performance comparison of the qudit (crosses) and qubit (circles) modes of operations. We optimize the squeezing parameter, λ, between values ranging from 0 to 0.1 as we are working in the weak-pump regime, for each distance, as well as the cut-off time for the qubit case. We assume a dark count probability of $p_{\text{dark}} = 1.6 \cdot 10^{-5}$, a memory storage efficiency of $\eta = 0.5$ (including photon detection), a SPDC repetition rate of $r_{\text{rep}} = 10^{-7}$s, and a qubit decoherence time of $T_d = 10$s. Additionally, the transmission probability, p_T is of the order of 10^{-3}, being $\sim 8 \cdot 10^{-3}$ for the shortest distance of ~ 200 km, and being $\sim 2 \cdot 10^{-3}$ for the longest distance of ~ 1200 km. In the **left figure**, the target fidelity is 0.9. The optimized value of the cut-off time is 1 s. In the **right figure**, the target fidelity is 0.95. Here, the optimized t_{cut} is always 0.1 s.

In Fig. 3.3, we show a comparison between the qudit and the qubit mode of operation when requiring a minimum average Bell pair fidelity of 0.90 (left figure) and 0.95 (right figure) of two event-ready entangled pairs (m=2). For the qubit mode of operation we optimize the cut-off

time to achieve the maximum distribution rate for a certain distance. We assume the same performance in terms of memory efficiency and coherence time for both modes of operation and optimize the squeezing parameter λ to achive the highest distribution rate. Our results show that the qudit mode of operation results in orders of magnitude larger distribution rates than the qubit mode. We also see that multiplexing increases the distribution rate for the qudit case while it surprisingly does not for the qubit mode of operation. This is because the attempt time increases as we increase the factor of multiplexing and the increase in success probability is not significant enough to outweigh this. In other words, multiplexing is worth implementing, if the rate at which the photons arrive at the ground stations, is higher than the communication time between them, which is not the case for the Micius parameters considered here where the SPDC source rate is 10 MHz. Note that increasing the repetition rate of the SPDC source would eventually result in a rate boost from multiplexing also in the qubit case.

Additionally, from Fig. 3.3, we see that the use of 2^m-dimensional qudits, where the dimensionality corresponds to the desired number of entangled pairs, enables entanglement over remarkably long distances of up to 1250 km. However, we see that, at this maximum distance, the entanglement rate drops to zero when the target fidelity is 0.95. The fidelity depends not only on the coherence time and the waiting time for the successful entanglement of all pairs, but also on the squeezing parameter (λ), the transmission probability (p_T), the memory efficiency (η), and the dark count probability (p_{dark}). In the simulations, the squeezing parameter is optimized to achieve the highest rate under the chosen fidelity cap. However, for distances ≥ 1250 km, it becomes impossible to find a squeezing parameter that ensures a target fidelity of 0.95 due to dark counts. This can be improved by either lowering the dark count rate of the detectors or improving the overall transmission probability. The transmission probability is influenced by factors such as the satellite's altitude and the size of its transmitters. Detection efficiency, on the other hand, can be enhanced by improving the detectors at ground stations. Therefore, while maintaining the same satellite, upgrading the ground station's detection systems could enable entanglement over even greater distances.

3.4. CONCLUSION

In summary, we have shown how satellite-assisted entanglement distribution can benefit significantly from adopting a qudit mode of operation when mutliple, high-fidelity, and event-ready entangled pairs are desired. Our simulations show that a qudit mode of operation results in several orders of magnitude higher distribution rates than a standard qubit mode of operation for all distances between 200-

1200km. Importantly, the qudit mode of operation does not require any substantial upgrades of existing quantum satellites payloads but rather upgrades of the quantum memories at the ground nodes, which are much more accessible. To achieve a general bound on the achievable rate, we have assumed negligible infidelities from the memory storage operation, except for the effect of limited coherence time. Although errors in current hardware do not quite satisfy this assumption for the target fidelities of 90% and 95% assumed in this work, we note that recent experiments with cavity-coupled diamond color centers have demonstrated spin-photon gates with infidelities of $\sim 2\%$, qubit gate errors of $\sim 1\%$ and measurement errors of $\sim 1-2\%$ [18] together with single photon storage efficiencies of $\sim 40\%$ [29] with clear paths to improvement. Additionally, using nearby nuclear memory spins, coherence times on the order of seconds have been demonstrated with the same hardware [38, 39], with the possibility to extend the coherence time to the order of minutes using weakly coupled nuclear spins [40]. We also note that Ref. [18] reports entanglement generation between two SiV qubit memories using a photonic qudit demonstrating the compatibility of this hardware with photonic qudits. This makes it conceivable that satellit-assisted high-quality entanglement distribution using the qudit mode of operation considered in this work could be realized with near-term hardware.

3.5. APPENDIX

3.5.1. FIDELITY

The fidelity of each entangled pair at the ground stations is defined as:

$$F(t) = \frac{\langle \Phi^+ | \rho_{\text{pair}} | \Phi^+ \rangle}{Tr(\rho)}, \tag{3.11}$$

where:

$$\begin{aligned} \langle \Psi^+ | \rho_{\text{pair}} | \Psi^+ \rangle \quad = \quad & 2^m p_f^2 \eta^2 \lambda^2 ((e^{-t/T_A} + (1-e^{-t/T_A})\epsilon_1) \\ & (e^{-t/T_B} + (1-e^{-t/T_B})\epsilon_1) + (1-e^{-t/T_A}) \\ & (1-e^{-t/T_B})(\epsilon_x^2 + \epsilon_y^2 + \epsilon_z^2)), \end{aligned} \tag{3.12}$$

$$
\begin{aligned}
Tr(\rho) \quad = \quad & 2^m p_T^2 \eta^2 \lambda^2 + 2^{m-1}(2^m+1) p_T^4 \lambda^4 \eta^4 \\
& + 2^{m+1} p_T \eta (1 - p_T \eta) \lambda^2 p_{\text{dark}} + 2^m (2^m+1) p_T^2 \eta^2 \\
& (1 - p_T \eta)^2 \lambda^4 \left(p_{\text{dark}} + 2 \right) + 2^{m+1}(2^m+1) \\
& \left(p_T^3 \eta^3 (1 - p_T \eta) \lambda^4 + p_T \eta (1 - p_T \eta)^3 \lambda^4 p_{\text{dark}} \right) \\
& + p_{\text{dark}}^2 \Big(2^{m-1}(2^m+1)(1 - p_T \eta)^4 \lambda^4 \\
& + 2^m (1 - p_T \eta)^2 \lambda^2 + 1 \Big) + \mathcal{O}(\lambda^6),
\end{aligned} \tag{3.13}
$$

$$
|\Phi^+\rangle = \frac{1}{\sqrt{2}} \left(|0\rangle|0\rangle + |1\rangle|1\rangle \right). \tag{3.14}
$$

Here, $|\Phi^+\rangle$ is the desired Bell pair, and ρ_{pair} is the (unnormalized) density matrix of a single pair of entangled memory qubits. In the qudit mode of operation, the latter corresponds to tracing out all other qubit pairs. The normalization of ρ_{pair} corresponds to the probability of obtaining successful heralding clicks that prepare the memories in this state. The denominator in Eq. (3.11) is the total probability of a successful heralding, which can be calculated as the trace over the full (unnormalized) density matrix, ρ including contributions from higher order photon terms and dark counts. Note that we adopt a lower bound on the fidelity by assuming that dark counts and higher-order photon terms results in states with zero overlap with the desired Bell states.

As stated in the main text, p_T is the total transmission probability and we explicitly include η as the memory storage efficiency. The time the pair is stored before successful entanglement of all desired pairs is achieved is t. Note that this varies from pair to pair in the qubit mode of operation as shown in Eq. (3.10), while $t = t_h$ in the qudit mode of operation. We let T_A and T_B denote the coherence times of Alice and Bobs memory qubits and let ϵ_1,ϵ_x, ϵ_y, and ϵ_z represent the relative error rates for Pauli errors in the I, X, Y, and Z bases, respectively. In our simulations, we set both decoherence times to $T_A = T_B = \tau_{\text{coh}}$ and assume a depolarizing channel with $\epsilon_1 = \epsilon_x = \epsilon_y = \epsilon_z = 1/4$.

3.5.2. CUT-OFF TIME CALCULATION.

Here, we show how we estimate the rate and fidelity for the qubit mode of operation when we have cut-off time and we want to entangle two pairs. In this scheme, the second pair needs to be entangled within the cut-off time, otherwise, the first entangled pair is discarded and we repeat the process again. To estimate the average number of attempts to successfully entangle two pairs within the cut-off time, we consider

the average number of tries assuming a successful entanglement generation i.e. that the pairs are generated within the cut-off time, $\langle n_{\text{succ}} \rangle$. The expression for this is similar to the one shown in Eq. (3.8), except that the sum over the second pair, i_2, is bounded by a finite number of tries given by the cut-off time, N_{cut}. This number of tries is defined as $N_{\text{cut}} = t_{\text{cut}}/D\tau_c$, where t_{cut} is the cut-off time, which is always smaller than the decoherence time of the quantum memories. Specifically,

$$\langle n_{\text{succ}} \rangle = \frac{D!}{(D-2)! p_{2\text{p}}} p_{\text{ent}}^2 (1-p_{\text{ent}})^{(2D-3)} \sum_{i_1=0}^{\infty} \sum_{i_2=0}^{N_{\text{cut}}-2} (i_1 + i_2 + 2)(1-p_{\text{ent}})^{i_2(D-1)+Di_1}, \tag{3.15}$$

where $p_{2\text{p}}$ is given by

$$p_{2\text{p}} = \frac{D!}{(D-2)!} p_{\text{ent}}^2 (1-p_{\text{ent}})^{(2D-3)} \sum_{i_1=0}^{\infty} \sum_{i_2=0}^{N_{\text{cut}}-2} (1-p_{\text{ent}})^{i_2(D-1)+Di_1},$$

and is the probability of successfully entangling two pairs within the cutoff time. Note that we still only allow for a single success per attempt as described in the main text. To estimate the average number of attempts, we also estimate the the average number of tries, $\langle n_{\text{fail}} \rangle$., to obtain one entangled pair but fail to entangle the second one within the cut-off time as well as the probability for this event. This is given by

$$\langle n_{\text{fail}} \rangle = N_{\text{cut}} + \langle n_1 \rangle = \frac{D!}{(D-1)!} p_{\text{ent}} (1-p_{\text{ent}})^{D-2} \sum_{i_1=0}^{\infty} (i_1 + 1)(1-p_{\text{ent}})^{Di_1} + N_{\text{cut}},$$

where $\langle n_1 \rangle$ is the average number of attempts to get the first pair. The probability of a failed attempt is $p_{\text{fail}} = (1-p_{\text{ent}})^{N_{\text{cut}}}$.

We now estimate the average number of attempt to successfully entangle two pairs within the cutoff time as

$$\langle n \rangle = \sum_{i=0}^{\infty} \big(i\langle n_{\text{fail}} \rangle + \langle n_{\text{succ}} \rangle\big) p_{\text{fail}}^i p_{\text{succ}} = \frac{1}{p_{\text{succ}}} \big(\big(\langle n_{\text{fail}} \rangle - \langle n_{\text{succ}} \rangle\big) p_{\text{fail}} + \langle n_{\text{succ}} \rangle\big), \tag{3.16}$$

where $p_{\text{succ}} = 1 - p_{\text{fail}}$. We note that $p_{\text{succ}} \approx p_{2\text{p}}$ for the parameters considered since the probability to heralding two pairs in the same attempt is very small. For the computation of the fidelity, we also truncate the upper limit of the sum for i_2.

$$\langle F(t)\rangle = \frac{D!}{2(D-2)!p_{2\text{p}}} p_{\text{ent}}^2 (1-p_{\text{ent}})^{2D-3} \sum_{i_1=0}^{\infty} \sum_{i_2=0}^{N_{\text{cut}}-2} (1-p_{\text{ent}})^{i_2(D-1)+Di_1} \big[F(\tau_h) + F(\tau_h + (i_2+1)\tau_c\big]$$

REFERENCES

[1] S. Wehner, D. Elkouss, and R. Hanson. *Quantum internet: A vision for the road ahead*. Oct. 2018. doi: 10.1126/science.aam9288. url: https://www.science.org/doi/10.1126/science.aam9288.

[2] S. Pironio, A. Acin, N. Brunner, N. Gisin, S. Massar, and V. Scarani. "Device-independent quantum key distribution secure against collective attacks". In: *New Journal of Physics* 11 (Apr. 2009). issn: 13672630. doi: 10.1088/1367-2630/11/4/045021.

[3] V. Scarani, H. Bechmann-Pasquinucci, N. J. Cerf, M. Dušek, N. Lütkenhaus, and M. Peev. "The security of practical quantum key distribution". In: *Reviews of Modern Physics* 81.3 (Sept. 2009), pp. 1301–1350. issn: 00346861. doi: 10.1103/RevModPhys.81.1301. url: https://journals.aps.org/rmp/abstract/10.1103/RevModPhys.81.1301.

[4] J. F. Fitzsimons. "Private quantum computation: an introduction to blind quantum computing and related protocols". In: *npj Quantum Information* 3.1 (June 2017), pp. 1–11. issn: 20566387. doi: 10.1038/S41534-017-0025-3. url: https://www.nature.com/articles/s41534-017-0025-3.

[5] R. Van Meter and S. J. Devitt. "The Path to Scalable Distributed Quantum Computing". In: *Computer* 49.9 (Sept. 2016), pp. 31–42. issn: 00189162. doi: 10.1109/MC.2016.291.

[6] L. de Forges de Parny, O. Alibart, J. Debaud, S. Gressani, A. Lagarrigue, A. Martin, A. Metrat, M. Schiavon, T. Troisi, E. Diamanti, P. Gélard, E. Kerstel, S. Tanzilli, and M. Van Den Bossche. "Satellite-based quantum information networks: use cases, architecture, and roadmap". In: *Communications Physics* 6.1 (2023), p. 12. doi: 10.1038/s42005-022-01123-7. url: https://doi.org/10.1038/s42005-022-01123-7.

[7] C. Liorni, H. Kampermann, and D. Bruß. "Quantum repeaters in space". In: *New Journal of Physics* 23.5 (May 2021), p. 053021. doi: 10.1088/1367-2630/abfa63. url: https://doi.org/10.1088%2F1367-2630%2Fabfa63.

[8] M. Gündoğan, J. S. Sidhu, V. Henderson, L. Mazzarella, J. Wolters, D. K. L. Oi, and M. Krutzik. “Proposal for space-borne quantum memories for global quantum networking”. In: *npj Quantum Information* 7.1 (2021), p. 128. doi: 10.1038/s41534-021-00460-9. url: https://doi.org/10.1038/s41534-021-00460-9.

[9] J. Wallnöfer, F. Hahn, M. Gündoğan, J. S. Sidhu, F. Wiesner, N. Walk, J. Eisert, and J. Wolters. “Simulating quantum repeater strategies for multiple satellites”. In: *Communications Physics* 5.1 (June 2022). doi: 10.1038/s42005-022-00945-9. url: https://doi.org/10.1038%2Fs42005-022-00945-9.

[10] S. Khatri, A. J. Brady, R. A. Desporte, M. P. Bart, and J. P. Dowling. “Spooky action at a global distance: analysis of space-based entanglement distribution for the quantum internet”. In: *npj Quantum Information* 7.1 (Jan. 2021). doi: 10.1038/s41534-020-00327-5. url: https://doi.org/10.1038%2Fs41534-020-00327-5.

[11] K. Boone, J.-P. Bourgoin, E. Meyer-Scott, K. Heshami, T. Jennewein, and C. Simon. “Entanglement over global distances via quantum repeaters with satellite links”. In: *Phys. Rev. A* 91 (5 May 2015), p. 052325. doi: 10.1103/PhysRevA.91.052325. url: https://link.aps.org/doi/10.1103/PhysRevA.91.052325.

[12] J. Yin, Y. Cao, Y.-H. Li, J.-G. Ren, S.-K. Liao, L. Zhang, W.-Q. Cai, W.-Y. Liu, B. Li, H. Dai, M. Li, Y.-M. Huang, L. Deng, L. Li, Q. Zhang, N.-L. Liu, Y.-A. Chen, C.-Y. Lu, R. Shu, C.-Z. Peng, J.-Y. Wang, and J.-W. Pan. “Satellite-to-Ground Entanglement-Based Quantum Key Distribution”. In: *Phys. Rev. Lett.* 119 (20 Nov. 2017), p. 200501. doi: 10.1103/PhysRevLett.119.200501. url: https://link.aps.org/doi/10.1103/PhysRevLett.119.200501.

[13] S.-K. Liao, W.-Q. Cai, J. Handsteiner, B. Liu, J. Yin, L. Zhang, D. Rauch, M. Fink, J.-G. Ren, W.-Y. Liu, Y. Li, Q. Shen, Y. Cao, F.-Z. Li, J.-F. Wang, Y.-M. Huang, L. Deng, T. Xi, L. Ma, T. Hu, L. Li, N.-L. Liu, F. Koidl, P. Wang, Y.-A. Chen, X.-B. Wang, M. Steindorfer, G. Kirchner, C.-Y. Lu, R. Shu, R. Ursin, T. Scheidl, C.-Z. Peng, J.-Y. Wang, A. Zeilinger, and J.-W. Pan. “Satellite-Relayed Intercontinental Quantum Network”. In: *Phys. Rev. Lett.* 120 (3 Jan. 2018), p. 030501. doi: 10.1103/PhysRevLett.120.030501. url: https://link.aps.org/doi/10.1103/PhysRevLett.120.030501.

[14] J. Yin, Y.-H. Li, S.-K. Liao, M. Yang, Y. Cao, L. Zhang, J.-G. Ren, W.-Q. Cai, W.-Y. Liu, S.-L. Li, R. Shu, Y.-M. Huang, L. Deng, L. Li, Q. Zhang, N.-L. Liu, Y.-A. Chen, C.-Y. Lu, X.-B. Wang, F. Xu, J.-Y. Wang, C.-Z. Peng, A. K. Ekert, and J.-W. Pan. "Entanglement-based secure quantum cryptography over 1,120 kilometres". In: *Nature* 582.7813 (June 2020). Number: 7813 Publisher: Nature Publishing Group, pp. 501–505. issn: 1476-4687. doi: 10.1038/s41586-020-2401-y. url: https://www.nature.com/articles/s41586-020-2401-y (visited on 08/14/2023).

[15] S. Krastanov, V. V. Albert, and L. Jiang. "Optimized Entanglement Purification". In: *Quantum* 3 (Feb. 2019), p. 123. issn: 2521-327X. doi: 10.22331/q-2019-02-18-123. url: https://doi.org/10.22331/q-2019-02-18-123.

[16] C. A. Pattison, G. Baranes, J. P. B. Ataides, M. D. Lukin, and H. Zhou. *Fast quantum interconnects via constant-rate entanglement distillation*. 2024. arXiv: 2408.15936 [quant-ph]. url: https://arxiv.org/abs/2408.15936.

[17] J. Ramette, J. Sinclair, N. P. Breuckmann, and V. Vuletić. "Fault-tolerant connection of error-corrected qubits with noisy links". In: *npj Quantum Information* 10.1 (2024), p. 58. doi: 10.1038/s41534-024-00855-4. url: https://doi.org/10.1038/s41534-024-00855-4.

[18] Y.-C. Wei, P.-J. Stas, A. Suleymanzade, G. Baranes, F. Machado, Y. Q. Huan, C. M. Knaut, S. W. Ding, M. Merz, E. N. Knall, U. Yazlar, M. Sirotin, I. W. Wang, B. Machielse, S. F. Yelin, J. Borregaard, H. Park, M. Lončar, and M. D. Lukin. "Universal distributed blind quantum computing with solid-state qubits". In: *Science* 388.6746 (2025), pp. 509–513. doi: 10.1126/science.adu6894. eprint: https://www.science.org/doi/pdf/10.1126/science.adu6894. url: https://www.science.org/doi/abs/10.1126/science.adu6894.

[19] N. Kalb, A. A. Reiserer, P. C. Humphreys, J. J. Bakermans, S. J. Kamerling, N. H. Nickerson, S. C. Benjamin, D. J. Twitchen, M. Markham, and R. Hanson. "Entanglement distillation between solid-state quantum network nodes". In: *Science* 356.6341 (June 2017), pp. 928–932. issn: 10959203. doi: 10.1126/science.aan0070. url: https://www.science.org/doi/10.1126/science.aan0070.

[20] L. Jiang, J. M. Taylor, K. Nemoto, W. J. Munro, R. Van Meter, and M. D. Lukin. "Quantum repeater with encoding". In: *Physical Review A* 79.3 (2009). issn: 1050-2947. doi: 10.1103/physreva.79.032325.

[21] W. J. Munro, K. Azuma, K. Tamaki, and K. Nemoto. *Inside Quantum Repeaters*. May 2015. doi: 10.1109/JSTQE.2015.2392076.

[22] Y. Zheng, H. Sharma, and J. Borregaard. "Entanglement Distribution with Minimal Memory Requirements Using Time-Bin Photonic Qudits". In: *PRX Quantum* 3.4 (2022). issn: 26913399. doi: 10.1103/PRXQuantum.3.040319.

[23] Z. Xie, Y. Liu, X. Mo, T. Li, and Z. Li. "Quantum entanglement creation for distant quantum memories via time-bin multiplexing". In: *Physical Review A* 104.6 (Dec. 2021), p. 062409. issn: 24699934. doi: 10.1103/PhysRevA.104.062409. url: https://journals.aps.org/pra/abstract/10.1103/PhysRevA.104.062409.

[24] O. A. Collins, S. D. Jenkins, A. Kuzmich, and T. A. B. Kennedy. "Multiplexed Memory-Insensitive Quantum Repeaters". In: *Phys. Rev. Lett.* 98 (6 Feb. 2007), p. 060502. doi: 10.1103/PhysRevLett.98.060502. url: https://link.aps.org/doi/10.1103/PhysRevLett.98.060502.

[25] C. Simon, H. de Riedmatten, and M. Afzelius. "Temporally multiplexed quantum repeaters with atomic gases". In: *Phys. Rev. A* 82 (1 July 2010), p. 010304. doi: 10.1103/PhysRevA.82.010304. url: https://link.aps.org/doi/10.1103/PhysRevA.82.010304.

[26] D. Lago-Rivera, J. V. Rakonjac, S. Grandi, and H. d. Riedmatten. "Long distance multiplexed quantum teleportation from a telecom photon to a solid-state qubit". In: *Nature Communications* 14.1 (2023), p. 1889. doi: 10.1038/s41467-023-37518-5. url: https://doi.org/10.1038/s41467-023-37518-5.

[27] B. Li, T. Coopmans, and D. Elkouss. "Efficient Optimization of Cutoffs in Quantum Repeater Chains". In: *IEEE Transactions on Quantum Engineering* 2 (2021), pp. 1–15. doi: 10.1109/TQE.2021.3099003.

[28] Á. G. Iñesta, G. Vardoyan, L. Scavuzzo, and S. Wehner. "Optimal entanglement distribution policies in homogeneous repeater chains with cutoffs". In: *npj Quantum Information* 9.1 (2023), p. 46. doi: 10.1038/s41534-023-00713-9. url: https://doi.org/10.1038/s41534-023-00713-9.

[29] M. K. Bhaskar, R. Riedinger, B. Machielse, D. S. Levonian, C. T. Nguyen, E. N. Knall, H. Park, D. Englund, M. Lončar, D. D. Sukachev, and M. D. Lukin. "Experimental demonstration of memory-enhanced quantum communication". In: *Nature* 580.7801 (2020), pp. 60–64. issn: 14764687. doi: 10.1038/s41586-020-

2103-5. url: https://doi.org/10.1038/s41586-020-2103-5.

[30] C. M. Knaut, A. Suleymanzade, Y. .-. Wei, D. R. Assumpcao, P. .-. Stas, Y. Q. Huan, B. Machielse, E. N. Knall, M. Sutula, G. Baranes, N. Sinclair, C. De-Eknamkul, D. S. Levonian, M. K. Bhaskar, H. Park, M. Lončar, and M. D. Lukin. "Entanglement of nanophotonic quantum memory nodes in a telecom network". In: *Nature* 629.8012 (2024), pp. 573–578. doi: 10.1038/s41586-024-07252-z. url: https://doi.org/10.1038/s41586-024-07252-z.

[31] A. Reiserer. "Colloquium: Cavity-enhanced quantum network nodes". In: *Rev. Mod. Phys.* 94 (4 Dec. 2022), p. 041003. doi: 10.1103/RevModPhys.94.041003. url: https://link.aps.org/doi/10.1103/RevModPhys.94.041003.

[32] J. Yin, Y. Cao, Y. H. Li, S. K. Liao, L. Zhang, J. G. Ren, W. Q. Cai, W. Y. Liu, B. Li, H. Dai, G. B. Li, Q. M. Lu, Y. H. Gong, Y. Xu, S. L. Li, F. Z. Li, Y. Y. Yin, Z. Q. Jiang, M. Li, J. J. Jia, G. Ren, D. He, Y. L. Zhou, X. X. Zhang, N. Wang, X. Chang, Z. C. Zhu, N. L. Liu, Y. A. Chen, C. Y. Lu, R. Shu, C. Z. Peng, J. Y. Wang, and J. W. Pan. "Satellite-based entanglement distribution over 1200 kilometers". In: *Science* 356.6343 (2017), pp. 1140–1144. issn: 10959203. doi: 10.1126/science.aan3211.

[33] A. Fedrizzi, R. Ursin, T. Herbst, M. Nespoli, R. Prevedel, T. Scheidl, F. Tiefenbacher, T. Jennewein, and A. Zeilinger. "High-fidelity transmission of entanglement over a high-loss free-space channel". In: *Nature Physics* 5.6 (2009), pp. 389–392. issn: 17452481. doi: 10.1038/nphys1255.

[34] V. D. Tubío, M. B. Aldecocea, J. van Dam, A. S. Sørensen, and J. Borregaard. *Satellite-assisted quantum communication with single photon sources and atomic memories*. 2024. arXiv: 2411.09533 [quant-ph]. url: https://arxiv.org/abs/2411.09533.

[35] S. Ritter, C. Nölleke, C. Hahn, A. Reiserer, A. Neuzner, M. Uphoff, M. Mücke, E. Figueroa, J. Bochmann, and G. Rempe. "An elementary quantum network of single atoms in optical cavities". In: *Nature* 484.7393 (Apr. 2012), pp. 195–200. issn: 00280836. doi: 10.1038/nature11023. url: https://www.nature.com/articles/nature11023.

[36] X. Liu, N. Bharos, L. Markovich, and J. Borregaard. "Error correlations in photonic qudit-mediated entanglement generation". In: *Phys. Rev. Res.* 6 (2 Apr. 2024), p. 023075. doi: 10.1103/PhysRevResearch.6.023075. url: https://

link.aps.org/doi/10.1103/PhysRevResearch.6.023075.

[37] C. Jones, K. D. Greve, and Y. Yamamoto. *A high-speed optical link to entangle quantum dots*. 2013. arXiv: 1310.4609 [quant-ph]. url: https://arxiv.org/abs/1310.4609.

[38] C. T. Nguyen, D. D. Sukachev, M. K. Bhaskar, B. Machielse, D. S. Levonian, E. N. Knall, P. Stroganov, R. Riedinger, H. Park, M. Lon čar, and M. D. Lukin. "Quantum Network Nodes Based on Diamond Qubits with an Efficient Nanophotonic Interface". In: *Phys. Rev. Lett.* 123 (18 Oct. 2019), p. 183602. doi: 10.1103/PhysRevLett.123.183602. url: https://link.aps.org/doi/10.1103/PhysRevLett.123.183602.

[39] P.-J. Stas, Y. Q. Huan, B. Machielse, E. N. Knall, A. Suleymanzade, B. Pingault, M. Sutula, S. W. Ding, C. M. Knaut, D. R. Assumpcao, Y.-C. Wei, M. K. Bhaskar, R. Riedinger, D. D. Sukachev, H. Park, M. Lončar, D. S. Levonian, and M. D. Lukin. "Robust multi-qubit quantum network node with integrated error detection". In: *Science* 378.6619 (2022), pp. 557–560. doi: 10.1126/science.add9771. eprint: https://www.science.org/doi/pdf/10.1126/science.add9771. url: https://www.science.org/doi/abs/10.1126/science.add9771.

[40] C. E. Bradley, J. Randall, M. H. Abobeih, R. C. Berrevoets, M. J. Degen, M. A. Bakker, M. Markham, D. J. Twitchen, and T. H. Taminiau. "A Ten-Qubit Solid-State Spin Register with Quantum Memory up to One Minute". In: *Phys. Rev. X* 9 (3 Sept. 2019), p. 031045. doi: 10.1103/PhysRevX.9.031045. url: https://link.aps.org/doi/10.1103/PhysRevX.9.031045.

4

SATELLITE-ASSISTED QUANTUM COMMUNICATION WITH SINGLE PHOTON SOURCES AND ATOMIC MEMORIES

V. Domínguez Tubío, M. Badás Aldecocea, J.van Dam, A. S. Sørensen, J. Borregaard

Satellite-based quantum repeaters are a promising means to reach global distances in quantum networking due to the polynomial decrease of optical transmission with distance in free space, in contrast to the exponential decrease in optical fibers. We propose a satellite-based quantum repeater architecture with trapped individual atomic qubits, which can serve both as quantum memories and true single photon sources. This hardware allows for nearly deterministic Bell measurements and exhibits long coherence times without the need for costly cryogenic technology in space. We develop a detailed analytical model of the repeater, which includes the main imperfections of the quantum hardware and the optical link, allowing us to estimate that high-rate and high-fidelity entanglement distribution can be achieved over inter-continental distances. In particular, we find that high fidelity entanglement distribution over thousands of kilometres at a rate of 100 Hz can be achieved with orders of magnitude fewer memory modes than conventional architectures based on optical Bell state measurements.

This chapter is based on the publication Phys. Rev. Res. 8, p.013099

4.1. INTRODUCTION

The implementation of a quantum internet opens a range of new opportunities for secure communication [1–3], enhanced sensing networks [4–6], and distributed quantum computing [7]. To exploit these opportunities in applications such as protecting and optimizing large-scale power distribution networks [8] or probing fundamental constants and geodesy [9], it is necessary to extend the range of quantum networks to distances of thousands of kilometres.

To carry out quantum communication, we need to use photons to transmit quantum information. However, transmission loss of an optical quantum signal cannot be compensated with standard classical amplification techniques due to the quantum no-cloning theorem [10]. Instead, quantum repeaters have been proposed, where the total distance is divided into smaller segments over which direct transmission is feasible. The segments are then combined either through quantum teleportation [11, 12] or quantum error correction [13, 14] at the repeater nodes to enable faithful transmission over the total distance.

For optical fiber-based quantum repeaters, the transmission between the repeater nodes decreases exponentially with distance and hundreds of repeater nodes are required to cover distances at the continental scale. Alternatively, fiber-based connections can be replaced with satellite-assisted free-space optical links where transmission decreases only polynomially with the distance [15–21]. For continental scales, this can reduce the required number of repeater nodes by orders of magnitude making up for the arguably higher cost of space-based quantum repeater nodes.

Quantum key distribution (QKD) has already been demonstrated with the Micius satellite over 1200 km [22]. Reaching larger distances by direct transmission, however, requires a high-orbit satellite due to the limitation from the line of sight of the ground receivers. This substantially increases the transmission loss, making high-rate quantum communication extremely challenging. Alternatively, multiple low-orbit satellites can operate in a quantum repeater architecture to efficiently compensate for the transmission loss and ensure line of sight between distant locations [16, 18, 23].

Previous theoretical work on satellite-based quantum repeaters assumes the use of probabilistic optical Bell state measurements (BSMs) [16], which requires multiplexing of thousands of memory modes in order to reach high-rate communication over global distances. Additionally, the availability of on-demand entangled photon pair sources are often assumed [16, 18–20], which remains an outstanding technological challenge [24]. Promising candidate systems are solid-state semiconductor quantum dots [25], which require cryogenic temperatures to function or multiplexing of SPDC sources [26] and single photon sources [27].

We propose a satellite-assisted quantum repeater protocol based on trapped individual atomic qubits. Individually trapped Alkali atoms can both function as efficient single-photon sources [28] and atomic memories due to their long coherence times [29, 30]. Furthermore, they enable nearly deterministic Bell state measurements through Rydberg-mediated two-atom gates [31–33] and the possibility of scaling to hundreds of qubits per repeater node [34, 35]. Additionally, laser-cooling of the atoms is sufficient to ensure long coherence times, which avoids the need for costly cryogenic technology in space.

We develop a detailed analytical model of the repeater protocol that considers the main imperfections of both the quantum hardware and the optical link budget. In contrast to Monte-Carlo-based simulations [18], the analytical model allows us to efficiently simulate long chains of quantum repeater nodes. We show that, for realistic satellite parameters and quantum hardware errors, we can get high-fidelity (≥ 0.9) entanglement distribution rates of 100 Hz over continental distances of up to 1500 km using 5 satellites with less than 200 quantum memory modes per satellite.

4.2. RESULTS

4.2.1. ARCHITECTURE

We consider a down-link scenario where photons are sent from the end-satellites to the ground stations, which is more robust to atmospheric turbulence than the reverse up-link scenario [23, 36]. A high-level sketch of a 3-node repeater is shown in Fig. 4.1a). The quantum repeater consists of different types of satellites. Some satellites act as emitters, sending photons to their neighbouring satellites or to the ground station. Others are receivers, that collect the photons sent by the emitter satellites. Both types of satellites are equipped with atomic quantum memories and act as quantum repeater nodes, as shown in Fig. 4.1b).

To distribute entanglement between the ground stations, atom-photon entanglement is generated at the repeater stations through pulsed excitation of the atoms. The generated photons are sent from the emitter nodes to the receiver ones, where the atom-photon entanglement is swapped to atom-atom entanglement by means of a linear optics Bell State Measurement (BSM). Once entanglement between two neighbouring elementary links has been successfully heralded, a nearly deterministic entanglement swap operation is performed through Rydberg-mediated atom-atom interactions. If the entanglement generation is successful in all elementary links, the two ground states will share an entangled pair.

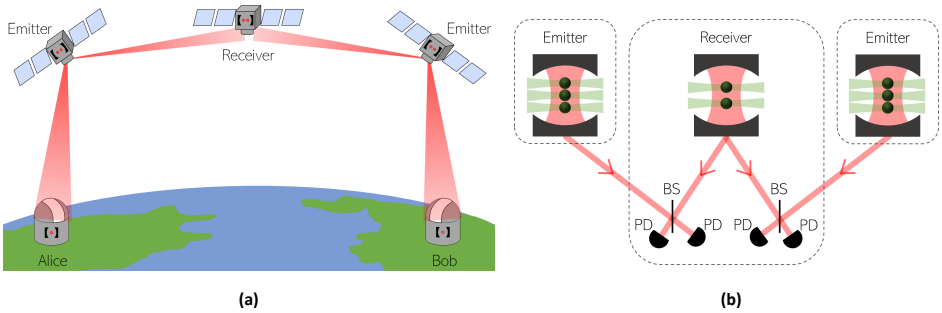

Figure 4.1: **Experimental setup. (a)** We consider a down-link scenario where the photons are transmitted from the end-satellites to the ground stations. Each of the satellites contains quantum memories and entanglement swaps are performed on the satellites to link the segments of the repeater (satellite-satellite or satellite-ground stations) once entanglement has been established. **(b)** Probabilistic BSM. The atom-photon entanglement generated through the emission of a photon from an atom is swapped to atom-atom entanglement within a receiver satellite by means of a linear optics Bell state measurement. This is done using a 50/50 beam splitter (BS) and single photon detectors.

4.2.2. ENTANGLEMENT GENERATION

For the generation of atom-atom entanglement, we consider a 'two-click' protocol [37], where each atom is entangled with a time-bin encoded single photon through pulsed excitation. This is then swapped to atom-atom entanglement by a linear optics Bell measurement. We focus on this scheme since it only requires phase stability on the time-scale of the time-bin separation and does not have the fundamental trade-off between rate and fidelity of 'single-click' protocols [38]. Furthermore, we consider a scenario where the entanglement swapping happens at a heralding station placed on the receiving satellite. The loss will thus only affect one of the photons and the usual advantage of the single-click protocol of having a higher rate for long distances is thus not applicable in this scenario.

We now describe the steps of the entanglement generation in more detail. Fig. 4.2a) shows how individual atoms are trapped with optical tweezers inside macroscopic, near-concentric optical cavities [34, 35, 39]. Throughout this paper, we will focus on an implementation with Rubidium (Rb) atoms though other Alkali atoms such as Cesium could also be used. The closed optical transition between the $5S_{1/2}$,$|F = 2, m_F = 2\rangle$ ground state and the $5P_{3/2}$, $|F' = 3, m_{F'} = 3\rangle$ excited state in ^{87}Rb allows for spin-photon entanglement through pulsed excitation. For simplicity, we first describe this process for a single atom and then discuss how to perform the operation for a collection of atoms.

First, the atom is prepared in a superposition of the spin states,

$$|\phi\rangle = \frac{1}{\sqrt{2}}(|0\rangle + |1\rangle). \tag{4.1}$$

by means of standard optical pumping and two-photon Raman driving [40, 41]. We imagine that $|0\rangle = |F = 1, m_F = 1\rangle$ and $|1\rangle = |F = 2, m_F = 2\rangle$ in the $5^2S_{1/2}$ ground state manifold. Next, a short optical π-pulse is applied to induce the transition, $|1\rangle \rightarrow |ex\rangle$, where $|ex\rangle = |F' = 3, m'_F = 3\rangle$ in the excited $5^2P_{3/2}$ manifold. The excited state will subsequently decay back to $|1\rangle$ by emission of an early cavity photon, $|e\rangle$. Next, two-photon Raman driving is used to flip the population of the ground states i.e. $|0\rangle \leftrightarrow |1\rangle$ after which a second optical π-pulse is applied resulting in the emission of a late photon, $|l\rangle$ if the atom is in the $|1\rangle$ state. Ideally, this procedure results in the spin-photon entangled state

$$|\psi\rangle_{sp} = \frac{1}{\sqrt{2}}(|0\rangle|e\rangle + |1\rangle|l\rangle). \tag{4.2}$$

When performing this operation on a collection of atoms it is important to prevent that the emission from one atom interferes with another. To this end, we propose to operate in a sequential manner where all atoms

are initially prepared in the state $(|0\rangle + |1\rangle)/\sqrt{2}$ and then addressed sequentially with the optical π-pulse for generation of atom-photon entanglement. An additional laser at 1530 nm addressing the transition between the $5^2P_{3/2}$ and $4^2D_{3/2}$ excited manifolds is applied to all atoms except the one subject to the optical π pulse. Specifically, a π-polarized laser will couple the excited $|ex\rangle$ to the $|ex'\rangle = |F'' = 3, m_{F''} = 3\rangle$ hyper-fine level of the $4^2D_{3/2}$ manifold. This is done to effectively shift the $|1\rangle \leftrightarrow |ex\rangle$ transition out of resonance for the other atoms since the excited dressed states will be detuned from the cavity resonance by $\pm\hbar\Omega$, where Ω is the Rabi frequency of the laser-driven $|ex\rangle \leftrightarrow |ex'\rangle$ transition [42]. Having $\Omega \gg g\sqrt{N}$, where g is the single photon Rabi frequency of the cavity coupled $|1\rangle \leftrightarrow |ex\rangle$ transition ensures that there is effectively no coupling of the atoms to the cavity field. In this way, atom-photon entanglement can be attempted with each atom sequentially as described above.

The photons collected from the cavity are transmitted to either one of the ground stations or another satellite depending on the specific location of the satellite in the repeater chain. In both cases, a linear optics BSM is performed at the destination to herald atom-atom entanglement, as shown in Fig. 4.1b). The latter is carried out with a 50/50 beam splitter and single photon detectors following the scheme of Ref. [37]. If the BSM is successful, meaning we have measured an early and a late photon, we have accomplished entanglement in an elementary link, i.e. satellite-satellite or satellite-ground entanglement,

$$|\psi\rangle_{sp} \otimes |\psi\rangle_{sp} \xrightarrow{BSM} |\psi\rangle = \frac{1}{\sqrt{2}}(|01\rangle \pm |01\rangle). \tag{4.3}$$

The phase of the superposition is determined by which detectors record the photons. Since this information is known, it is possible to change the phase with local qubit operations, if necessary.

4.2.3. ENTANGLEMENT SWAP

Following the successful atom-atom entanglement generation of neighboring links in the setup, we carry out a SWAP between the entangled atoms of the different links. Previous satellite-based quantum repeater schemes have considered photonic Bell measurements similar to the entanglement generation step [16, 17, 20] to achieve this. However, the downside of performing a photonic BSM is that it has an intrinsic failure probability of 50%, which has a detrimental effect on the overall rate of the repeater. To circumvent this, we consider nearly-deterministic Bell measurement between pair of atoms through the Rydberg interaction. To do so, the atoms are spatially re-arranged. This can be performed on a timescale of milliseconds [34, 40], which is on the order of the communication time between segments for the parameters considered

below. This is different from the situation in the entanglement generation step where the typical time scale of the local operations is on the microsecond scale for typical experimental parameters [34, 35] and thus negligible compared to the communication time.

A Rydberg-mediated CZ gate between the two atoms [43–45] is assumed for the Bell measurement. Since the originally proposed schemes in Ref. [43], there have been a number of further developments to increase the performance of Rydberg-mediated two-atom gates [44, 45] leading to experimentally reported gate fidelities exceeding 99% [33]. To illustrate the basic idea of how the Rydberg-interaction allows for a two-atom controlled phase gate, we focus, however, on one of the original schemes of Ref. [43] illustrated in Fig. 4.2b) for simplicity. First, a π pulse is applied to the control atom which makes the transition $|1\rangle \rightarrow |r\rangle$, where $|r\rangle$ is a Rydberg state with a high principal quantum number ($n \approx 60$). Then, a 2π pulse is applied to the target atom. If the control atom is in state $|0\rangle$, this pulse will make the transition $|1\rangle \rightarrow |r\rangle \rightarrow -|1\rangle$ on the target atom. However, if the control atom is in the Rydberg state, the Rydberg interaction will shift the transition out of resonance such that the target atoms remain essentially unperturbed by the pulse. A final π pulse brings the population of the control atom back to $|1\rangle$ and concludes the gate. This operation amounts ideally to a controlled phase gate between the atoms, which is sufficient to perform a Bell state measurement.

To realize a Bell measurement, it is necessary to apply a Hadmard gate on the target atom before the CZ gate and a Hadamard gate on the control atom after the gate, which can be done with two-photon Raman driving [29, 41]. The qubit states are then measured by first driving the closed $|1\rangle \leftrightarrow |ex\rangle$ transition and collecting the emitted light which detects if the atom is in the $|1\rangle$ state. If no light is detected, the atom is either in the $|0\rangle$ state or it could have been lost from the trap. The latter can result from the re-arrangement step, the two-atom gate or simply from imperfect vacuum. To herald whether the atom was lost, a Raman drive is applied to bring the population from $|0\rangle$ to $|1\rangle$ followed by a second detection. If light is collected, the atom was in the $|0\rangle$ state while if no light was collected, the atom is assumed lost. We note that this means that the Bell measurement is in fact not deterministic since there is a non-zero probability that the atom was lost in which case the operation fails.

4.2.4. PERFORMANCE

To evaluate the performance of the repeater protocol we model a number of imperfections at both the quantum hardware level as well as in the optical transmission budget. Below, we describe these imperfections at a high level and refer to Appendix 4.4.1 and the supplemental

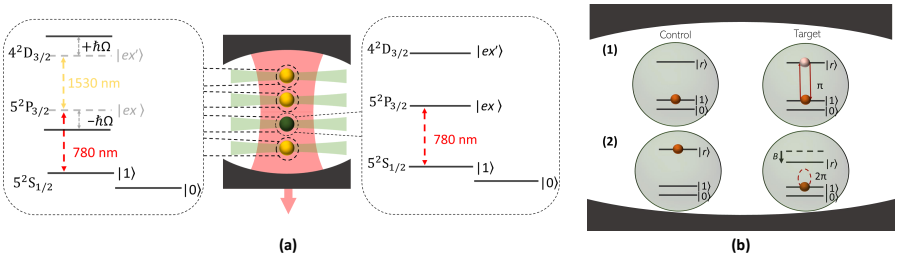

Figure 4.2: **Individually trapped atoms in a cavity as the main hardware. (a)** The quantum memories chosen are Rubidium (Rb) atoms in a cavity, which also work as emitters. With a laser resonant with the $|1\rangle \rightarrow |ex\rangle$ transition, the atom is excited to the $|ex\rangle$ state from which it will decay back to the $|1\rangle$ state with the emission of a photon. To selectively address only one atom in an entangling attempt, the other atoms are shifted out of resonance through strong driving of the $|ex\rangle \rightarrow |ex'\rangle$ transition. **(b)** Nearly deterministic BSM. After the elementary links are entangled a nearly deterministic Bell state measurement is carried out to distribute entanglement between Alice and Bob. The latter is performed by applying a CNOT gate between the atoms and a Hadamard gate in the control atom. To perform the 2-qubit gate, we exploit the well-known Rydberg blockade: The $|1\rangle \rightarrow |r\rangle$ transition of the target atom is resonant with our driving field if (1) the control atom is in state $|0\rangle$ but (2) shifted out of resonance by the Rydberg interaction if the control atom is in state $|r\rangle$.

material [46] for additional details of the modelling. At the quantum hardware level, we consider different imperfections in the entanglement generation, the quantum memories, and the entanglement swap.

Entanglement generation: In the generation of spin-photon entanglement, we consider undesired two-photon emissions and imperfect coupling to the cavity mode. After the entangled photon is sent from the emitter to the receiver, a probabilistic optical BSM is performed. The photons interfering may not be perfectly indistinguishable, which is accounted for by including a non-unity visibility. The efficiency of the detector and the coupling losses from free space to fiber are also included in the link budget (see below). Moreover, dark counts can generate a "click" in the detectors, despite no photon being transmitted, which we include with a non-zero dark count probability.

Quantum memories: The atom-atom entanglement will decohere over time due to dephasing of the spin state of the atoms. We model this as single qubit dephasing channels acting on each atomic qubit leading to an exponential decrease of coherence with time. Furthermore, the atoms can get lost from the traps due to imperfect vacuum, which we model as an erasure channel with an exponential decay of the qubit population with time.

Entanglement SWAP: After entanglement between neighboring links is successfully achieved, we carry out the atomic Bell measurements in all the satellites of the chain to enable entanglement swapping to the ground stations. To account for imperfections in the CZ-gate, we assume that the gate succeeds perfectly with some probability p_{swap} while with probability $1-p_{\text{swap}}$ the swap results in a 'garbage' state with zero fidelity with the desired Bell state. In addition, we also include a finite probability that the atoms participating in the Bell measurement are lost, which also destroys the entanglement but is an heralded error.

Optical link budget: We compute free space propagation losses assuming a fundamental Gaussian beam under transmitter pointing jitter. The latter is assumed to be described by a radially varying Rayleigh probability distribution function. Furthermore, in satellite-to-ground links, we include the atmospheric effects of Rayleigh scattering and beam widening due to turbulence. Finally, internal losses in the terminals, due to non-ideal operation of the optical elements (i.e. absorption in lenses and mirrors) are included.

In our simulations, we consider two different satellites. One has the characteristics of the Micius satellite [22], namely a telescope with 15 cm radius and 0.41 μrad pointing error. In addition, we consider an improved second satellite, with a 50-centimeter radius telescope. In both cases, the satellite orbit is at a height of 500 km from the surface of the Earth, the same as the Micius satellite, and both ground stations have a 60-centimeter radius telescope. We also assume the satellites to be in a 'string of pearls' configuration following an equatorial orbit.

The ground stations are assumed to be at a height of 2000 meters to avoid Mie scattering. Mie scattering is produced by particles of size comparable to the wavelength of light, mainly due to atmospheric aerosols. These particles are more abundant in the lower atmosphere and can be neglected for higher elevations [47].

As detailed in the supplemental material [46], we can derive an analytical estimate of the fidelity of final Bell pairs distributed between the ground stations taking into account all of the aforementioned errors and losses. In order to do this, we adopt a model where errors either lead to a completely dephased Bell state of the from $\rho_{\text{deph}} = (|01\rangle\langle 01| + |10\rangle\langle 10|)/2$ or end up in a non-specified 'garbage' state $|g\rangle$ with zero overlap with the desired target state $|\psi\rangle = (|01\rangle + |10\rangle)/\sqrt{2}$. In the entanglement generation, two-photon errors, memory dephasing and non-perfect optical visibility results in errors of the first type. We model the errors from dark counts as resulting in a garbage state as a worst case scenario. This allows us to express the density matrix describing the entangled pairs in the elementary links as $\rho_{\text{link}} = \alpha|\psi\rangle\langle\psi| + \beta\rho_{\text{deph}} + \gamma|g\rangle\langle g|$. The dependence of the coefficients α, β, and γ on the physical parameters such as two-photon emission probability, transmission loss, dark counts and memory coherence time are given in the supplemental material [46].

Finally, we model the imperfect entanglement swap at the repeater nodes as succeeding with probability p_{swap} resulting in an error free swap while with probability $1 - p_{\text{swap}}$, the swap results in a garbage state. This allows us obtain a compact expression of the final entangled state between the end-nodes of the repeater

$$\begin{aligned}\rho_{\text{AB}} &= p_{\text{swap}}^{n_{\text{sat}}}\left(A[n_{\text{sat}}]|\psi\rangle\langle\psi| + B[n_{\text{sat}}]\rho_{\text{deph}}\right) + C[n_{\text{sat}}]|g\rangle\langle g| \\ &\quad + \left(1 - p_{\text{swap}}^{n_{\text{sat}}}\right)(A[n_{\text{sat}}] + B[n_{\text{sat}}])\,|g\rangle\langle g|, \end{aligned} \tag{4.4}$$

where $p_{\text{swap}}^{n_{\text{sat}}}$ is the probability of no faulty entanglement swap operations across the chain of n_{sat} satellites. The coefficients $A[n_{\text{sat}}]$, $B[n_{\text{sat}}]$ and $C[n_{\text{sat}}]$ can straightforwardly be found from combining $(n_{\text{sat}} + 1)$ states of the form ρ_{link} (see supplemental material for details [46]). Note that, in general, the coefficients α, β, and γ will be different for each of the elementary links. From Eq. (5.25), it follows that the fidelity of the final state with the target Bell state is $F_{\text{AB}} = p_{\text{swap}}^{n_{\text{sat}}} \frac{A[n_{\text{sat}}]+B[n_{\text{sat}}]/2}{A[n_{\text{sat}}]+B[n_{\text{sat}}]+C[n_{\text{sat}}]}$.

For the computation of the rate, we assume that N_{mem} photons are transmitted in each elementary link entangling attempt using $2N_{\text{mem}}$ atoms per emitter satellite since each satellite covers two elementary links. In each attempt, we assume that the N_{mem} photons are emitted within a time assumed negligible compared to the communication time between the links, which is on the order of milliseconds. We therefore set the repetition time of the entangling attempt to match the longest communication time between links in the repeater chain.

After each attempt, the entanglement in a link is either swapped if the neighboring link is also successful or discarded before a new attempt is made. We choose this mode of operation because for quantum memories with second long coherence times, as considered in this work, the communication time between elementary links is too long to maintain high fidelity entanglement by storing successful links for multiple entanglement attempts. It is therefore desirable to have enough multiplexing to ensure near-deterministic entanglement generation in the elementary links [48].

To estimate the rate of the repeater, we first consider the probability of generating n Bell pairs in a single elementary link, which is simply

$$p_{(g,s)}(n) = \binom{N_{\text{mem}}}{n} p_{\text{link},(g,s)}^{n} (1 - p_{\text{link},(g,s)})^{N_{\text{mem}}-n} \tag{4.5}$$

where $p_{\text{link},(g,s)}$ is the success probability per photon for ground-satellite (g) or satellite-satellite links (s). This expression is valid in the regime where the optical transmission is limited by beam divergence rather than pointing errors since the latter can induce correlated errors, whereas the binomial distribution assumes uncorrelated loss.. We verify that this is the case for realistic pointing errors though Monte-Carlo simulations of the distribution of entangled pairs in an elementary link (see supplemental materials for details [46]). Since the number of entangled pairs between the ground stations will be limited by the link with the smallest number of successful pairs, we can express the probability of generating n entangled pairs between the ground stations, assuming deterministic swapping, as

$$\begin{aligned} p(n) \quad = \quad & \Big(\sum_{i=0}^{n_{\text{sat}}-1} \binom{n_{\text{sat}}-1}{i} p_s(n)^i p_s(>n)^{n_{\text{sat}}-(i+1)} \Big) \\ & \cdot \Big(\sum_{j=0}^{2} \binom{2}{j} p_g(n)^j p_g(>n)^{2-j} \Big) \\ & - p_s(>n)^{n_{\text{sat}}-1} p_g(>n)^2, \end{aligned} \tag{4.6}$$

where $p_{(g,s)}(>n) = \sum_{i=n+1}^{N_{\text{mem}}} p_{(g,s)}(i)$.

Since the entanglement swapping is only near-deterministic due to the possibility of atom loss, we need to include the probability of losing some of these pairs due to failed entanglement swaps. This modifies the probability for establishing n entangled pairs between the ground stations to

$$p_f(n) = \sum_{i=n}^{N_{\text{mem}}} \binom{i}{n} p(i) (1 - p_{\text{loss}})^n p_{\text{loss}}^{i-n}, \tag{4.7}$$

where p_{loss} is the probability to unsuccessfully combine the entangled pairs in the elementary links to achieve an entangled pair between the

ground stations due to loss of at least one atom in any of the elementary link pairs. The final average rate of the repeater is then estimated as

$$R = \frac{\sum_{i=1}^{N_{\text{mem}}} i p_f(i)}{T_{\text{com}}}, \tag{4.8}$$

where we have assumed that the repetition rate is set by T_{com} which is the longest, round-trip communication time between elementary links. Additional details about the calculation of the rate and fidelity can be found in the supplementary material where we provide detailed expressions for $p_{\text{link},(g,s)}$, p_{loss} and T_{com}.

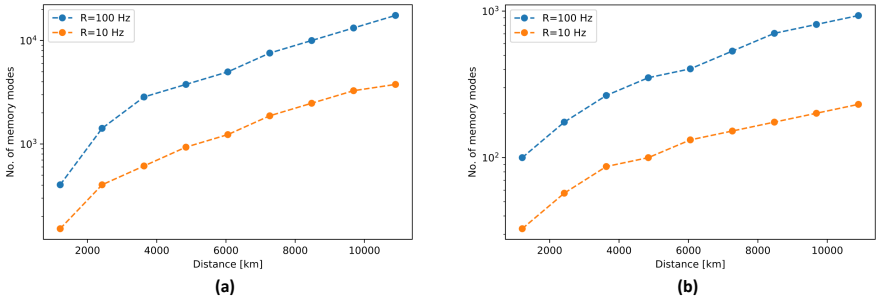

Figure 4.3: **Multiplexing capabilities required to reach a rate of 10Hz (orange) or 100Hz (blue) and a fidelity of 0.9 in the entanglement distribution protocol in a satellite chain of 5 satellites.** **(a)** Number of memory modes needed in a satellite with the characteristics of Micius, i.e. the same size of the telescope ($r = 0.15$ m), pointing error ($\sigma = 0.41$ μrad) and height ($h = 500$ km), as a function of the distance between ground stations. **(b)** Number of memory modes needed in a satellite with a bigger telescope radius than Micius ($r = 0.5$ m) as a function of the distance between ground stations.

Rather than using the rate analysis described above to estimate the achievable rate and fidelity for a fixed number of atoms, N_{mem}, we instead estimate the number of atoms needed to achieve a certain target rate and fidelity. We do this to get a sense of the multiplexing capabilities needed to reach fidelities above 90% compatible with secret key distillation [49] and rates above 10Hz (100 Hz) such that at least 10 (100) entangled pairs could be distributed within the second long memory time that we assume for the ground state memories. Since the satellites are moving in orbit, the rate is estimated as the average rate during the time-window where ground-satellite communication is

Parameters considered for the simulations		
Prob. of the emitter to emit a single photon	p_1	0.99
Prob. of the emitter to emit two photons	p_2	0.002
Collection efficiency	η_{coll}	0.49
Visibility of the photons	$\mathcal{V}$	0.999
Prob. of losing an atom in the SWAP	$p_{\text{loss,swap}}$	0.1
Effective loss time in satellite	$T_{\text{loss,sat}}$	0.01 s
Effective loss time in ground station	$T_{\text{loss,gstat}}$	1.5 s
Fidelity of the swap	p_{swap}	0.995
Dark detection probability	p_{dark}	10^{-6}
Decoherence time in satellite	$\tau_{\text{c,sat}}$	1.5 s
Decoherence time in ground station	$\tau_{\text{c,gstat}}$	10 s
Photon detection efficiency	η	0.98
Transmission probabilities in the elementary links		
Trans. prob. sat.-ground. ($r = 0.15$m)	$p_{\text{T,sat-ground}}$	0.14
Trans. prob. sat.-ground. ($r = 0.5$m)	$p_{\text{T,sat-ground}}$	0.33
Trans. prob. sat.-sat. ($r = 0.15$m)	$p_{\text{T,sat-sat}}$	0.052 - 0.0007
Trans. prob. sat.-sat. ($r = 0.5$m)	$p_{\text{T,sat-sat}}$	0.55-0.03

Table 4.1: Assumed values of the parameters in the model. The assumed values are compatible with current or near-term technology. The parameters that are different from the ones shown in this table are indicated in the figures. The collection efficiency is defined as $\eta_{\text{coll}} = p\eta_{\text{cav,coll}}$, where $p = 0.99$ is the probability of emitting in the cavity mode, and $\eta_{\text{cav,coll}} = 0.5$ is the collection efficiency from the cavity to free space. The effective loss coherence times depends on the quality of the vacuum in the atomic memories and is assumed to be higher for ground stations than on the satellites. The values of the transmission probability between satellites shown are the ones for the shortest distance between ground stations (~ 1300 km) and for the longest one(~ 12000km) to provide a sense of the relevant regime.

possible. This window is about 5 min for the satellite height of 500km considered here.

In Fig. 4.3 we plot the necessary number of memory modes per repeater node, to reach a certain rate of entanglement between the ground stations, in this case 10 Hz or 100 Hz, and a fidelity ≥ 0.9 of the final Bell pair as a function of distance assuming a chain of five satellites. The parameters considered in the simulation are shown in Table 4.1.

From the comparison of Figures 4.3 a) and b), it is seen that increasing the radius of the satellite mirrors relaxes the multiplexing requirements up to two orders of magnitude. While the Micius-like satellite requires more than 1000 memory modes to get a rate of 100 Hz for a distance of 3500km between ground stations, the upgraded satellite only requires ~ 200 memories. Additionally, the upgraded satellite only requires around 1000 memory modes to reach a rate of 100 Hz over distances ≥ 8000 km. This is an order of magnitude less than found in optical BSM architectures for similar satellite characteristics [16].

We chose to target a final fidelity of ≥ 0.9 since this allows for direct extraction of secure encryption keys through quantum key distribution [49]. If higher fidelity entanglement is required, this can, in principle be achieved through entanglement purification [50]. Increasing the rate from the targeted 10Hz or 100Hz can be achieved by increasing the amount of multiplexing. Increasing the number of memory modes in Fig 4.3 by a certain factor will result in roughly the same increase in rate.

As seen from table 4.1, quantum operations with %-error level is sufficient to reach a final fidelity ≥ 0.9. Lower error budgets in the quantum hardware will naturally increase the performance of the repeater. While errors at the 0.1% level are within reach of current neutral atom based hardware, entanglement purification techniques could also be employed to leverage the effect of non-perfect operations at the expense of a slower distribution rate.

4.3. CONCLUSION

In summary, we have proposed a satellite-assisted quantum repeater architecture based on individually trapped alkali atoms, which has several desirable features for functioning as quantum payloads. In particular, the ability to perform nearly deterministic BSMs with Rydberg-mediated two-qubit gates significantly lowers the amount of multiplexing needed to establish entanglement at continental distances compared to protocols based on probabilistic linear optics BSMs [16]. Additionally, the use of atoms as single photon sources circumvents the need for entangled photon sources and absorptive quantum memories.

We developed a simple but accurate analytical model of the repeater

architecture that allowed us to compute how expensive, in the sense of the number of memory modes per repeater station, it is to get high-fidelity entanglement at continental distances using the setup we propose. From this model, we estimated that a chain of 5 satellites with a 50-centimeter radius telescope, enables high-fidelity ($F \geq 0.9$) entanglement at a rate of 100 Hz with less than 200 atoms per repeater station at a range of 1500 km.

We believe that our model can be readily adapted to provide first-order estimates of the performance for other satellite-assisted quantum repeater architectures based on heralded entanglement generation and entanglement swapping also with different quantum hardware. This is due to the characterization of the effect of the physical errors into simple lower-bound estimates of the fidelity of the final state. Notably our model allows for easy and fast simulation of long quantum repeater chains in contrast to Monte Carlo-based simulations [18] where the computational overhead increases rapidly with the length of the repeater chain.

In addition to the promise of long-distance entanglement distribution, satellite-assisted quantum repeaters also open up new tools for more fundamental tests of nature. In particular, the atomic hardware considered here opens up new opportunities for quantum-enhanced sensor networks relevant for searches for topological dark matter [51], global time-keeping [4], and tests of the interplay between gravity and quantum mechanics [52].

4.4. APPENDIX

4.4.1. MODELLING OF ERRORS

In this appendix, we provide more details on our model of hardware imperfections and transmission loss in the satellite repeater chain. Specifically, we describe how we model two-photon emission errors, dark counts, quantum memory dephasing, and atom loss. Finally, we describe our model of the optical transmission including beam divergence, pointing jitter, and atmospheric absorption. Additional details can be found in the supplementary material [46].

In the first step of the protocol, for establishing entanglement between the spin of the emitter and the photon, we take into account two-photon emissions and that the photons may not be emitted into the cavity mode. The collected photons are sent to the closest satellite or to the ground station for the spin-spin entanglement generation. The photons will reach their destination with probability p_T, computed using the optical link budget explained later in this section. These free space and atmospheric losses are modelled as a fictitious beam splitter with transmission p_T. The transmission of a single photon is modelled as

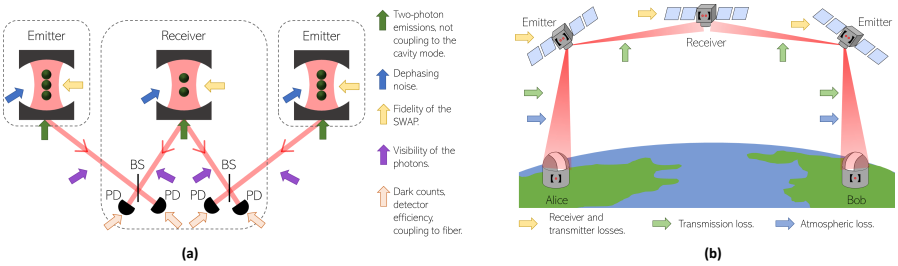

Figure 4.4: **Errors considered in the protocol.** **(a)** Schematic representation of the quantum setup used and possible errors that can happen. Two-photon emissions and imperfect coupling to the cavity mode are taken into account when modelling the atom-photon entanglement generation. Dark counts, detector efficiency and coupling to the fiber are included as imperfections in the Bell state measurements carried out in the receivers. Non-perfect visibility of the photons involved in the Bell state measurement is also included. Finally, we include dephasing of the atoms and imperfections of the SWAP operation. **(b)** Schematic representation of the transmission losses. In the satellite-satellite link, we take into account transmission losses due to the propagation of the Gaussian beam and the pointing jitter of the emitter. In the satellite-ground station link, we also consider the effect of the atmosphere, i.e. the Rayleigh scattering due to molecules. Additionally, losses originated in the terminals are also added to the model.

follows:

$$\hat{a}^{\dagger}_{\mathrm{ph}}|0\rangle_{\mathrm{ph}}|0\rangle_{\mathrm{E}} \rightarrow \sqrt{p_{\mathrm{T}}}\hat{a}^{\dagger}_{\mathrm{ph}}|0\rangle_{\mathrm{ph}}|0\rangle_{\mathrm{E}} + \sqrt{1-p_{\mathrm{T}}}\hat{a}^{\dagger}_{\mathrm{E}}|0\rangle_{ph}|0\rangle_{\mathrm{E}}, \tag{4.9}$$

where $\hat{a}^{\dagger}_{\mathrm{ph}}$ is the creation operator for the collected mode while $\hat{a}^{\dagger}_{\mathrm{E}}$ is the creation of a non-collected (environment) photon. Once the photon reaches the receiver, a photonic Bell state measurement is performed between the emitted photon and a photon emitted from an atom in the receiver system. The two photons may not be perfectly indistinguishable and the efficiency of the single photon detectors and the coupling from free space to fiber is not perfect. These factors are added to the model as the visibility of the photons, the detector and the coupling efficiency. Moreover, dark counts can generate a "click" in the detectors, when there is no photon to measure, which is considered in the dark count probability. The photonic Bell state measurement is modelled as a 50/50 beam splitter where just single photon emissions are considered indistinguishable leading to interference terms. In other words, we do not consider interference between photons from two-photon emissions since these will likely be emitted with very different temporal envelopes resulting in negligible interference effects. As a result of the above imperfections, the final atom-atom entangled states are captured by probabilistic mixtures of the ideal Bell state, a dephased state, and a non-specified garbage state with fidelity zero (which includes e.g. the $|00\rangle$ and $|11\rangle$ states) as specified in the supplemental material [46].

The entanglement is "stored" in the hyperfine spin of the Rubidium atoms but decoheres with time. We model this as a dephasing channel, where the coherence (off-diagonal terms of the density matrix) decayes exponentially with time as $\exp(-t/\tau_c)$, where τ_c is the coherence time of the atoms (assumed different for ground and satellites as detailed in Tab. 4.1). In addition, we assume that the atoms can get lost due to imperfect vacuum. We model this by assuming that with probability $\exp(-t/T_{\mathrm{loss}})$ an atom is lost after a time t, where T_{loss} is an effective loss time (also assumed different for satellite and ground).

After entanglement between elementary links is successfully achieved, we carry out the SWAP in all the satellites of the chain. To do so, the tweezers move the atoms that have established entanglement with their counterparts at the end of their respective elementary links to the top positions of the cavity, such that we know where the successfully entangled atoms are. The imperfections of the entanglement swap are modelled as described in the main text.

As shown in Fig. 4.4b), we include a number of imperfections and loss for the optical link budget. The free space propagation losses are computed considering a fundamental Gaussian beam under transmitter pointing jitter. The latter is assumed to be described by a radially varying Rayleigh probability distribution function, which is the result of the combination of centered Gaussian probability density functions

in both the vertical and the horizontal directions. The joint Gaussian probability density function of the pointing jitter is given by

$$f(x_0, y_0; \sigma) = \frac{1}{2\pi\sigma^2} \exp\left(-\frac{x_0^2 + y_0^2}{2\sigma^2}\right) \tag{4.10}$$

where x_0 and y_0 are the coordinates of the pointing error in the receiver's aperture plane and σ is the pointing jitter's standard deviation for both directions. The effect of pointing errors is that the center of the Gaussian beam profile is not aligned with the center of the receiver. In the regime where the width σ, of the pointing jitter is small compared to the beam waist at the receiver, w, the effect of pointing jitter will be small and the transmission will be dominated by beam divergence. This allows us to use the binomial distribution approximation of the number of success full pairs in an elementary link used in our model (see Eq. (4.5)) using the average transmission probability wrt. to the pointing jitter. From numerical Monte-Carlo simulations, we find that for $w/\sigma \geq 10$, the binomial distribution approximation is good (see the supplemental material for further details [46]). For realistic pointing errors and beam focusing characteristics [53], this requirement is fulfilled [46]. In satellite-to-ground links, the atmospheric effects have been included in the model using simulated atmospheric transmission from Ref. [54] and assuming that beam wandering is dominated by transmitter pointing jitter.

4.5. SUPPLEMENTARY MATERIAL

In this supplemental material we present the details of the quantum repeater model discussed in the main text. We start by discussing the different steps at the hardware level, detailing the modelling of errors that can happen in the spin-photon entanglement generation, the transmission loss between elementary links, imperfections in the optical Bell state measurement, imperfect quantum memories, and errors in the atomic entanglement swap operation. Finally, we present the details of the optical link budget including modelling of beam divergence, pointing jitter, and atmospheric effects.

4.5.1. QUANTUM HARDWARE MODELLING

SPIN-PHOTON ENTANGLEMENT

Here we consider imperfections in the spin-photon entanglement generation. Two-photon emissions and imperfect coupling to the cavity mode are captured by considering the following type of state:

$$\rho_{\text{emit}} = \alpha_e |\psi\rangle\langle\psi| + \beta_e |\psi_{\text{multi}}\rangle\langle\psi_{\text{multi}}| + \eta_e \rho_{\text{deph1}} + \gamma_e \rho_{\text{deph2}}, \tag{4.11}$$

where $|\psi\rangle = \frac{1}{\sqrt{2}}\left(|0\rangle|e\rangle_{\text{ph}} + |1\rangle_{\text{ph}}|l\rangle\right)$ is the desired state, which we obtain with probability α_{e}. Here $|0\rangle/|1\rangle$ are the qubit states of the atom while $|e\rangle_{\text{ph}}/|l\rangle_{\text{ph}}$ denotes an early/late collected photon. The state $|\psi_{\text{multi}}\rangle = \frac{1}{\sqrt{2}}\left(|0\rangle|2e\rangle_{\text{ph}} + \ +|1\rangle|2l\rangle_{\text{ph}}\right)$ represents undesirable two-photon emissions where both photons are collected, which we obtain with probability β_{e}. We neglect any coherence between the state $|\psi\rangle$ and $|\psi_{\text{multi}}\rangle$ for simplicity since it will have a negligible effect in the later parts of the protocol, as detailed below. The dephased states $\rho_{\text{deph,1}}$ and $\rho_{\text{deph,2}}$ represents the loss of one (or multiple) photon(s) to the environment (e.g. through emission into non-collected modes/spontaneous emission), which leaks information about the spin state. Specifically, we define $\rho_{\text{deph,1}} = (|0\rangle\langle 0|\otimes|e\rangle_{\text{ph}}\langle e| + |1\rangle\langle 1|\otimes|l\rangle_{\text{ph}}\langle l|)/2$ and $\rho_{\text{deph,2}} = (|0\rangle\langle 0| + |1\rangle\langle 1|) \otimes |0\rangle_{\text{ph}}\langle 0|)/2$. The probability of getting a dephased state with a photon in the collected mode is thus η_{e} while the probability to have a dephased state with zero photons collected is γ_{e}. We estimate the probabilities above as

$$\alpha_{\text{e}} = p_1\eta_{\text{coll}}, \tag{4.12}$$
$$\beta_{\text{e}} = \eta_{\text{coll}}^2 p_2, \tag{4.13}$$
$$\gamma_{\text{e}} = p_1(1-\eta_{\text{coll}}) + (1-\eta_{\text{coll}})^2 p_2 + p_0, \tag{4.14}$$
$$\eta_{\text{e}} = 2p_2\eta_{\text{coll}}(1-\eta_{\text{coll}}) \tag{4.15}$$
$$\tag{4.16}$$

where $\eta_{\text{coll}} = p\eta_{\text{cav,coll}}$ is the total collection efficiency, where we take into account the collection efficiency of the cavity, $\eta_{\text{cav,coll}}$; and the probability of emitting in the cavity mode, p. The probability of emitting a single photon is p_1, and p_2 is the probability of two-photon emissions. As a final note, p_0 is the probability of not emitting any photon at all, which we have assumed results in a dephased state.

FREE SPACE TRANSMISSION

The free space and atmospheric loss is modelled as a fictitious beam splitter with transmission p_{T} determined from the optical link budget (See Section 4.5.3). The transmission of a single photon state is thus modelled as

$$\hat{a}^\dagger_{\text{ph}}|0\rangle_{\text{ph}}|0\rangle_{\text{E}} \rightarrow \sqrt{p_{\text{T}}}\hat{a}^\dagger_{\text{ph}}|0\rangle_{\text{E}} + \sqrt{1-p_{\text{T}}}\hat{a}^\dagger_{\text{E}}|0\rangle_{\text{ph}}|0\rangle_{\text{E}}, \tag{4.17}$$

where subscript 'E' denotes the loss mode. So, for example, for the state $|\psi\rangle$ we will have that either the state is transmitted with probability p_{T}, or that the photon is lost with probability $1-p_{\text{T}}$ and the atom is left in a dephased state $\rho_{\text{deph,2}}$. The state that reaches the receiver after being transmitted from the emitter is the following:

$$\rho_{\text{trans}} = \alpha_t|\psi\rangle\langle\psi| + \beta_t|\psi_{\text{multi}}\rangle\langle\psi_{\text{multi}}| + \eta_t\rho_{\text{deph},1} + \gamma_t\rho_{\text{deph},2}, \tag{4.18}$$

with:

$$\begin{aligned}
\alpha_t &= p_T p_1 \eta_{\text{coll}}, && (4.19)\\
\beta_t &= \eta_{\text{coll}}^2 p_T^2 p_2, && (4.20)\\
\gamma_t &= (1-p_T)p_1\eta_{\text{coll}} + p_1(1-\eta_{\text{coll}}) + (1-p_T)^2\eta_{\text{coll}}^2 p_2 \\
&\quad + 2p_2\eta_{\text{coll}}(1-\eta_{\text{coll}})(1-p_T) + (1-\eta_{\text{coll}})^2 p_2, && (4.21)\\
\eta_t &= 2\eta_{\text{coll}}^2 p_2 p_T(1-p_T) + 2p_2\eta_{\text{coll}}(1-\eta_{\text{coll}})p_T. && (4.22)
\end{aligned}$$

4

PHOTONIC BELL MEASUREMENT

Once the photons from the emitter and from the receiver meet at the receiver station, a Bell state measurement is performed between them to obtain atom-atom entanglement across the elementary links. For the photon generated at the receiver station, we assume negligible transmission loss but imperfect collection from the cavity. The BSM is performed with a 50/50 beam splitter, and we assume that photonic interference only occurs for the case where the two input states are of the form $|\psi\rangle$ i.e. that there is no photonic interference for the error terms in Eq. (4.18) which has a photonic component. This is justified by the fact that those error terms originates from cases where two photons were initially emitted from an atom. The probability that those two photons are emitted in the exact same mode (e.g. with the same temporal envelope) is limited and hence we do not expect strong interference between them.

We assume that the beam splitter transformations is of the following form:

$$|e\rangle_1 \to \frac{1}{\sqrt{2}}(|e\rangle_3 + |e\rangle_4) \quad ; \quad |e\rangle_2 \to \frac{1}{\sqrt{2}}(|e\rangle_3 - |e\rangle_4) \tag{4.23}$$

$$|l\rangle_1 \to \frac{1}{\sqrt{2}}(|l\rangle_2 + |l\rangle_3) \quad ; \quad |l\rangle_2 \to \frac{1}{\sqrt{2}}(|l\rangle_3 - |l\rangle_4). \tag{4.24}$$

In the case of input state $|\psi\rangle \otimes |\psi\rangle$, the output state of the beam splitter is:

$$\begin{aligned}
|\psi\rangle_1 \otimes |\psi\rangle_2 \to \frac{1}{2}\Bigg(&\frac{1}{\sqrt{2}}(|el\rangle_3|0\rangle_4 - |0\rangle_3|el\rangle_4)\frac{1}{\sqrt{2}}(|01\rangle + |10\rangle)|0\rangle_E \\
&+ \frac{1}{\sqrt{2}}(|l\rangle_3|e\rangle_4 - |e\rangle_3|l\rangle_4)\frac{1}{\sqrt{2}}(|01\rangle - |10\rangle)|0\rangle_E\Bigg) \\
+\frac{1}{2}\Bigg(&|00\rangle\frac{1}{\sqrt{2}}(|ee\rangle_3|0\rangle_4 - |0\rangle_3|ee\rangle_4) + |11\rangle\frac{1}{\sqrt{2}}(|ll\rangle_3|0\rangle_4 - |0\rangle_3|ll\rangle_4)\Bigg).
\end{aligned} \tag{4.25}$$

Post-selecting on detecting an early and a late photon, we will project the atoms into an entangled state of the form $|\psi\rangle = \frac{1}{\sqrt{2}}(|01\rangle \pm |10\rangle)$. The sign of the superposition depends on which detectors recorded the photons and can always be corrected by a local atomic unitary if desired. The probability of this successful projection is 1/2 from the expression above.

We assume that the rest of the possible combinations between input states do not result in photonic interference as explained above. Thus, for example, if the input states are $|\psi_{\text{multi}}\rangle \otimes |\psi_{\text{multi}}\rangle$, the beam splitter transformations are assumed to be:

$$|2e\rangle_1 \rightarrow \frac{1}{2\sqrt{2}}\left((b_{e3}^\dagger)^2 + 2\left(b_{e3}^\dagger b_{e4}^\dagger\right) + (b_{e4}^\dagger)^2\right)|0\rangle_3|0\rangle_4, \tag{4.26}$$

$$|2e\rangle_2 \rightarrow \frac{1}{2\sqrt{2}}\left((d_{e3}^\dagger)^2 + 2\left(d_{e3}^\dagger d_{e4}^\dagger\right) + (d_{e4}^\dagger)^2\right)|0\rangle_3|0\rangle_4, \tag{4.27}$$

where $b^\dagger$ and $d^\dagger$ are orthogonal creation operators. The resulting output state is then:

$$\begin{aligned}|\psi_{\text{multi}}\rangle \otimes |\psi_{\text{multi}}\rangle \rightarrow\ & \frac{1}{8}(|01\rangle(|2b_e2d_l\rangle_3|0\rangle_4 + |2b_e\rangle_3|2d_l\rangle_4 + |2d_l\rangle_3|2b_e\rangle_4 + \\ & |0\rangle_3|2b_e2d_l\rangle_4) + |10\rangle(|2b_l2d_e\rangle_3|0\rangle_4 + |2b_l\rangle_3|2d_e\rangle_4 + \\ & |2d_e\rangle_3|2b_l\rangle_4 + |0\rangle_3|2b_l2d_e\rangle_4)) + \frac{1}{8}(|00\rangle(|2b_e2d_e\rangle_3|0\rangle_4 + \\ & |0\rangle_3|2b_e2d_3\rangle_4) + |11\rangle(|2b_l2d_l\rangle_3|0\rangle_4 + \\ & |0\rangle_3|2b_l2d_l\rangle_4))\end{aligned} \tag{4.28}$$

Therefore, with probability 1/2, we will project either into state $|01\rangle$ or $|10\rangle$ by heralding on an early and late detection.

So far, we have neglected the effect of dark counts in the detectors. A dark count is when a detector clicks for a vacuum input. The probability of this happening is p_{dark} i.e. a detector will click when receiving vacuum input with probability p_{dark}. In principle, dark counts could affect the outcome of the Bell measurements when the incident fields contain the desired number of photons as considered above. However, since $p_{\text{dark}} \ll 1$ for realistic detectors and the probability of receiving two photons is also very small, we can neglect higher order terms such as the cases where we receive two photons and have a dark counts. Consequently, dark counts will have a negligible effect for the cases where two (or more) photons arrive at the receiver station. However, we do need to include the effect of dark counts for terms with only one or no photons arriving at the receiver station. This amounts to the combinations $\{|\psi\rangle\langle\psi|, \rho_{\text{deph},2}\}$, $\{\rho_{\text{deph},1}, \rho_{\text{deph},2}\}$, and $\{\rho_{\text{deph},2}, \rho_{\text{deph},2}\}$. For the two first combinations the probability of a (false) success due to

dark counts will be p_{dark} to lowest order and for the third combination, it will be p_{dark}^2. For all combinations, the resulting state of the atoms will be an equal mixture of the states $|01\rangle, |10\rangle, |00\rangle$, and $|11\rangle$.

Collecting all possible combinations of input states, the state after the beam splitter is the following:

$$\alpha_{\text{BS}}\mathcal{V}|\psi\rangle\langle\psi| + (\beta_{\text{BS}} + \alpha_{\text{BS}}(1-\mathcal{V}))\,\rho_{\text{deph}} + \gamma_{\text{BS}}|g\rangle\langle g|, \tag{4.29}$$

where we have defined $|g\rangle\langle g|$ as a garbage state which contains all terms of the form $|00\rangle, |11\rangle$ and $\rho_{\text{deph}} = |01\rangle\langle 10| + |10\rangle\langle 01|$. We have also introduced the visibility, $\mathcal{V}$ of the photons which accounts for the photons not being perfectly indistinguishable even for the input state $|\psi\rangle \otimes |\psi\rangle$. If the visibility is 0, we will have a dephased state, if it is 1, we will have a Bell state. The coefficients above are given by:

$$\alpha_{\text{BS}} = \eta^2\alpha_{\text{t}}\alpha_{\text{e}}/2, \tag{4.30}$$

$$\begin{aligned}\beta_{\text{BS}} = {} & 1/2\,(p_{\text{dark}}(1-\eta)(\eta(\alpha_{\text{t}}\gamma_{\text{e}} + \gamma_{\text{t}}\alpha_{\text{e}} + \gamma_{\text{t}}\eta_{\text{e}} + \eta_{\text{t}}\gamma_{\text{e}}) + p_{\text{dark}}(1-\eta)\gamma_{\text{t}}\gamma_{\text{e}}) + \\ & + \eta^2(\alpha_{\text{t}}\eta_{\text{e}} + \eta_{\text{t}}\alpha_{\text{e}} + \eta_{\text{t}}\eta_{\text{e}})) + \eta^2/4\,(\alpha_{\text{t}}\beta_{\text{e}} + \beta_{\text{t}}\alpha_{\text{e}} + \eta_{\text{t}}\beta_{\text{e}} + \beta_{\text{t}}\eta_{\text{e}}) + \\ & \eta^2\beta_{\text{t}}\beta_{\text{e}}/8,\end{aligned} \tag{4.31}$$

$$\begin{aligned}\gamma_{\text{BS}} = {} & (1-\eta)p_{\text{dark}}\,(1/2\,(\eta(\alpha_{\text{t}}\gamma_{\text{e}} + \gamma_{\text{t}}\alpha_{\text{e}} + \gamma_{\text{t}}\eta_{\text{e}} + \eta_{\text{t}}\gamma_{\text{e}}) + \\ & (1-\eta)p_{\text{dark}}\gamma_{\text{t}}\gamma_{\text{e}})),\end{aligned} \tag{4.32}$$

where η is the single photon detection efficiency. Note that the state in Eq. (4.29) is not normalized. The normalization constant corresponds to the probability of success i.e. that an early and late click is recorded.

QUANTUM MEMORIES

We consider the limited coherence time of the quantum memories to be captured by a general Pauli noise channel. Thus the decoherence of an atomic Bell pair is captured by the noise channel:

$$\begin{aligned}\Delta(\rho) = {} & p_{\text{c1}}p_{\text{c2}}\rho + [(1-p_{\text{c1}})p_{\text{c2}} \\ & \sum_{i=\{x,y,z,0\}} \epsilon_i\,(\sigma_i \otimes \mathbb{I})\,\rho\,(\sigma_i \otimes \mathbb{I}) + p_{\text{c1}}(1-p_{\text{c2}}) \sum_{j=\{x,y,z,0\}} \epsilon_j\left(\mathbb{I} \otimes \sigma_j\right)\rho\left(\mathbb{I} \otimes \sigma_j\right) \\ & +(1-p_{\text{c1}})(1-p_{\text{c2}}) \sum_{i,j=\{x,y,z,0\}} \left(\epsilon_i\epsilon_j\left(\sigma_i \otimes \sigma_j\right)\rho\left(\sigma_i \otimes \sigma_j\right)\right)\Bigg],\end{aligned} \tag{4.33}$$

where $\sigma_x, \sigma_y, \sigma_z$ are the Pauli matrices and σ_0 is the identity matrix; and $p_{\text{c1,2}} = e^{-t/\tau_{\text{c,i}}}$ where $\tau_{\text{c},i}$ is the coherence time of the atoms. In our simulations, we assumed the dominant noise to be pure dephasing such that $\epsilon_x = \epsilon_y = 0$ and $\epsilon_z = \epsilon_0 = 1/2$. Additionally, we also consider the possibility that atoms are lost due to imperfect vacuum. This is

expressed as an erasure channel with an effective decoherence time, T_{loss} such that the probability of losing an atom is:

$$p_{\text{loss,vac}} = 1 - e^{-t/T_{\text{loss}}}, \tag{4.34}$$

where t is the time the atom stays in the trap. The loss of an atom is, however, ultimately detected once the atom is measured and we therefore consider it to be a heralded error that does not affect the fidelity of the final pair but only the distribution rate.

Note that quantum states are stored for different amounts of time, depending on whether the memories are in a ground station, an end-satellite or a emitter/receiver satellite between the two end-sattelites. The memories at the end-satellites need to store the quantum states for the time it takes to receive an heralding signal from both the ground station and the neighboring satellite and to subsequently perform an entanglement swap operation. This time is $\max\{2L_{sat-sat}/c, 2L_{sat-ground}/c\}+T_{\text{swap}}$, where c is the speed of light and $L_{sat-sat}$ is the satellite-satellite distance and $L_{sat-ground}$ is the distance between the specific end-satellite and its corresponding ground station. The memories at the emitter satellites between the two end-satellites have to store the quantum states for a time $2L_{sat-sat}/c+T_{swap}$, while the memories at the receiver satellites only have to store the quantum states for the time of the entanglement swap T_{swap}. Finally, the memories at the ground stations have to store the quantum states for long enough that they can receive signals from all satellites about which pairs where successfully swapped. Therefore, the required storage time will be $\max\{2L_{sat-sat}/c-L_{sat-ground}/c, L_{sat-ground}/c\}+L_{ground-endsat}/c+T_{\text{swap}}$, where $L_{ground-endsat}$ is the distance between the ground station and the end-satellite at the opposite end of the repeater.

Including the effect of the decoherence of the atomic memories on the stored Bell pairs in the elementary links updates Eq. (4.29) to:

$$\alpha|\psi\rangle\langle\psi| + \beta\rho_{\text{deph}} + \gamma|g\rangle\langle g|, \tag{4.35}$$

where:

$$\begin{aligned}
\alpha &= p_{\text{b}}\mathcal{V}\alpha_{\text{BS}}, && (4.36)\\
\beta &= p_{\text{deph}}\left(\beta_{\text{BS}} + \alpha_{\text{BS}}(1-\mathcal{V})\right), && (4.37)\\
\gamma &= ((1-p_{\text{b}})\mathcal{V}\alpha_{\text{BS}} + (1-p_{\text{deph}})\left(\beta_{\text{BS}} + \alpha_{\text{BS}}(1-\mathcal{V})\right) + \gamma_{\text{BS}}, && (4.38)
\end{aligned}$$

and where the probabilities for a general Pauli noise channel are:

$$\begin{aligned}
p_{\text{b}} &= p_1p_2 + (1-p_1)(1-p_2)\left(\epsilon_x^2+\epsilon_y^2+\epsilon_z^2+\epsilon_0^2\right) + \\
&\quad (p_1(1-p_2)+p_2(1-p_1))\,\epsilon_0, && (4.39)\\
p_{\text{deph}} &= p_1p_2 + ((p_1(1-p_2)+p_2(1-p_1))\,(\epsilon_z+\epsilon_0) + \\
&\quad (1-p_1)(1-p_2)\left(\epsilon_x^2+\epsilon_y^2+\epsilon_z^2+\epsilon_0^2\right)\Big). && (4.40)
\end{aligned}$$

Since we assume dephasing noise as the dominant decoherence error in our setup, we put $\epsilon_z = \epsilon_0 = 1/2$ and $\epsilon_x = \epsilon_y = 0$. As we will discuss later, atomic loss can be treated as an overall probability of losing an end-to-end entangled pair.

SWAP

A high-level sketch of the swap operation is shown in Fig. 4.5. Prior to the swap operation, the (entangled) states of the elementary links are of the following form:

$$\alpha|\psi\rangle\langle\psi| + \beta\rho_{\text{deph}} + \gamma|g\rangle\langle g|, \tag{4.41}$$

where α, β and γ are given in Eqs. (4.36), (4.37) and (4.38) respectively. The input state of the first swap is:

$$\begin{aligned}&\left(\alpha_0|\psi\rangle\langle\psi| + \beta_0\rho_{\text{deph}} + \gamma_0|g\rangle\langle g|\right)_{12} \otimes \\ &\left(\alpha_1|\psi\rangle\langle\psi| + \beta_1\rho_{\text{deph}} + \gamma_1|g\rangle\langle g|\right)_{34},\end{aligned} \tag{4.42}$$

which is followed by a CNOT gate on qubits 2-3, a Hadamard gate on qubit 2, and the measurement of both qubits. In this expression, we have included a sub-index on the coefficients $\{\alpha, \beta, \gamma\}$ since the states of the elementary links can in general be different due to e.g. different transmission probabilities. As a final note, we can lose an atom as a result of a gate operation. This loss is heralded in the measurement of the swap, and therefore not considered in the computation of the fidelity. However, it does affect the rate of entanglement and we assign a probability $p_{\text{loss,swap}}$ of losing an atom in the SWAP operation.

For the measurement of the spins, we use the states we considered for the generation of spin-photon entanglement, i.e. $|0\rangle = |\text{F} = 1, \text{m}_\text{F} = 1\rangle, |1\rangle = |\text{F} = 2, \text{m}_\text{F} = 2\rangle$ and $|ex\rangle = |\text{F} = 3, \text{m}_\text{F} = 3\rangle$, as there is a closed optical transition between $|1\rangle \rightarrow |ex\rangle$. Driving this transition, we can collect emitted photons to determine if the atom is in state $|1\rangle$. If no photons are detected, a π pulse between the $|0\rangle$ and $|1\rangle$ states is applied. The optical transition is then driven again which should lead to the detection of photons unless the atom was lost. In this way, we can detect the state of the atom as well as determine if the atom was lost or not.

After a successful (i.e. no atom loss detected) swap operation the swapped state will be of the form

$$A[1]|\psi\rangle\langle\psi| + B[1]\rho_{\text{deph}} + C[1]|g\rangle\langle g|, \tag{4.43}$$

where:

$$A[1] = \alpha_0\alpha_1, \tag{4.44}$$

$$B[1] = \beta_0(\alpha_1 + \beta_1) + \alpha_0\beta_1, \tag{4.45}$$

$$C[1] = \gamma_0(\alpha_1 + \beta_1) + \gamma_1(\alpha_0 + \beta_0) + p_2\gamma_0\gamma_1. \tag{4.46}$$

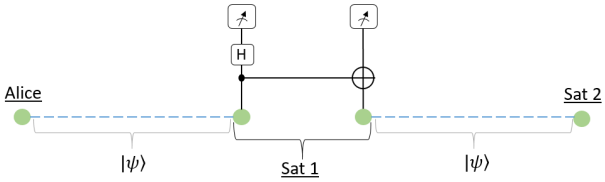

Figure 4.5: Deterministic swap. We have established entanglement between Alice and Satellite 1, and Satellite 1 and Satellite 2. To have entanglement between Alice and Satellite 2, we carry out a nearly deterministic SWAP, which is a CNOT gate between the two atoms at Satellite 1 which have established entanglement successfully between Alice and Satellite 2 respectively. After the CNOT, a Hadarmad gate (H) is performed in the control qubit, and, as a final step, both qubits are measured.

The state after performing n entanglement swaps is described by the recursive expressions:

$$A[n] = A[n-1]\alpha_n, \tag{4.47}$$

$$B[n] = A[n-1]\beta_n + B[n-1](\alpha_n + \beta_n), \tag{4.48}$$

$$C[n] = \gamma_n(A[n-1] + B[n-1]) + \\ +C[n-1](\alpha_n + \beta_n + p_2\gamma_n). \tag{4.49}$$

Lastly, we also consider the fidelity of the swap operation. We assume that with probability, p_{swap}, the swap operation is pefect while with probability $1-p_{\text{swap}}$, the resulting state is a garbage state, which amounts to a lower bound on the fidelity of the swapped state. Thus, after n_{sat} swaps (the number of swaps is equal to the number of satellites), the end-to-end entangled pair will be of the form

$$\rho_{\text{AB}} = p_{\text{swap}}^{n_{\text{sat}}}\left(A[n_{\text{sat}}]|\psi\rangle\langle\psi| + B[n_{\text{sat}}]\rho_{\text{deph}}\right) + \\ \left(\left(1-p_{\text{swap}}^{n_{\text{sat}}}\right)(A[n_{\text{sat}}] + B[n_{\text{sat}}]) + C[n_{\text{sat}}]\right)|g\rangle\langle g|, \tag{4.50}$$

The fidelity conditioned on not losing any of the atoms is then:

$$F_{\text{AB}} = \frac{\langle\psi|\rho_{\text{AB}}|\psi\rangle}{Tr(\rho_{\text{AB}})} = p_{\text{swap}}^{n_{\text{sat}}}\frac{A[n_{\text{sat}}] + B[n_{\text{sat}}]/2}{A[n_{\text{sat}}] + B[n_{\text{sat}}] + C[n_{\text{sat}}]}. \tag{4.51}$$

4.5.2. RATE

As discussed in the main paper, the average rate of the repeater is estimated as

$$R = \frac{\sum_{i=1}^{N_{\text{mem}}} i p_f(i)}{T_{\text{com}}}, \tag{4.52}$$

where T_{com} which is the longest communication time between elementary links and

$$p_f(n) = \sum_{i=n}^{N_{\text{mem}}} \binom{i}{n} p(i)(1-p_{\text{loss}})^n p_{\text{loss}}^{i-n}, \tag{4.53}$$

$$\begin{aligned} p(n) = & \Big(\sum_{i=0}^{n_{\text{sat}}-1} \binom{n_{\text{sat}}-1}{i} p_s(n)^i p_s(>n)^{n_{\text{sat}}-(i+1)}\Big) \cdot \\ & \Big(\sum_{j=0}^{2} \binom{2}{j} p_g(n)^j p_g(>n)^{2-j}\Big) + \\ & - p_s(>n)^{n_{\text{sat}}-1} p_g(>n)^2, \end{aligned} \tag{4.54}$$

$$p_{(g,s)}(n) = \binom{N_{\text{mem}}}{n} p_{\text{link},(g,s)}^n (1-p_{\text{link},(g,s)})^{N_{\text{mem}}-n}, \tag{4.55}$$

and $p_{(g,s)}(>n) = \sum_{i=n+1}^{N_{\text{mem}}} p_{(g,s)}(i)$.

The success probabilities of the entanglement generation in the elementary links, $p_{\text{link},(g,s)}$ are

$$p_{\text{link},(g,s)} = \alpha_{\text{BS}} + \beta_{\text{BS}} + \gamma_{\text{BS}}, \tag{4.56}$$

corresponding to the normalization in Eq. (4.29). The overall probability of loosing an entangled pair between the ground stations due to atomic loss is p_{loss}. This includes both cases where atoms are lost in the swap operation and due to imperfect vaccum conditions. We can express this as

$$\begin{aligned} p_{\text{loss}} = & \; p_{\text{loss,gstat}}^2 \left(p_{\text{loss,end-sat}}\right)^2 \left(p_{\text{loss,receiver-sat}}\right)^{(n_{sat}-1)/2} \cdot \\ & \left(p_{\text{loss,emitter-sat}}\right)^{(n_{sat}-3)/2}, \end{aligned} \tag{4.57}$$

where

$$p_{\text{loss,gstat}} = 1 - e^{-t'/T'_{loss}}, \tag{4.58}$$

$$\begin{aligned} p_{\text{loss,x-sat}} = & \; e^{(-2t_x/T_{loss})} p_{loss,swap} + 2e^{-t_x/T_{loss}} \left(1 - e^{-t_x/T_{loss}}\right) + \\ & + \left(1 - e^{-t_x/T_{loss}}\right)^2. \end{aligned} \tag{4.59}$$

The different storage times t', t_x ($x = \{\text{end, receiver, or emitter}\}$) are the different storage times discussed in Sec. 4.5.1. Note, that we allow

for different effective loss times of the atoms on ground (T'_{loss}) and on satellites (T_{loss}) since it is conceivable that better vacuum and hence longer effective loss time can be obtained on ground than on satellites.

4.5.3. OPTICAL LINK BUDGET

In this section, the models developed to compute the propagation losses occurring in a link between two terminals are considered. The architecture proposed in this paper includes both inter-satellite and space-to-ground optical links. For inter-satellite links, the propagation losses include pointing jitter and beam divergence. Furthermore, in space-to-ground links, the losses due to atmospheric effects are also included. The following sections explain in detail the models developed to account for these effects.

BEAM DIVERGENCE AND POINTING JITTER

In an optical link between two terminals (see Fig. 4.6), the beam diverges creating a far-field intensity pattern in the aperture plane of the receiver. In the single photon regime, the probability density function of finding the photon on the xy-plane of the receiver, considering a given link distance z and a Gaussian beam profile, is

$$P(x,y) = \frac{2}{\pi w(z)^2} \exp\left(\frac{-2\left(x^2+y^2\right)}{w(z)^2}\right), \tag{4.60}$$

where

$$w(z) = w_0 \sqrt{1+\left(\frac{z}{z_{\text{R}}}\right)^2}, \tag{4.61}$$

in the absence of pointing errors. The transmitter pointing jitter, will displace the center of the Gaussian beam from the center of the receiver optical axis as shown in figure 4.6. For a given pointing error (x_0, y_0) the probability of capturing the photon is given by the convolution

$$\begin{aligned} P(x_0,y_0) \quad = \quad & \int_{-\infty}^{\infty}\int_{-\infty}^{\infty} I_0\left(\frac{w_0}{w(z)}\right)^2 \exp\left(\frac{-2\left(x^2+y^2\right)}{w(z)^2}\right) \cdot \\ & P_R(x-x_0, y-y_0)\, dx\, dy, \end{aligned} \tag{4.62}$$

where $P_R(x,y)$ is the pupil aperture function of the receiver given by

$$P_R(x,y) = \begin{cases} 1 & x^2+y^2 \leq r_R^2 \\ 0 & \text{else} \end{cases} \tag{4.63}$$

with r_R being the radius of the receiver and (x_0, y_0) is the displacement of the optical axis of the receiver with respect to the optical axis of the beam.

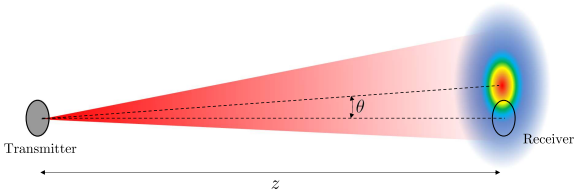

Figure 4.6: Gaussian beam propagation between two terminals through free space. The transmitter angular pointing jitter will deviate the center of the beam from the center of the receiver optical axis

The transmitter pointing jitter is usually characterized by a Gaussian probability density function for x_0 and y_0 of the form [55]

$$f_{XY}(x_0, y_0) = \frac{1}{\sigma_{xy}(z)^2 2\pi} \exp\left(-\frac{x_0^2 + y_0^2}{2\sigma_{xy}(z)^2}\right) \tag{4.64}$$

where $\sigma_{xy}(z)$ is the standard deviation of the displacement. The displacement of the beam in the xy plane is determined by the transmitter angular pointing error, θ (see Fig. 4.6). Under the small angle approximation, and considering that both the azimuthal and elevation angular errors are statistically equal, the standard deviation is $\sigma_{xy}(z) \approx \sigma_\theta z$, where σ_θ is the standard deviation of the angular transmitter pointing error [56].

In our rate analysis, we have assumed that the probability of receiving k out of N_{mem} photons in an elementary link follows a binomial distribution (see Sec. 4.5.1), using the averaged probability $\bar{P} = \int P(x_0, y_0) f_{XY}(x_0, y_0) dx_0 dy_0$. This approximation is valid in the regime where we are dominated by beam divergence rather than pointing jitter, i.e. when $w(z) \gg \sigma_{xy}$. For long distances, $z \gg 1$, we have that $w(z) \approx w_0 z / z_{\text{R}}$, where $z_{\text{R}} = \pi w_0^2 / \lambda$ is the Rayleigh distance (ee Eq. (4.61)). Since $\sigma_{xy}(z) \approx \sigma_\theta z$, it follows that by choosing a small enough beamwaist, w_0, we can ensure that $w(z) \gg \sigma_{xy}$.

In our simulations, we have assumed a pointing jitter of $\sigma_\theta = 0.47\,\mu$rad in the transmitter consistent with the Micius satellite [22] and light emitted from the Rb-atoms has a wavelength of $\lambda = 780$ nm. We choose a beamwaist of $w_0 = \lambda/(10\pi\sigma_\theta) = 0.054$ m, which ensures that $w(z)/\sigma_{xy} = 10$ in the simulations. We note that since the value of w_0 is much smaller than the smallest transmitter's radius $r_T = 0.15$ m considered for the Micius like satellite, the effect of clipping in the transmitter's telescope is negligible.

To check the validity of the binomial approximation for $w(z)/\sigma_{xy} = 10$,

we compare the true average probability distribution of a link

$$\overline{\Pr}(k; N_{\text{mem}}) = \int \Pr(k; N_{\text{mem}}, P(x_0, y_0)) f_{XY}(x_0, y_0) dx_0 dy_0, \tag{4.65}$$

with a binomial distribution $\Pr(k; N_{\text{mem}}, \bar{P})$. The two distributions in the limiting cases (shortest and largest elementary link distance considered) are plotted for specific values in Figs. 4.7. The difference in mean and standard deviation are shown in Figs. 4.8. The error in the mean is negligible ($< 10^{-10}$) and the standard deviation error is between 2% and 14% of the mean. The skewness for both distributions were found to be $\lesssim 0.4$ and thus non-significant.

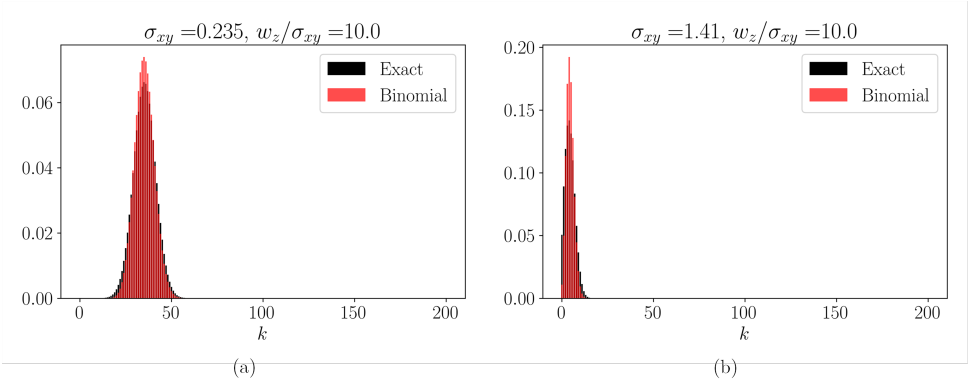

Figure 4.7: Histograms corresponding to the number of photons captured ($\sigma_\theta = 0.47$ μrad, $r_T = 0.5$ m, $r_R = 0.5$ m and $N_{\text{mem}} = 200$). In black is the exact histogram obtained through Monte Carlo simulations and in red is the approximate binomial distribution (with the same average $\overline{k}$), for (a) $z = 500$ km and (b) $z = 3000$ km.

ATMOSPHERIC LOSS

In this section, the photon losses due to the atmospheric effects are considered. These losses will be included in the model developed for the space-to-ground links. Atmospheric turbulence loss model When an optical beam propagates through the atmosphere, the turbulence will create wavefront errors that will be detrimental to the link. In a downlink scenario, the beam spread induced by the atmospheric turbulence can be neglected (ref. [36], chapter 12). Hence the beam-spread due to the atmospheric turbulence is not considered in the space-to-ground links on our model. Furthermore, the atmospheric turbulence will also create a beam wander on the receiver's aperture plane. This beam

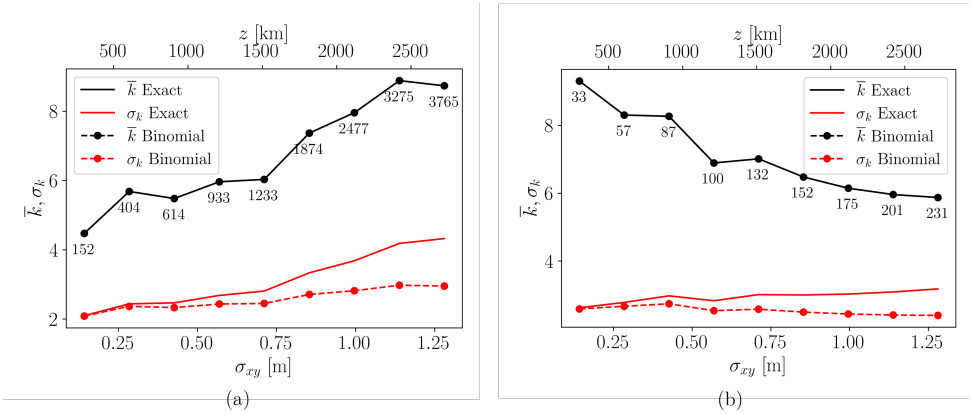

Figure 4.8: Values for mean $\overline{k}$ and standard deviation σ_k of the distributions of the number of photons captured for different distances between intersatellite elementary links for the (a) Micius satellite and (b) upgraded satellite. The numbers below the mean value are the number of memory modes considered for each point. Values are for elementary link distances and the number of memory modes obtained from the $R = 10$ Hz in Figure 3a of the main paper. Note that the error in the mean is negligible resulting in overlapping curves for the binomial and exact distribution.

wander can be modeled as a part of the transmitter pointing jitter, as their effects are the same (stochastic displacement of the beam center from the receiver's optical axis). However, for a downlink, the beam wander effect due to the transmitter pointing jitter will be dominant for reasonable turbulence regimes and the contribution from turbulence can therefore be neglected (ref. [36], chapter 12.6.2).

Atmospheric transmission loss model The atmospheric transmittance loss is due to four effects: Molecular absorption, molecular scattering, aerosol absorption, aerosol scattering. The beam attenuation due to these can be modeled with Beer's law as [57]

$$\frac{P_\lambda(\mathcal{L})}{P_\lambda(0)} = \exp\left[-\int_0^{\mathcal{L}} \alpha_\lambda(z)dz\right] \tag{4.66}$$

where $P(\mathcal{L})$ is the signal intensity after travelling a distance $\mathcal{L}$ through the atmosphere, z is the distance coordinate, and $\alpha_\lambda(z)$ is the attenuation coefficient (a result of the sum of the attenuation coefficients of the absorption and scattering of molecules and aerosols).

The wavelength dependence is due to the dependence of the absorption and scattering phenomena on the wavelength. Considering

that the length $\mathcal{L}$ is given for a beam with zenith angle $\zeta = 0°$, the atmospheric attenuation coefficient can to good approximation be considered as a constant of position [58] such that the atmospheric transmittance loss for a zenith angle ζ can be computed as

$$\frac{P(\mathcal{L}')}{P(0)} = \exp\left[-\mathcal{L}'\alpha_\lambda\right] = \eta^{\sec(\zeta)} \tag{4.67}$$

where $\eta = \exp\left[-\mathcal{L}\alpha_\lambda\right]$ is the transmittance for the zenith angle $\zeta = 0°$. For large zenith angles $\zeta > 60°$ the parallel plane approximation of the atmosphere is no longer applicable and the geometrical correction factor has to be changed to [57]

$$\frac{P(\mathcal{L}')}{P(0)} = \eta^{m(\zeta)} \tag{4.68}$$

$$m(\zeta) = \begin{cases} \sec\zeta & \zeta \leq 60° \\ \dfrac{1}{\cos\zeta + 0.505572(96.07995 - \zeta)^{-1.664}} & 60° < \zeta < 90° \end{cases} \tag{4.69}$$

Simulated values for the transmittance η, for different zenith angles can be found in [54]. In space-to-ground links, the main contributor to the atmospheric attenuation of light is the Rayleigh scattering due to molecules [57] assuming that the ground stations are placed at 2 km altitude where the Mie scattering is negligible [54]. This is because the aerosol density is very low at these altitudes and therefore the Mie scattering can be neglected. The wavelength considered in this work is 780 nm (see Figure 2 of the main paper), so according to Figure 15 in Ref. [54], a value of $\eta \approx 0.95$ is used for our simulations.

REFERENCES

[1] C. H. Bennett and G. Brassard. “Quantum cryptography: Public key distribution and coin tossing”. In: *Theoretical Computer Science* 560 (2014). Theoretical Aspects of Quantum Cryptography – celebrating 30 years of BB84, pp. 7–11. issn: 0304-3975. doi: https://doi.org/10.1016/j.tcs.2014.05.025. url: https://www.sciencedirect.com/science/article/pii/S0304397514004241.

[2] A. K. Ekert. “Quantum cryptography based on Bell’s theorem”. In: *Phys. Rev. Lett.* 67 (6 Aug. 1991), pp. 661–663. doi: 10.1103/PhysRevLett.67.661. url: https://link.aps.org/doi/10.1103/PhysRevLett.67.661.

[3] S. Pirandola, U. L. Andersen, L. Banchi, M. Berta, D. Bunandar, R. Colbeck, D. Englund, T. Gehring, C. Lupo, C. Ottaviani, J. L. Pereira, M. Razavi, J. S. Shaari, M. Tomamichel, V. C. Usenko, G. Vallone, P. Villoresi, and P. Wallden. “Advances in quantum cryptography”. In: *Adv. Opt. Photon.* 12.4 (Dec. 2020), pp. 1012–1236. doi: 10.1364/AOP.361502. url: https://opg.optica.org/aop/abstract.cfm?URI=aop-12-4-1012.

[4] P. Kómár, E. M. Kessler, M. Bishof, L. Jiang, A. S. Sørensen, J. Ye, and M. D. Lukin. “A quantum network of clocks”. In: *Nature Physics* 10.8 (2014), pp. 582–587. doi: 10.1038/nphys3000. url: https://doi.org/10.1038/nphys3000.

[5] X. Guo, C. R. Breum, J. Borregaard, S. Izumi, M. V. Larsen, T. Gehring, M. Christandl, J. S. Neergaard-Nielsen, and U. L. Andersen. “Distributed quantum sensing in a continuous-variable entangled network”. In: *Nature Physics* 16.3 (2020), pp. 281–284. doi: 10.1038/s41567-019-0743-x. url: https://doi.org/10.1038/s41567-019-0743-x.

[6] L.-Z. Liu, Y.-Z. Zhang, Z.-D. Li, R. Zhang, X.-F. Yin, Y.-Y. Fei, L. Li, N.-L. Liu, F. Xu, Y.-A. Chen, and J.-W. Pan. “Distributed quantum phase estimation with entangled photons”. In: *Nature Photonics* 15.2 (2021), pp. 137–142. doi: 10.1038/s41566-020-00718-2. url: https://doi.org/10.1038/s41566-020-00718-2.

[7] H. Buhrman and H. Röhrig. “Distributed Quantum Computing”. In: *Mathematical Foundations of Computer Science 2003*. Ed. by B. Rovan and P. Vojtáš. Lecture Notes in Computer Science. Berlin, Heidelberg: Springer, 2003, pp. 1–20. isbn: 978-3-540-45138-9. doi: 10.1007/978-3-540-45138-9_1.

[8] Z. Tang, P. Zhang, W. O. Krawec, and L. Wang. “Quantum Networks for Resilient Power Grids: Theory and Simulated Evaluation”. In: *IEEE Transactions on Power Systems* 38.2 (2023), pp. 1189–1204. doi: 10.1109/TPWRS.2022.3172374.

[9] B. C. Nichol, R. Srinivas, D. P. Nadlinger, P. Drmota, D. Main, G. Araneda, C. J. Ballance, and D. M. Lucas. “An elementary quantum network of entangled optical atomic clocks”. In: *Nature* 609.7928 (2022), pp. 689–694. doi: 10.1038/s41586-022-05088-z. url: https://doi.org/10.1038/s41586-022-05088-z.

[10] W. K. Wootters and W. H. Zurek. “A single quantum cannot be cloned”. In: *Nature* 299.5886 (1982), pp. 802–803. doi: 10.1038/299802a0. url: https://doi.org/10.1038/299802a0.

[11] L. .-. Duan, M. D. Lukin, J. I. Cirac, and P. Zoller. “Long-distance quantum communication with atomic ensembles and linear optics”. In: *Nature* 414.6862 (2001), pp. 413–418. doi: 10.1038/35106500. url: https://doi.org/10.1038/35106500.

[12] N. Sangouard, C. Simon, H. de Riedmatten, and N. Gisin. “Quantum repeaters based on atomic ensembles and linear optics”. In: *Rev. Mod. Phys.* 83 (1 Mar. 2011), pp. 33–80. doi: 10.1103/RevModPhys.83.33. url: https://link.aps.org/doi/10.1103/RevModPhys.83.33.

[13] S. Muralidharan, J. Kim, N. Lütkenhaus, M. D. Lukin, and L. Jiang. “Ultrafast and Fault-Tolerant Quantum Communication across Long Distances”. In: *Phys. Rev. Lett.* 112 (25 June 2014), p. 250501. doi: 10.1103/PhysRevLett.112.250501. url: https://link.aps.org/doi/10.1103/PhysRevLett.112.250501.

[14] W. J. Munro, A. M. Stephens, S. J. Devitt, K. A. Harrison, and K. Nemoto. “Quantum communication without the necessity of quantum memories”. In: *Nature Photonics* 6.11 (2012), pp. 777–781. doi: 10.1038/nphoton.2012.243. url: https://doi.org/10.1038/nphoton.2012.243.

[15] L. de Forges de Parny, O. Alibart, J. Debaud, S. Gressani, A. Lagarrigue, A. Martin, A. Metrat, M. Schiavon, T. Troisi, E. Diamanti, P. Gélard, E. Kerstel, S. Tanzilli, and M. Van Den Bossche. "Satellite-based quantum information networks: use cases, architecture, and roadmap". In: *Communications Physics* 6.1 (2023), p. 12. doi: 10.1038/s42005-022-01123-7. url: https://doi.org/10.1038/s42005-022-01123-7.

[16] C. Liorni, H. Kampermann, and D. Bruß. "Quantum repeaters in space". In: *New Journal of Physics* 23.5 (May 2021), p. 053021. doi: 10.1088/1367-2630/abfa63. url: https://doi.org/10.1088%2F1367-2630%2Fabfa63.

[17] M. Gündoğan, J. S. Sidhu, V. Henderson, L. Mazzarella, J. Wolters, D. K. L. Oi, and M. Krutzik. "Proposal for space-borne quantum memories for global quantum networking". In: *npj Quantum Information* 7.1 (2021), p. 128. doi: 10.1038/s41534-021-00460-9. url: https://doi.org/10.1038/s41534-021-00460-9.

[18] J. Wallnöfer, F. Hahn, M. Gündoğan, J. S. Sidhu, F. Wiesner, N. Walk, J. Eisert, and J. Wolters. "Simulating quantum repeater strategies for multiple satellites". In: *Communications Physics* 5.1 (June 2022). doi: 10.1038/s42005-022-00945-9. url: https://doi.org/10.1038%2Fs42005-022-00945-9.

[19] S. Khatri, A. J. Brady, R. A. Desporte, M. P. Bart, and J. P. Dowling. "Spooky action at a global distance: analysis of space-based entanglement distribution for the quantum internet". In: *npj Quantum Information* 7.1 (Jan. 2021). doi: 10.1038/s41534-020-00327-5. url: https://doi.org/10.1038%2Fs41534-020-00327-5.

[20] K. Boone, J.-P. Bourgoin, E. Meyer-Scott, K. Heshami, T. Jennewein, and C. Simon. "Entanglement over global distances via quantum repeaters with satellite links". In: *Phys. Rev. A* 91 (5 May 2015), p. 052325. doi: 10.1103/PhysRevA.91.052325. url: https://link.aps.org/doi/10.1103/PhysRevA.91.052325.

[21] D. L. Bakker, Y. Jong, B. P. F. Dirks, and G. C. Amaral. "A Best-Path Approach to the Design of a Hybrid Space–Ground Quantum Network with Dynamic Constraints". In: *Photonics* 11.3 (2024). issn: 2304-6732. doi: 10.3390/photonics11030268. url: https://www.mdpi.com/2304-6732/11/3/268.

[22] J. Yin, Y.-H. Li, S.-K. Liao, M. Yang, Y. Cao, L. Zhang, J.-G. Ren, W.-Q. Cai, W.-Y. Liu, S.-L. Li, R. Shu, Y.-M. Huang, L. Deng, L. Li, Q. Zhang, N.-L. Liu, Y.-A. Chen, C.-Y. Lu, X.-B. Wang, F. Xu, J.-Y. Wang, C.-Z. Peng, A. K. Ekert, and J.-W. Pan.

"Entanglement-based secure quantum cryptography over 1,120 kilometres". In: *Nature* 582.7813 (June 2020). Number: 7813 Publisher: Nature Publishing Group, pp. 501–505. issn: 1476-4687. doi: 10.1038/s41586-020-2401-y. url: https://www.nature.com/articles/s41586-020-2401-y (visited on 08/14/2023).

[23] M. Gündoğan, J. S. Sidhu, V. Henderson, L. Mazzarella, J. Wolters, D. K. L. Oi, and M. Krutzik. "Proposal for space-borne quantum memories for global quantum networking". In: *npj Quantum Information* 7.1 (Aug. 2021). doi: 10.1038/s41534-021-00460-9. url: https://doi.org/10.1038%2Fs41534-021-00460-9.

[24] A. Anwar, C. Perumangatt, A. Villar, A. Lohrmann, and A. Ling. "Development of compact entangled photon-pair sources for satellites". In: *Applied Physics Letters* 121.22 (Nov. 2022), p. 220503. issn: 0003-6951. doi: 10.1063/5.0109702. eprint: https://pubs.aip.org/aip/apl/article-pdf/doi/10.1063/5.0109702/16485971/220503_1_online.pdf. url: https://doi.org/10.1063/5.0109702.

[25] C. Schimpf, M. Reindl, F. Basso Basset, K. D. Jöns, R. Trotta, and A. Rastelli. "Quantum dots as potential sources of strongly entangled photons: Perspectives and challenges for applications in quantum networks". In: *Applied Physics Letters* 118.10 (Mar. 2021), p. 100502. issn: 0003-6951. doi: 10.1063/5.0038729. eprint: https://pubs.aip.org/aip/apl/article-pdf/doi/10.1063/5.0038729/14544746/100502_1_online.pdf. url: https://doi.org/10.1063/5.0038729.

[26] K. C. Chen, P. Dhara, M. Heuck, Y. Lee, W. Dai, S. Guha, and D. Englund. "Zero-Added-Loss Entangled-Photon Multiplexing for Ground- and Space-Based Quantum Networks". In: *Phys. Rev. Appl.* 19 (5 May 2023), p. 054029. doi: 10.1103/PhysRevApplied.19.054029. url: https://link.aps.org/doi/10.1103/PhysRevApplied.19.054029.

[27] Q. Zhang, X.-H. Bao, C.-Y. Lu, X.-Q. Zhou, T. Yang, T. Rudolph, and J.-W. Pan. "Demonstration of a scheme for the generation of "event-ready" entangled photon pairs from a single-photon source". In: *Phys. Rev. A* 77 (6 June 2008), p. 062316. doi: 10.1103/PhysRevA.77.062316. url: https://link.aps.org/doi/10.1103/PhysRevA.77.062316.

[28] J. McKeever, A. Boca, A. D. Boozer, R. Miller, J. R. Buck, A. Kuzmich, and H. J. Kimble. “Deterministic Generation of Single Photons from One Atom Trapped in a Cavity”. In: *Science* 303.5666 (2004), pp. 1992–1994. doi: 10.1126/science.1095232. eprint: https://www.science.org/doi/pdf/10.1126/science.1095232. url: https://www.science.org/doi/abs/10.1126/science.1095232.

[29] D. Bluvstein, H. Levine, G. Semeghini, T. T. Wang, S. Ebadi, M. Kalinowski, A. Keesling, N. Maskara, H. Pichler, M. Greiner, V. Vuletić, and M. D. Lukin. “A quantum processor based on coherent transport of entangled atom arrays”. In: *Nature* 604.7906 (Apr. 2022), pp. 451–456. doi: 10.1038/s41586-022-04592-6. url: https://doi.org/10.1038%2Fs41586-022-04592-6.

[30] A. W. Young, W. J. Eckner, W. R. Milner, D. Kedar, M. A. Norcia, E. Oelker, N. Schine, J. Ye, and A. M. Kaufman. “Half-minute-scale atomic coherence and high relative stability in a tweezer clock”. In: *Nature* 588.7838 (Dec. 2020), pp. 408–413. doi: 10.1038/s41586-020-3009-y. url: https://doi.org/10.1038%2Fs41586-020-3009-y.

[31] H. Levine, A. Keesling, G. Semeghini, A. Omran, T. T. Wang, S. Ebadi, H. Bernien, M. Greiner, V. Vuleti ć, H. Pichler, and M. D. Lukin. “Parallel Implementation of High-Fidelity Multiqubit Gates with Neutral Atoms”. In: *Phys. Rev. Lett.* 123 (17 Oct. 2019), p. 170503. doi: 10.1103/PhysRevLett.123.170503. url: https://link.aps.org/doi/10.1103/PhysRevLett.123.170503.

[32] Z. Fu, P. Xu, Y. Sun, Y.-Y. Liu, X.-D. He, X. Li, M. Liu, R.-B. Li, J. Wang, L. Liu, and M.-S. Zhan. “High-fidelity entanglement of neutral atoms via a Rydberg-mediated single-modulated-pulse controlled-phase gate”. In: *Phys. Rev. A* 105 (4 Apr. 2022), p. 042430. doi: 10.1103/PhysRevA.105.042430. url: https://link.aps.org/doi/10.1103/PhysRevA.105.042430.

[33] S. J. Evered, D. Bluvstein, M. Kalinowski, S. Ebadi, T. Manovitz, H. Zhou, S. H. Li, A. A. Geim, T. T. Wang, N. Maskara, H. Levine, G. Semeghini, M. Greiner, V. Vuletić, and M. D. Lukin. “High-fidelity parallel entangling gates on a neutral-atom quantum computer”. In: *Nature* 622.7982 (Oct. 2023), pp. 268–272. doi: 10.1038/s41586-023-06481-y. url: https://doi.org/10.1038%2Fs41586-023-06481-y.

[34] W. Huie, S. G. Menon, H. Bernien, and J. P. Covey. “Multiplexed telecommunication-band quantum networking with atom arrays in optical cavities”. In: *Phys. Rev. Res.* 3 (4 Dec. 2021), p. 043154. doi: 10.1103/PhysRevResearch.3.043154. url: https:

//link.aps.org/doi/10.1103/PhysRevResearch.3.043154.

[35] J. P. Covey, H. Weinfurter, and H. Bernien. “Quantum networks with neutral atom processing nodes”. In: *npj Quantum Information* 9.1 (2023), p. 90. doi: 10.1038/s41534-023-00759-9. url: https://doi.org/10.1038/s41534-023-00759-9.

[36] L. C. Andrews and R. L. Phillips. *Laser Beam Propagation Through Random Media*. 1000 20th Street, Bellingham, WA 98227-0010 USA: SPIE, Sept. 2005. isbn: 978-0-8194-5948-0. doi: 10.1117/3.626196. url: http://link.aip.org/link/doi/10.1117/3.626196 (visited on 06/07/2022).

[37] S. D. Barrett and P. Kok. “Efficient high-fidelity quantum computation using matter qubits and linear optics”. In: *Phys. Rev. A* 71 (6 June 2005), p. 060310. doi: 10.1103/PhysRevA.71.060310. url: https://link.aps.org/doi/10.1103/PhysRevA.71.060310.

[38] C. Cabrillo, J. I. Cirac, P. García-Fernández, and P. Zoller. “Creation of entangled states of distant atoms by interference”. In: *Phys. Rev. A* 59 (2 Feb. 1999), pp. 1025–1033. doi: 10.1103/PhysRevA.59.1025. url: https://link.aps.org/doi/10.1103/PhysRevA.59.1025.

[39] E. Deist, J. A. Gerber, Y.-H. Lu, J. Zeiher, and D. M. Stamper-Kurn. “Superresolution Microscopy of Optical Fields Using Tweezer-Trapped Single Atoms”. In: *Phys. Rev. Lett.* 128 (8 Feb. 2022), p. 083201. doi: 10.1103/PhysRevLett.128.083201. url: https://link.aps.org/doi/10.1103/PhysRevLett.128.083201.

[40] D. Bluvstein, H. Levine, G. Semeghini, T. T. Wang, S. Ebadi, M. Kalinowski, A. Keesling, N. Maskara, H. Pichler, M. Greiner, V. Vuletić, and M. D. Lukin. “A quantum processor based on coherent transport of entangled atom arrays”. In: *Nature* 604.7906 (2022), pp. 451–456. doi: 10.1038/s41586-022-04592-6. url: https://doi.org/10.1038/s41586-022-04592-6.

[41] H. Levine, D. Bluvstein, A. Keesling, T. T. Wang, S. Ebadi, G. Semeghini, A. Omran, M. Greiner, V. Vuleti ć, and M. D. Lukin. “Dispersive optical systems for scalable Raman driving of hyperfine qubits”. In: *Phys. Rev. A* 105 (3 Mar. 2022), p. 032618. doi: 10.1103/PhysRevA.105.032618. url: https://link.aps.org/doi/10.1103/PhysRevA.105.032618.

[42] Y. Li and J. Thompson. *High-rate and high-fidelity modular interconnects between neutral atom quantum processors*. 2024. arXiv: 2401.04075 [quant-ph].

[43] D. Jaksch, J. I. Cirac, P. Zoller, S. L. Rolston, R. Côté, and M. D. Lukin. “Fast Quantum Gates for Neutral Atoms”. In: *Phys. Rev. Lett.* 85 (10 Sept. 2000), pp. 2208–2211. doi: 10.1103/PhysRevLett.85.2208. url: https://link.aps.org/doi/10.1103/PhysRevLett.85.2208.

[44] H. Levine, A. Keesling, G. Semeghini, A. Omran, T. T. Wang, S. Ebadi, H. Bernien, M. Greiner, V. Vuleti ć, H. Pichler, and M. D. Lukin. “Parallel Implementation of High-Fidelity Multiqubit Gates with Neutral Atoms”. In: *Phys. Rev. Lett.* 123 (17 Oct. 2019), p. 170503. doi: 10.1103/PhysRevLett.123.170503. url: https://link.aps.org/doi/10.1103/PhysRevLett.123.170503.

[45] S. Jandura and G. Pupillo. “Time-Optimal Two- and Three-Qubit Gates for Rydberg Atoms”. In: *Quantum* 6 (May 2022), p. 712. issn: 2521-327X. doi: 10.22331/q-2022-05-13-712. url: https://doi.org/10.22331/q-2022-05-13-712.

[46] V. Dominguez Tubio, M. Badas Aldecocea, J. van Dam, A. Sorensen, and J. Borregaard. “Suplementary material: Satellite-assisted quantum communication with single photon sources and atomic memories”. In: (2024).

[47] E. Brattich, E. Serrano Castillo, F. Giulietti, J.-B. Renard, S. N. Tripathi, K. Ghosh, G. Berthet, D. Vignelles, and L. Tositti. “Measurements of aerosols and charged particles on the BEXUS18 stratospheric balloon”. In: *Annales Geophysicae* 37.3 (June 2019). Publisher: Copernicus GmbH, pp. 389–403. issn: 0992-7689. doi: 10.5194/angeo-37-389-2019. url: https://angeo.copernicus.org/articles/37/389/2019/ (visited on 11/14/2023).

[48] O. A. Collins, S. D. Jenkins, A. Kuzmich, and T. A. B. Kennedy. “Multiplexed Memory-Insensitive Quantum Repeaters”. In: *Phys. Rev. Lett.* 98 (6 Feb. 2007), p. 060502. doi: 10.1103/PhysRevLett.98.060502. url: https://link.aps.org/doi/10.1103/PhysRevLett.98.060502.

[49] F. Xu, X. Ma, Q. Zhang, H.-K. Lo, and J.-W. Pan. “Secure quantum key distribution with realistic devices”. In: *Rev. Mod. Phys.* 92 (2 May 2020), p. 025002. doi: 10.1103/RevModPhys.92.025002. url: https://link.aps.org/doi/10.1103/RevModPhys.92.025002.

[50] M. Victora, S. Tserkis, S. Krastanov, A. S. de la Cerda, S. Willis, and P. Narang. “Entanglement purification on quantum networks”. In: *Phys. Rev. Res.* 5 (3 Sept. 2023), p. 033171. doi: 10.1103/PhysRevResearch.5.033171. url: https:

//link.aps.org/doi/10.1103/PhysRevResearch.5.033171.

[51] A. Belenchia, M. Carlesso, Ö. Bayraktar, D. Dequal, I. Derkach, G. Gasbarri, W. Herr, Y. L. Li, M. Rademacher, J. Sidhu, D. K. Oi, S. T. Seidel, R. Kaltenbaek, C. Marquardt, H. Ulbricht, V. C. Usenko, L. Wörner, A. Xuereb, M. Paternostro, and A. Bassi. "Quantum physics in space". In: *Physics Reports* 951 (2022). Quantum Physics in Space, pp. 1–70. issn: 0370-1573. doi: https://doi.org/10.1016/j.physrep.2021.11.004. url: https://www.sciencedirect.com/science/article/pii/S0370157321004142.

[52] D. E. Bruschi, C. Sabín, A. White, V. Baccetti, D. K. L. Oi, and I. Fuentes. "Testing the effects of gravity and motion on quantum entanglement in space-based experiments". In: *New Journal of Physics* 16.5 (May 2014), p. 053041. doi: 10.1088/1367-2630/16/5/053041. url: https://dx.doi.org/10.1088/1367-2630/16/5/053041.

[53] A. Carrasco-Casado, K. Shiratama, D. Kolev, P. Trinh, T. Fuse, S. Fuse, K. Kawaguchi, Y. Hashimoto, M. Hyodo, T. Sakamoto, T. Kunisada, and M. Toyoshima. "Prototype Development and Validation of a Beam-Divergence Control System for Free-Space Laser Communications". In: *Frontiers in Physics* 10 (May 2022). doi: 10.3389/fphy.2022.878488.

[54] D. Giggenbach and A. Shrestha. "Atmospheric absorption and scattering impact on optical satellite-ground links". In: *International Journal of Satellite Communications and Networking* 40.2 (2022), pp. 157–176. issn: 1542-0981. doi: 10.1002/sat.1426. url: https://onlinelibrary.wiley.com/doi/abs/10.1002/sat.1426 (visited on 05/31/2023).

[55] K. Kiasaleh. "On the probability density function of signal intensity in free-space optical communications systems impaired by pointing jitter and turbulence". In: *Optical Engineering* 33.11 (Nov. 1994), pp. 3748–3757. issn: 0091-3286, 1560-2303. doi: 10.1117/12.181939. url: http://www.spiedigitallibrary.org/journals/optical-engineering/volume-33/issue-11/0000/On-the-probability-density-function-of-signal-intensity-in-free/10.1117/12.181939.full (visited on 04/08/2023).

[56] M. Badás, P. Piron, J. Bouwmeester, and J. Loicq. "On the optimum far-field irradiance distribution using Laguerre-Gaussian beams for intersatellite free-space optical communications". In: *Optics Express* 32.18 (Aug. 2024), pp. 31597–31620. issn: 1094-4087. doi: 10.1364/OE.533250. url: https://opg.optica.org/

oe/abstract.cfm?uri=oe-32-18-31597 (visited on 08/16/2024).

[57] H. Hemmati. *Near-Earth Laser Communications*. CRC Press, 2009. isbn: 1-4200-1544-3. url: http://books.google.com/books?id=hiFPrD55GD8C&pgis=1 (visited on 05/23/2022).

[58] S. Khatri, A. J. Brady, R. A. Desporte, M. P. Bart, and J. P. Dowling. "Spooky action at a global distance: analysis of space-based entanglement distribution for the quantum internet". In: *npj Quantum Information* 7.1 (Jan. 2021). Number: 1 Publisher: Nature Publishing Group, pp. 1–15. issn: 2056-6387. doi: 10.1038/s41534-020-00327-5. url: http://www.nature.com/articles/s41534-020-00327-5 (visited on 04/05/2023).

5

QUANTUM KEY DISTRIBUTION IN THE IBERIAN PENINSULA

V. Domínguez Tubío, M. Badás Aldecocea, D. Bakker, G.C. Amaral, D.López, J. Borregaard

The development of a quantum network promises breakthroughs in secure communication, distributed computing, and precision sensing. An application of quantum communication currently implemented is quantum key distribution (QKD), which provides information-theoretic security unattainable by classical means. While optical fiber-based QKD networks suffer from exponential loss, satellite-assisted quantum communication offers a scalable solution for long-distance secure key exchange. In this work, we propose and evaluate a satellite-based QKD setup covering the Iberian Peninsula, linking Madrid with Barcelona, Bilbao, and Lisbon. Our proposed setup uses a Low-Earth-Orbit (LEO) state-of-the-art satellite equipped with a spontaneous parametric down-conversion (SPDC) source to distribute entangled photon pairs to ground stations. Considering vibrations in the satellite, we optimize the beam waist to enhance the transmission probability and improve the secret key rate (SKR). Our results show that we achieve key rates sufficient for a real-world application, such as secure communication between hospitals, using hybrid classical-quantum protocols. Our results highlight the viability of near-term satellite-based QKD networks for national-scale secure communications.

This chapter is based on the publication Optica Quantum 4.1, pp. 22-30

5.1. INTRODUCTION

The realization of a quantum internet holds the potential to revolutionize multiple fields, including secure communication [1–3], high-precision sensing networks [4–6], and distributed quantum computing [7]. In particular, quantum key distribution (QKD) enables communication with information-theoretic security, a level of protection unattainable by classical methods.

Quantum communication relies on photons to carry quantum information. However, their transmission is limited by loss and, unlike classical signals, quantum signals cannot be amplified using conventional techniques due to the no-cloning theorem [8]. To mitigate this, quantum repeater architectures have been proposed. These divide the total distance into shorter segments, where quantum information can be transmitted directly. The segments are then connected using quantum teleportation [9, 10] or quantum error correction [11, 12] at the repeater nodes, enabling faithful transmission over the total distance. In fiber-based systems, however, signal attenuation increases exponentially with distance, requiring hundreds of repeater nodes for continental-scale coverage.

Satellite-based free-space QKD offers a promising alternative for long-distance communication without the need for complex repeater infrastructures. Notably, the Micius satellite has demonstrated QKD over distances from 500 to 7,000 km using a trusted-node architecture [13, 14]. More recently, entanglement-based QKD was successfully achieved without relying on a trusted node, decreasing the risk of eavesdroppers, reaching up to 1,200 km [15, 16]—distances well beyond the capability of terrestrial fiber networks.

Fiber-based QKD has also made significant progress, enabling high-speed, secure communication across metropolitan areas. Recent demonstrations include the protection of multiple VPNs [17] and secure data exchange between hospitals in the Madrid area via a trusted-node QKD network [18]. The next logical step is to extend these capabilities from city-scale to national-scale coverage.

To this end, we propose a satellite-based QKD architecture to interconnect major cities across the Iberian Peninsula— Madrid with Barcelona, Bilbao, and Lisbon—as shown in Fig. 5.1(a). Our system employs a satellite like Micius in a Low-Earth-Orbit (LEO) equipped with a spontaneous parametric down-conversion (SPDC) source to distribute entangled photon pairs to multiple ground stations, implementing the BBM92 protocol [16]. In our setup, we consider the vibrations in the satellite, the pointing jitter, and the pumping laser of the source and optimize them such that it increases the transmission probability that reaches the ground stations. This jitter optimization comes with finding the best value for the size of the telescope and the best beam waist in real time while the telescope is at the line of sight of the ground

stations.

We evaluate the system's performance with and without optimization, demonstrating that the latter significantly enhances the secret key rate (SKR)—by a factor of approximately 10. A single satellite link proves sufficient to support secure communication across the Iberian Peninsula. Our results show that the SKR is adequate to support existing QKD use cases such as hospital-to-hospital encryption demonstrated in the MAD-QCI project, using hybrid protocols where the quantum layer handles key generation and classical layers manage key expansion via IPsec. Furthermore, we check that for more demanding use cases such as supporting VPN services using the ETSI-QKD-014 protocol [17], we would need to improve some hardware of the setup, such as the entangled photon pair source.

5.2. MODEL

We focus on a downlink configuration, where photons are transmitted from a satellite to ground stations. This setup is preferred because atmospheric disturbances are generally less severe than in the uplink case, where photons travel from the ground to the satellite [19, 20]. Specifically, we consider a single satellite like Micius, with telescopes of radius of 15 cm, entangled photon source rate of $5 \cdot 10^6$ ph/s and pointing jitters of $\sim 10^{-6}$ rad, in a low Earth orbit (LEO) at an altitude of approximately 400 km, following a medium-inclination trajectory at a latitude of 42°, passing over the Iberian Peninsula, as illustrated in Fig. 5.1(b). The satellite carries an onboard entangled photon source that probabilistically generates polarization-entangled photon pairs.

At the ground stations, photons are measured randomly in either the Z or X basis. Only those detected in the same basis are retained in classical memories through postselection. We employ the BBM92 protocol, following the approach demonstrated by the Micius satellite [16]. The figure of merit that we base our analysis on is the extracted key material; in general, the value is presented as a certain amount of **bits per second** (bps), but eventually it may also be convenient to also express it in terms of **bits per satellite pass**. The calculation involves three main steps, which are discussed in the Sections to follow: the model of the photonic qubit states generated by the entangled photon-pair source on-board the satellite; the effect of the optical channels between the satellite and the ground stations (always considered in pairs); and the effect of the measurement performed by the receivers in the presence of noise.

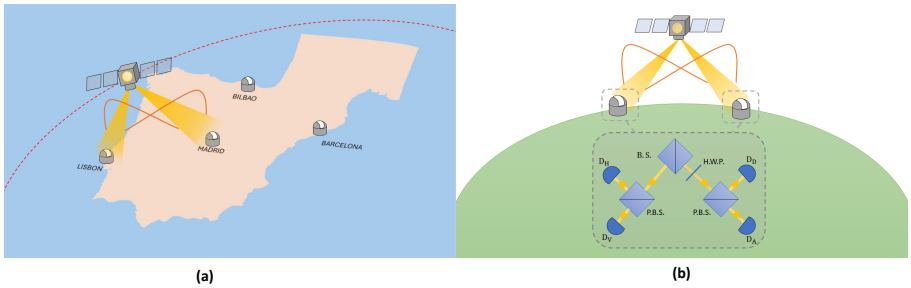

Figure 5.1: **Experimental setup. (a)** Ground stations of the regional quantum key distribution (QKD) network that we want to implement. The central node is Madrid, and the key distribution is always between Madrid and any of the other cities (Barcelona, Bilbao and Lisbon). **(b)** We consider a downlink scenario, with an entangled photon source firing photons from the satellite to the ground stations. At the ground stations, the photons are randomly measured in the X or Z basis. To perform such a measurement, the photons go through a 50/50 beam splitter (B.S.), followed by a half-wave plate (H.W.P.) in one of the outputs, which changes the basis of the input photons. Finally, before measuring, the photons go through a polarizing beam splitter (P.B.S.) such that we measure different polarizations- horizontal (D_H), vertical (D_V), diagonal (D_D) and antidiagonal (D_A)- at the output ports of the B.S.

5.2.1. ENTANGLED PHOTON PAIR SOURCE

We consider an SPDC source as our probabilistic source of entangled photonic pairs. A pump laser is used to drive a nonlinear optical crystal in both the clockwise and anticlockwise directions simultaneously, generating down-converted polarization-entangled photon pairs with orthogonal polarizations [15, 21].

$$
\begin{aligned}
|\psi_{\text{source}}\rangle = (1-\lambda)\,(|0,0\rangle_{A,B} + \\
\frac{\sqrt{2}\lambda^{1/2}}{(1-\lambda)^{1/2}}\frac{1}{\sqrt{2}}(|H\rangle_A|V\rangle_B + |V\rangle_A|H\rangle_B) + \\
\frac{\sqrt{3}\lambda}{1-\lambda}\frac{1}{\sqrt{3}}(|2H\rangle_A|2V\rangle_B + |HV\rangle_A|HV\rangle_B + \\
|2V\rangle_A|2H\rangle_B)),
\end{aligned}
\tag{5.1}
$$

where the subscripts A and B correspond to two different spatial modes directed toward the ground stations of Alice and Bob respectively, $|H\rangle$ and $|V\rangle$ denote the horizontal and vertical polarization states, respectively. The state $|\psi\rangle = 1/\sqrt{2}\,(|H\rangle_A|V\rangle_B + |V\rangle_A|H\rangle_B)$ denotes the desired state which corresponds to a maximally entangled state with anticorrelated polarization.

The term $\mu = 2\lambda$ is the average number of photon pairs generated by one pump laser, characterised by the brightness of the SPDC source [21]. The source operates in a weak-pump regime, where $\lambda \ll 1$, implying that the probability of emitting a photon pair is as well much less than one. However, it improves the fidelity by reducing multi-photon events ($\propto |2H\rangle_A|2V\rangle_B + |HV\rangle_A|HV\rangle_B + |2V\rangle_A|2H\rangle_B$). In other words, there is trade-off between the rate and the fidelity of entanglement. In our simulation, we optimize λ such that it gives us the higher SKR possible.

5.2.2. PHOTON TRANSMISSION

Photon loss during transmission to the two ground stations will change the received state from the one emitted by the SPDC source. We model this by passing the state in Eq.(5.16) through fictitious beam splitters in each spatial model and polarization, where one output of the beam splitters corresponds to the loss, while the other is the transmitted mode. By considering the different spatial modes in the transmission probability, we take into account the asymmetry of the channels due to the different distances from the satellite to each of the ground stations.

The free space transmission probability is built upon the one presented in Ref. [22], which includes divergence, atmospheric absorption, and pointing jitter. For a more accurate estimation of the number of entangled photon-pairs captured by the ground station per second, an optical propagation model based on Ref. [23], which accounts for the

truncation of the beam in the transmitter, is used (see Appendix 5.5.1). This model enables the accurate evaluation of the average photon capture probability of each downlink channel accounting for both the diffraction effects and the pointing jitter. By changing the beamwaist of the transmitted spatial Gaussian mode, i.e. w_0, the average photon capture probability $\overline{\eta}$ can be maximized. Fig. 5.2 shows the optimization of the beamwaist for the parameters used in the simulations of this paper. The results show that an optimum beamwaist can be found that maximizes the average photon capture probability. This maximum is the result of two counteracting effects when increasing the beamwaist. On the one hand, increasing the beamwaist increases the collimation of the beam and therefore results in a smaller spread of the spatial mode on the receiver aperture plane. On the other hand, as the beamwaist increases the truncation effects due to the finite aperture of the transmitter start to be relevant. These truncation effects account for the telescope's transmission probability and the diffraction induced due to the edges of the aperture.

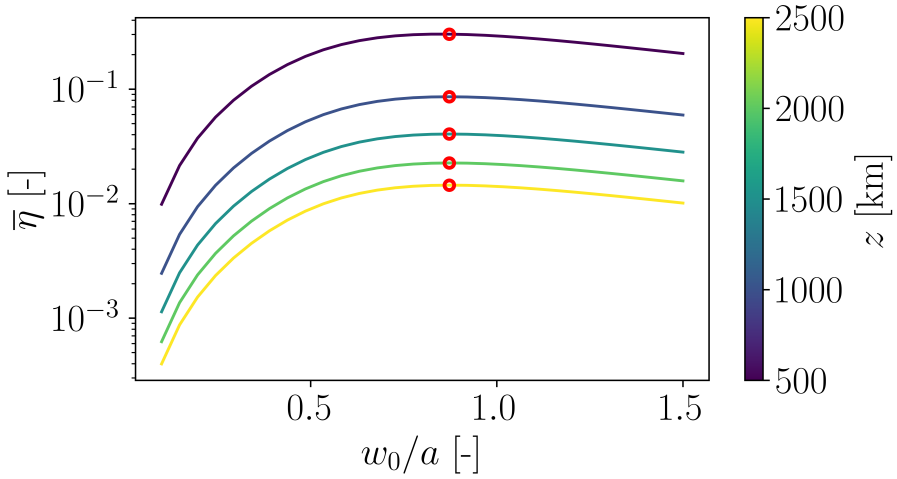

Figure 5.2: Optimization of the beamwaist for a pointing jitter $\sigma_{\text{PJ}} = 0.47\ \mu$rad, satellite's aperture $a = 15$ cm and ground station's aperture radius of 60 cm

As a result of this optimization the spatial spread of the single photon mode in the ground station's aperture plane can be significantly reduced, compared to a case in which $w_0 << a$. This optimum beam, when combined with the pointing jitter statistics, yields to a higher average photon capture probability $\overline{\eta}$. However, this effect comes along

with an increase on the fluctuation of the photon capture probability η around the average $\overline{\eta}$. Although this fluctuations can be very detrimental in classical communication links [23], this is not the case for quantum entanglement distribution. As shown in the Supplemental Material, the average photon capture probability is what matters on quantum entanglement distribution protocols affected by the pointing jitter stochastic process.

The effect of the atmospheric channel in the performance of the system has also been modeled. The atmospheric attenuation and scattering model presented in [24] has been used. Regarding the atmospheric turbulence, under weak turbulence conditions, the effect of beam spread and wander has been considered negligible for the downlinks at limited zenith angles considered in this work [19]. Moreover, the turbulence induced scintillation and the resulting coupling efficiency on the detector is accounted for on the coupling efficiency (CL) – this efficiency is obtained assuming an adaptive optics system on the ground station. Furthermore, other dynamic atmospheric effects that significantly impact the quality of the QKD link depending on time of day and weather are also taken into account. This is possible due to the framework developed in [24], where the sun irradiance – used to calculate the stray light impinging on the single-photon detectors – and atmospheric parameters – such as cloud coverage factor, weather visibility, and the relative angle between the satellite and the ground station telescope – are extracted at the ground station locations and used to determine noise levels and photon losses dynamically. We also model false detections assuming that there is a probability p_{dark} that a detector clicks despite no photon being received. We assume that this event translates into a detected state with zero fidelity with respect to the desired entangled state, leading to a lower bound in the overall fidelity measured at the ground.

5.2.3. PHOTON MEASUREMENT

At the ground stations, the incoming photons are randomly measured in either the Z basis—defined by the states $|H\rangle$ (horizontal) and $|V\rangle$ (vertical)—or the X basis, defined by $|D\rangle = (|H\rangle + |V\rangle)/\sqrt{2}$ (diagonal) and $|A\rangle = (|H\rangle - |V\rangle)/\sqrt{2}$ (antidiagonal). To implement this random-basis measurement, the photons first pass through a 50/50 beam splitter (BS). At one of the BS output ports, a half-wave plate (HWP) is used to rotate the measurement basis from Z to X. Both outputs are then directed into a polarizing beam splitter (PBS), which spatially separates the polarization components, as illustrated in Fig. 5.1(b).

Assuming the ideal entangled state $|\psi\rangle$ is received at the ground stations, it evolves as follows:

$$\frac{1}{\sqrt{2}}\left(|H\rangle_{A_a}|V\rangle_{B_a}+|V\rangle_{A_a}|H\rangle_{B_a}\right)\xrightarrow{B.S.}$$
$$\frac{1}{\sqrt{2}}\left(\frac{1}{\sqrt{2}}\left(|H\rangle_{A_c}+i|H\rangle_{A_d}\right)\frac{1}{\sqrt{2}}\left(|V\rangle_{B_c}+i|V\rangle_{B_d}\right)+\right.$$
$$\left.\frac{1}{\sqrt{2}}\left(|V\rangle_{A_c}+i|V\rangle_{A_d}\right)\frac{1}{\sqrt{2}}\left(|H\rangle_{B_c}+i|H\rangle_{B_d}\right)\right). \tag{5.2}$$

Here, the subscripts A_c, A_d, B_c, and B_d refer to the different spatial modes after the beam splitter for photons A and B, respectively. The output ports labelled "d" undergo a basis transformation via a HWP: $|H\rangle \rightarrow |D\rangle$ and $|V\rangle \rightarrow |A\rangle$.

Subsequently, each output passes through a PBS, which separates the polarization components before detection. The resulting state just before measurement is:

$$\frac{1}{2\sqrt{2}}\left(|H\rangle_{A_c}|0\rangle_{A_f}|0\rangle_{B_e}|V\rangle_{B_f}+i|H\rangle_{A_e}|0\rangle_{A_f}|0\rangle_{B_g}|A\rangle_{B_h}+\right.$$
$$i|D\rangle_{A_g}|0\rangle_{A_h}|0\rangle_{B_e}|V\rangle_{B_f}-|D\rangle_{A_g}|0\rangle_{A_h}|0\rangle_{B_g}|A\rangle_{B_h}+$$
$$|0\rangle_{A_e}|V\rangle_{A_f}|H\rangle_{B_e}|0\rangle_{B_f}+i|0\rangle_{A_e}|V\rangle_{A_f}|D\rangle_{B_g}|0\rangle_{B_h}+$$
$$\left.i|0\rangle_{A_g}|A\rangle_{A_h}|H\rangle_{B_e}|0\rangle_{B_f}-|0\rangle_{A_g}|A\rangle_{A_h}|D\rangle_{B_g}|0\rangle_{B_h}\right). \tag{5.3}$$

From Eq. (5.25), we observe that in half of the cases, the photon pairs are measured in the same basis (either Z or X). Consequently, during post-selection, approximately 50% of the events are discarded to ensure only measurements in matching bases are kept.

5.2.4. SECRET KEY RATE

The computation of the secret key rate (SKR) follows the model shown in [24], where both the assumption of depolarizing channel and Werner states produced by the entangled photon-pair source have been used. This analysis enables one to split the effect of losses and decoherence (loss of fidelity) in the channel, calculating them separately only to combine them when calculating the final secret key rate expression:

$$SKR = R_{\text{final}} \cdot (\max(0, 1-(1+\xi)\mathcal{H}(\text{QBER}))). \tag{5.4}$$

In the expression above, $\mathcal{H}$ is Shannon's entropy function, $\xi = 1.22$ is a factor representing the inneficiency of the classical protocol required for key extraction [21], and the QBER is calculated based on the total state fidelity (see Appendix 5.5.2).

$$\text{QBER} = \frac{1-\frac{3\mathcal{F}+1}{4}}{2}. \tag{5.5}$$

R_{final} depends on the rate of the source in the satellite and the total channel efficiency, i.e., source to ground station detector. This term can be decomposed in three main ones: the free-space path loss, governed by the divergence of the beam; the atmospheric attenuation factor, governed by the weather condition; and the detector efficiency, which varies significantly in case one chooses cryogenically-cooled detectors (higher efficiency, but fibre coupling is required), or free-space-coupled detectors (lower efficiency, no fibre coupling). For the purpose of this analysis, we choose to operate under the assumption that fibre coupling can be efficiently implemented via adaptive optics correction strategies, leading to an overall net improvement in the channel quality with the more efficient superconducting nanowire single-photon detectors (SNPDs). This assumption is also tied to a lower system jitter and lower detector dead times, which lead to higher signal-to-noise ratio (due to narrower available detection time windows and detection saturation rates).

In summary, the transmission from the satellite to the ground stations follows the expression

$$\begin{aligned} p_{T,A} &= \overline{\eta}_{Sat-GndA} \mathrm{ATML}_{Sat-GndA} \mathrm{CL}_{Sat-GndA} \\ p_{T,B} &= \overline{\eta}_{Sat-GndB} \mathrm{ATML}_{Sat-GndB} \mathrm{CL}_{Sat-GndB}. \end{aligned}$$

$\overline{\eta}$ accounts for the diffraction and pointing jitter losses (see Section 5.2.2), ATML for atmospheric attenuation and scattering loss, CL for coupling loss, and GndA/GndB for the two ground stations of interest. The detailed description of how each of these terms is evaluated can be found in the Supplemental Material. The reason for evaluating the two paths individually is the channel asymmetry during satellite transit, not only in terms of the dynamic conditions (such as weather condition) but also the distance between the spacecraft and either ground station.

Equipped with the overall loss term, the probabilities – per attempt – associated with the detection of a valid pair can be translated into raw detection rates via the source pair emission rate R. These are further translated into expected secret key rate using a key extraction algorithm that implements: basis reconciliation, error correction, and privacy amplification. As mentioned before, depending on the channel quality, the raw detection material that must be spent in order to produce a final key will change according to the classical protocols being used. Since this procedure can be quite computationally intensive and would have to be executed for each time step at each satellite pass, a look-up table was generated by feeding the software with a grid of parameters (QBER and block length).

5.3. PERFORMANCE

To evaluate the protocol's performance and quantify its optimization, we compute the SKR per satellite pass that reaches the ground stations over the course of one month—specifically, April 2025—while accounting for real-time weather conditions. Our analysis focuses on three links: Madrid–Barcelona, Madrid–Bilbao, and Madrid–Lisbon. We begin by computing the SKR per pass and, based on this, derive the usable secret key material per pass (see section 5.2.4). By averaging the usable key material per pass and taking into account the percentage of successful passes, we obtain the average secret key material rate, which we then compare against the requirements of Telefónica and JPMorgan use cases.

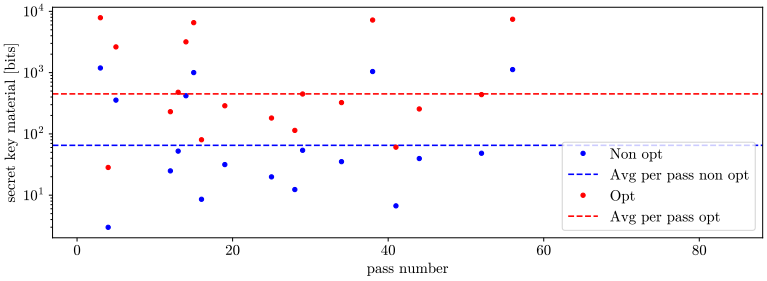

Figure 5.3: **Secret key material between Madrid and Bilbo** The blue data shows the usable key without carrying out the beam optimization, and the red data shows the results when applying the dynamical optimization of the beam. The discontinuous red line shows the average key per pass.

In Fig.5.3, we present the secret key material per satellite pass and its average for both the non-optimized and optimized cases on the Madrid–Bilbao link. The figure shows that real-time beam optimization results in an increase of the average secret key material by a factor of ten.

Links	Non opt [keys/s]	Telefonica	JPMorgan	Opt [keys/s]	Telefonica	JPMorgan
Mad-Bilb	0.003	No	No	0.018	Yes	No
Mad-Bcn	0.002	No	No	0.012	Yes	No
Mad-Lis	0.002	No	No	0.018	Yes	No

Table 5.1: Results for an entangled photon source like Micius $5.9 \cdot 10^6$ Hz[16].

Table 5.1 summarizes the computed results for the different links and compares them against two use cases: Telefónica, which requires 256 keys every 12 hours (equivalent to 0.006 keys/s), and JPMorgan, which

requires 256 keys every 2 minutes (2.13 keys/s). We observe that the 12-hour key renewal, used for communication between hospitals, is achieved across all links when the dynamic beam optimization is carried out.

However, for the more demanding use case of QKD-based VPNs, where the key must be refreshed every 2 minutes, the required key rate is not met. To get to such key requirements, we would need to improve the entangled photon source rate and reduce the coupling loss, CL, which we consider 0.5 due to the scintillation effect of the lowest parts of the atmosphere [25–27]. This coupling efficiency could be increased by considering free space coupling into the single photon detectors [28], or multimode fiber coupling [29, 30]. Additionally, we could use a constellation of satellites like Micius.

5.4. CONCLUSION

In summary, we have demonstrated how single-satellite architectures enable the extension of quantum key distribution (QKD) from metropolitan-scale deployments [18] to national-scale distances. Furthermore, we introduced a dynamic beam optimization method that accounts for satellite pointing jitter and varying satellite-ground distances, maximizing the transmission probability. This optimization allows us to meet the key rate requirements even for the current use cases of secure communication between two hospitals [18], using state-of-the-art satellite technology [16].

Our approach employs an entanglement-based QKD protocol, which eliminates the need for trusted nodes in the key distribution process, thereby reducing the risk of eavesdropping.

By upgrading the rate of the entangled photon source and improving the coupling efficiency, we could also meet the requirement for the most demanding use case [17].

To extend quantum communication to larger distances, the integration of quantum memories onboard satellites is needed [22, 24, 31, 32]. Currently, we assume trusted ground stations for classical information storage. However, incorporating quantum memories at the ground level would allow for the use of untrusted ground stations and enable the distribution of entanglement across nodes. This would open the door to a broader range of quantum technologies beyond QKD, including blind quantum computing [33, 34] and quantum-enhanced sensing networks [4–6].

In existing use cases, hybrid quantum algorithms are typically employed, where only the first layer involves quantum processing. As a natural progression, future work should investigate fully quantum algorithms and their corresponding key rate requirements.

5.5. APPENDIX

5.5.1. FREE SPACE CHANNEL MODEL

The model to calculate the probability of the single photon emitted by the satellite being captured by the ground station is detailed in this appendix. This model considers the effects of the beam propagation and the pointing jitter in a coupled manner. Furthermore, as the maximum average photon capture probability is obtained when the spatial Gaussian mode describing the single photon in the transmitter aperture is highly truncated, the model presented in this appendix also accounts for the diffraction effects due to this truncation. A more detailed explanation of this model can be found in [23].

The beamwaist w_0 of the spatial Gaussian mode is located at the satellite's telescope aperture. The telescope on board the satellite has a radius a. The field at the ground station's aperture plane, located at a distance z, can be computed numerically through Fresnel propagation [35]. This propagation gives the probability density function of the spatial location of the single photon, i.e. $I(x, y)$, in the ground station's aperture plane. Then, a convolution can be performed to compute the probability of capturing the single photon when the center of the beam is displaced to (x_0, y_0) in the ground station's reference system. This convolution can be computed using the convolution theorem by

$$g(x_0, y_0) = \mathcal{F}^{-1}\mathcal{F}(I) \cdot \mathcal{F}(A) \tag{5.6}$$

where $A(x, y)$ is the aperture function of the ground station's telescope and $\mathcal{F}$ is the bidimensional Fourier transform. The satellite pointing jitter is modeled as a bidimensional Gaussian probability density function of the location of the center of the beam at the ground station frame of reference (x_0, y_0),

$$f_{\mathrm{PJ}}(x_0, y_0) = \frac{1}{2\sigma^2} \exp\left(-\frac{x_0^2 + y_0^2}{2\sigma^2}\right) \tag{5.7}$$

where $\sigma = z\sigma_{\mathrm{PJ}}$, and σ_{PJ} is the angular pointing jitter. By combining the previous equations, the probability density function of the photon capture probability can be computed as [36]

$$f(\eta) = \iint_{\mathbb{R}^2} f_{\mathrm{PJ}}(x_0, y_0)\, \delta[\eta - g(x_0, y_0)]\, dx_0\, dy_0 \tag{5.8}$$

where $\delta(x)$ is the Dirac delta function. Finally, the average of this probability density function gives the average photon capture probability. As shown in the Supplementary Material, the latter is to be maximized in the context of quantum entanglement based QKD for optimal performance of the system. This maximization is done by varying the beamwaist w_0 of the spatial Gaussian mode transmitted.

5.5.2. FIDELITY OF THE FINAL STATE

In this appendix, we provide a more detailed calculation of how we compute the fidelity required for the secret key rate computation. The final state is of the form:

$$\rho_{\text{final}} = A|\psi\rangle\langle\psi| + B\rho_{\text{deph}} + C\rho_{\text{garb}}, \tag{5.9}$$

where $|\psi\rangle$ is the desired target state which gives fidelity 1, ρ_{deph} are the multi-photon states, where one photon for each elementary link has been lost, resulting in a dephased states which gives fidelity smaller than one, and ρ_{garb} is the non-specified 'garbage' density matrix with zero overlap with the desired target state. The (normalized) density matrix of the dephased state is the following:

$$\begin{aligned}\rho_{\text{deph}} = (5|H\rangle|V\rangle\langle H|\langle V| + 5|V\rangle|H\rangle\langle V|\langle H| + \\ |H\rangle|H\rangle\langle H|\langle H| + |V\rangle|V\rangle\langle V|\langle V|)/12,\end{aligned} \tag{5.10}$$

being the fidelity of the previous state:

$$F_{\text{deph}} = \langle\psi|\rho_{\text{deph}}|\psi\rangle = 5/12. \tag{5.11}$$

Therefore, the overall fidelity is:

$$F = \frac{\langle\psi|\rho_{\text{final}}|\psi\rangle}{Tr(\rho_{\text{final}})} = \frac{A + \frac{5}{12}B}{A + B + C}, \tag{5.12}$$

where the parameters A, B, C are the following:

$$A = \lambda(1-\lambda)p_{\text{T,A}}p_{\text{T,A}}, \tag{5.13}$$

$$B = 5\lambda^2 p_{\text{T,A}}p_{\text{T,B}}(1-p_{\text{T,A}})(1-p_{\text{T,B}}), \tag{5.14}$$

$$\begin{aligned}C = {} & \lambda(1-\lambda)\big(p_{\text{T,A}}(1-p_{\text{T,B}})p_{\text{dark}} + p_{\text{T,B}}(1-p_{\text{T,A}})p_{\text{dark}} \\ & + (1-p_{\text{T,A}})(1-p_{\text{T,B}})p_{\text{dark}}^2\big) \\ & + \lambda^2\big(3p_{\text{T,A}}(1-p_{\text{T,A}})(1-p_{\text{T,B}})^2 p_{\text{dark}} + \\ & 3p_{\text{T,B}}(1-p_{\text{T,B}})(1-p_{\text{T,A}})^2 p_{\text{dark}} \\ & + \frac{3}{2}(1-p_{\text{T,A}})^2(1-p_{\text{T,B}})^2 p_{\text{dark}}^2\big) + \\ & \frac{1}{2}(1-\lambda)^2 p_{\text{dark}}^2.\end{aligned} \tag{5.15}$$

5.6. SUPPLEMENTARY MATERIAL

In this supplemental material we present the details of the quantum key distribution model discussed in the main text. We start by discussing

the different steps at the hardware level, detailing the modelling of the spontaneous parametric down-conversion (SPDC) source, the transmission loss from the satellite to the ground station and the setup at the ground stations. Finally, we present the details of the transmission loss due to pointing jitter and beam divergence. The average photon capture probability as a performance parameter is justified. Furthermore, the effect of truncation due to the finite transmitter aperture in the transmitted beam and the resulting average photon capture probability are studied. Additionally, the optimum Gaussian beams are presented with and without the effects of truncation.

5.7. QUANTUM HARDWARE MODELLING

5.7.1. SPONTANEOUS PARAMETRIC DOWN-CONVERSION SOURCE

Here, we consider second-photon emissions in the entangled photon source. Following the work shown in [21], the expression for the spontaneous-parametric down conversion (SPDC) source is the following:

$$
\begin{aligned}
|\psi_{\text{source}}\rangle = (1-\lambda)\,(|0,0\rangle_{A,B} + \\
\frac{\sqrt{2}\lambda^{1/2}}{(1-\lambda)^{1/2}}\frac{1}{\sqrt{2}}(|H\rangle_A|V\rangle_B + |V\rangle_A|H\rangle_B) + \\
\frac{\sqrt{3}\lambda}{1-\lambda}\frac{1}{\sqrt{3}}\big(|2H\rangle_A|2V\rangle_B + |HV\rangle_A|HV\rangle_B + |2V\rangle_A|2H\rangle_B\big)\Big),
\end{aligned}
\tag{5.16}
$$

where $\mu = 2\lambda$ is the average number of photon pairs generated by one pump laser, characterised by the brightness of the SPDC source. The state $1/\sqrt{2}\,(|H\rangle_A|V\rangle_B + |V\rangle_A|H\rangle_B) = |\psi\rangle$ is the desired entangled state, and $1/\sqrt{3}\big(|2H\rangle_A|2V\rangle_B + |HV\rangle_A|HV\rangle_B + |2V\rangle_A|2H\rangle_B\big) = |\psi_{\text{multi}}\rangle$ is the two-photon state.

5.7.2. FREE-SPACE, ATMOSPHERE PROPAGATION AND PHOTON MEASUREMENT

After the SPDC source, the photons are sent from the satellite to the ground stations. The free space and atmospheric loss are modelled as a fictitious beam splitter with transmission p_T determined by the optical link budget. The transmission of a single photon is the following:

$$\hat{a}^{\dagger}_{H,A(B)}|0\rangle_{A,(B)}|0\rangle_{E_A,(E_B)} \rightarrow \sqrt{p_{T,A(B)}}\hat{a}^{\dagger}_{H,A(B)}|0\rangle_{A,(B)}|0\rangle_{E_A,(E_B)} + \sqrt{1-p_{\mathrm{T,A(B)}}}\hat{a}^{\dagger}_{H,E_A(E_B)}|0\rangle_{A(B)}|0\rangle_{E_A,(E_B)}, \quad (5.17)$$

$$\hat{a}^{\dagger}_{V,A(B)}|0\rangle_{A,(B)}|0\rangle_{E_A,(E_B)} \rightarrow \sqrt{p_{T,A(B)}}\hat{a}^{\dagger}_{V,A(B)}|0\rangle_{A,(B)}|0\rangle_{E_A,(E_B)} + \sqrt{1-p_{\mathrm{T,A(B)}}}\hat{a}^{\dagger}_{V,E_A(E_B)}|0\rangle_{A(B)}|0\rangle_{E_A,(E_B)}, \quad (5.18)$$

where the subscripts A and B denote the different spatial modes, and the subscript E denotes the loss mode. So, for example, for the state $|\psi\rangle$ we will have that the state is transmitted with probability $p_{\mathrm{T,A}}p_{\mathrm{T,B}}$, or that we lose a photon in one of the arms with probability $p_{\mathrm{T,A(B)}}(1-p_{\mathrm{T,B(A)}})$ leaving a dephased state $\rho_{\mathrm{deph0,A(B)}} \otimes |0\rangle_{\mathrm{B(A)}}\langle 0|$, where $\rho_{\mathrm{deph0}} = \frac{1}{2}(|H\rangle\langle H| + |V\rangle\langle V|)$, or that with probability $(1-p_{\mathrm{T,A}})(1-p_{\mathrm{T,B}})$ we lose both photons. Mathematically, it goes as follows:

$$\begin{aligned}|\psi\rangle \rightarrow\ & \frac{1}{\sqrt{2}}\big(\sqrt{p_{\mathrm{T,A}}p_{\mathrm{T,B}}}(|H\rangle_A|0\rangle_{E_A}|V\rangle_B|0\rangle_{E_B} + |V\rangle_A|0\rangle_{E_A}|H\rangle_B|0\rangle_{E_B}) + \\ & \sqrt{p_{\mathrm{T,A}}(1-p_{\mathrm{T,B}})}\big(|H\rangle_A|0\rangle_{E_A}|0\rangle_{E_B}|V\rangle_{E_B} + |V\rangle_A|0\rangle_{E_A}|0\rangle_B|H\rangle_{E_B}\big) + \\ & \sqrt{p_{\mathrm{T,B}}(1-p_{\mathrm{T,A}})}\big(|0\rangle_A|H\rangle_{E_A}|V\rangle_B|0\rangle_{E_B} + |0\rangle_A|V\rangle_{E_A}|H\rangle_B|0\rangle_{E_B}\big) + \\ & \sqrt{(1-p_{\mathrm{T,A}})(1-p_{\mathrm{T,B}})}\big(|0\rangle_A|H\rangle_{E_A}|0\rangle_B|V\rangle_{E_B} \\ & + |0\rangle_A|V\rangle_{E_A}|0\rangle_B|H\rangle_{E_B}\big)\big). \end{aligned} \quad (5.19)$$

After the photons pass through the atmosphere, they reach the ground stations. There, photons are randomly measured either in the Z basis- defined by the states $|H\rangle$ and $|V\rangle$- or in the X basis- defined by $|D\rangle = (|H\rangle + |V\rangle)/\sqrt{2}$ and $|A\rangle = (|H\rangle - |V\rangle)/\sqrt{2}$. To implement this random-basis measurement, the photons first pass through a 50/50 beam splitter (BS). At one of the BS output ports, a half-wave plate (HWP) is used to rotate the measurement basis from Z to X. Both outputs are then directed into a polarizing beam splitter (PBS), which spatially separates the polarization components.

We assume that the beam splitter transformations are of the following form:

$$|H\rangle_1 \rightarrow \frac{1}{\sqrt{2}}(|H\rangle_3 + |H\rangle_4) \quad ; \quad |H\rangle_2 \rightarrow \frac{1}{\sqrt{2}}(|H\rangle_3 - |H\rangle_4) \quad (5.20)$$

$$|V\rangle_1 \rightarrow \frac{1}{\sqrt{2}}(|V\rangle_3 + |V\rangle_4) \quad ; \quad |V\rangle_2 \rightarrow \frac{1}{\sqrt{2}}(|V\rangle_3 - |V\rangle_4). \quad (5.21)$$

Assuming the ideal entangled state $|\psi\rangle$ is received at the ground stations, it evolves as follows:

$$\frac{1}{\sqrt{2}}\left(|H\rangle_{A_a}|V\rangle_{B_a}+|V\rangle_{A_a}|H\rangle_{B_a}\right)\xrightarrow{B.S.}$$
$$\frac{1}{\sqrt{2}}\left(\frac{1}{\sqrt{2}}\left(|H\rangle_{A_c}+i|H\rangle_{A_d}\right)\frac{1}{\sqrt{2}}\left(|V\rangle_{B_c}+i|V\rangle_{B_d}\right)+\right.$$
$$\left.\frac{1}{\sqrt{2}}\left(|V\rangle_{A_c}+i|V\rangle_{A_d}\right)\frac{1}{\sqrt{2}}\left(|H\rangle_{B_c}+i|H\rangle_{B_d}\right)\right). \tag{5.22}$$

Here, the subscripts A_c, A_d, B_c, and B_d refer to the different spatial modes after the beam splitter for photons A and B, respectively. The output ports labelled "d" undergo a basis transformation via a HWP: $|H\rangle \rightarrow |D\rangle$ and $|V\rangle \rightarrow |A\rangle$.

Subsequently, each output passes through a PBS, which separates the polarization components before detection. The resulting state just before measurement is:

$$\frac{1}{2\sqrt{2}}\left(|H\rangle_{A_c}|0\rangle_{A_f}|0\rangle_{B_e}|V\rangle_{B_f}+i|H\rangle_{A_e}|0\rangle_{A_f}|0\rangle_{B_g}|A\rangle_{B_h}+i|D\rangle_{A_g}|0\rangle_{A_h}|0\rangle_{B_e}|V\rangle_{B_f}-\right.$$
$$|D\rangle_{A_g}|0\rangle_{A_h}|0\rangle_{B_g}|A\rangle_{B_h}+|0\rangle_{A_e}|V\rangle_{A_f}|H\rangle_{B_e}|0\rangle_{B_f}+i|0\rangle_{A_e}|V\rangle_{A_f}|D\rangle_{B_g}|0\rangle_{B_h}+$$
$$\left.i|0\rangle_{A_g}|A\rangle_{A_h}|H\rangle_{B_e}|0\rangle_{B_f}-|0\rangle_{A_g}|A\rangle_{A_h}|D\rangle_{B_g}|0\rangle_{B_h}\right). \tag{5.23}$$

From Eq. (5.23), we observe that in half of the cases, the photon pairs are measured in the same basis (either Z or X). Consequently, during postselection, approximately 50% of the events are discarded to ensure only measurements in matching bases are kept.

Additionally, we take into account dark counts in the detectors. A dark count is when a detector clicks for a vacuum input. The probability of this happening is p_{dark}, i.e. a detector will click when receiving vacuum input with probability p_{dark}. Since $p_{\text{dark}}, p_T \ll 1$, we discard third-order terms, implying that we will not consider terms with probability $p_T^2 p_{\text{dark}}, p_{\text{dark}}^2 p_T$ and similar. Therefore, from Eq.(5.19), and considering that we postselect states with opposite polarizations in the same basis, we get the desired state, $|\psi\rangle$, with probability $\lambda(1-\lambda)p_{\text{T,A}}p_{\text{T,B}}$, with probability $\lambda(1-\lambda)p_{T,A(B)}(1-p_{T,B(A)})p_{\text{dark}}$ one of the photons has gotten lost in transmission, and with probability $\lambda(1-\lambda)(1-p_{\text{T,A}})(1-p_{\text{T,B}})p_{\text{dark}}^2$, both photons get lost in transmission.

In the case of the two-photon state, $|\psi_{\text{multi}}\rangle$, discarding third-order terms, we can lose one photon in each arm, which leads to the following dephased state:

$$\rho_{\text{deph}} = \frac{1}{12}\left(5|H\rangle_A|V\rangle_B\langle H|_A\langle V|_B+5|V\rangle_A|H\rangle_B\langle V|_A\langle H|_B+\right.$$
$$\left.|H\rangle_A|H\rangle_B\langle H|_A\langle H|_B+|V\rangle_A|V\rangle_B\langle V|_A\langle V|_B\right), \tag{5.24}$$

where, considering that we post-select the measurements with opposite polarizations in the same basis, we will get the aforementioned depolarized state with probability $5\lambda^2 p_{\mathrm{T,A}} p_{\mathrm{T,B}} (1-p_{\mathrm{T,B}})(1-p_{\mathrm{T,A}})$. Additionally, we can also lose three photons and get a valid measurement due to dark counts with probabilities $3\lambda^2 p_{\mathrm{T,A}}(1-p_{\mathrm{T,A}})(1-p_{\mathrm{T,B}})^2 p_{\mathrm{dark}}$ and $3\lambda^2 p_{\mathrm{T,B}}(1-p_{\mathrm{T,B}})(1-p_{\mathrm{T,A}})^2 p_{\mathrm{dark}}$.

We can also measure states that give zero fidelity with probabilities $3\lambda^2(1-p_{\mathrm{T,A}})^2(1-p_{\mathrm{T,B}})^2 p_{\mathrm{dark}}^2/2$, $(1-\lambda)^2 p_{\mathrm{dark}}^2/2$.

Therefore, we can write the final state as:

$$\rho_{\mathrm{final}} = A|\psi\rangle\langle\psi| + B\rho_{\mathrm{deph}} + C\rho_{\mathrm{garb}}, \tag{5.25}$$

where ρ_{deph} is the dephased state shown in Eq.(5.24), and ρ_{garb} is the non-specified 'garbage' density matrix with zero overlap with the desired target state.

$$A = \lambda(1-\lambda) p_{\mathrm{T,A}} p_{\mathrm{T,B}}, \tag{5.26}$$

$$B = 5\lambda^2 p_{\mathrm{T,A}} p_{\mathrm{T,B}} (1-p_{\mathrm{T,A}})(1-p_{\mathrm{T,B}}), \tag{5.27}$$

$$\begin{aligned} C \;=\; & \lambda(1-\lambda)\big(p_{\mathrm{T,A}}(1-p_{\mathrm{T,B}})p_{\mathrm{dark}} + p_{\mathrm{T,B}}(1-p_{\mathrm{T,A}})p_{\mathrm{dark}} + \\ & (1-p_{\mathrm{T,A}})(1-p_{\mathrm{T,B}})p_{\mathrm{dark}}^2\big) + 3\lambda^2\big(p_{\mathrm{T,A}}(1-p_{\mathrm{T,B}})^2(1-p_{\mathrm{T,A}})p_{\mathrm{dark}} + \\ & p_{\mathrm{T,B}}(1-p_{\mathrm{T,A}})^2(1-p_{\mathrm{T,B}})p_{\mathrm{dark}}\big) + \\ & \frac{3}{2}\lambda^2(1-p_{\mathrm{T,B}})^2(1-p_{\mathrm{T,A}})^2 p_{\mathrm{dark}}^2 + \frac{1}{2}(1-\lambda)^2 p_{\mathrm{dark}}^2. \end{aligned} \tag{5.28}$$

5.8. FIDELITY

To compute the fidelity, we consider the final state from Eq.(5.25), where $|\psi\rangle$ gives fidelity 1, ρ_{garb} are all the states that give fidelity zero, and ρ_{deph} are the multi-photon states, where one photon for each elementary link has been lost, resulting in a dephased state which gives fidelity smaller than one. To know the exact fidelity that, on average, these states give, we go to Eq.(5.24) and consider the terms where one photon has been lost in each elementary link. The (normalized) density matrix of this state is the following:

$$\begin{aligned} \rho_{\mathrm{deph}} \;=\; & \frac{1}{12}\big(5|H\rangle_A|V\rangle_B\langle H|_A\langle V|_B + 5|V\rangle_A|H\rangle_B\langle V|_A\langle H|_B + \\ & |H\rangle_A|H\rangle_B\langle H|_A\langle H|_B + |V\rangle_A|V\rangle_B\langle V|_A\langle V|_B\big) \end{aligned} \tag{5.29}$$

And the average fidelity this dephased state gives is:

$$F_{\text{deph}} = \langle\psi|\rho_{\text{deph}}|\psi\rangle = 5/12 \tag{5.30}$$

And the overall fidelity is:

$$F = \frac{\langle\psi|\rho_{\text{final}}|\psi\rangle}{Tr(\rho_{\text{final}})} = \frac{A + \frac{5}{12}B}{A + B + C}. \tag{5.31}$$

5.9. FREE SPACE CHANNEL MODELLING

In this section we show the models developed for evaluating the free space channel losses. Firstly the average photon capture probability as a performance parameter for a downlink channel under a stochastic pointing jitter is justified. Then, a model to accurately compute the average photon capture probability is presented. This model consider the truncation effects on the transmitted single photon spatial modes. Finally, the atmospheric channel model used for our analysis is explained.

5.9.1. AVERAGE PHOTON CAPTURE PROBABILITY

In this section, a demonstration of the average photon-pair capture probability as a valuable parameter to evaluate the performance of quantum entanglement distribution from a satellite is presented.

Consider a Gaussian beam traveling from the transmitter satellite to the ground station. Although in reality the light beam would deviate from an ideal Gaussian shape (due to e.g. atmospheric turbulence and truncation due to finite aperture), this shape can be considered for the present discussion. In Sec. 5.9.2 the effect of the truncation due to the finite transmitter aperture is considered. As seen by the ground station, the transmitter's pointing jitter will stochastically deviate the center of the Gaussian beam from the center of the receiver's aperture. This stochastic deviation will in turn create variations of the photon capture probability in the free space channel.

To evaluate the process of capturing a photon at the ground station under the stochastic nature of the pointing jitter, the different timescales involved in the system have to be thoroughly assessed. We have three different timescales that have to be considered in an scenario involving a satellite downlink:

1. *Timescale of the link distance variation*. This timescale refers to the characteristic time in which the distance between the transmitter (satellite) and the receiver (ground station) significantly changes. A significant change would be one that has a non-negligible impact on the photon capture probability due to the change in the link distance. This timescale is usually in the order of minutes for the LEO satellite considered, $\tau_D = \mathcal{O}(10^1)$ seconds.

2. *Timescale of the pointing jitter*. This timescale is the correlation time of the pointing jitter process. Due to the nature of the microvibration sources onboard satellites and the limitations of the fine pointing assembly this is usually in the order of milliseconds, $\tau_{PJ} = \mathcal{O}(10^{-3})$ seconds [37].

3. *Timescale of the photon emission*. The rate at which the single photons are emitted from the source is also relevant for the discussion. On demand single photon sources of interest to this application can work on the order of MHz∼GHz [16, 38]. Therefore, the characteristic timescale of this process is $\tau_{SPS} = 1/\nu_{SPS} = \mathcal{O}(10^{-6}) \sim \mathcal{O}(10^{-9})$ seconds.

Considering these timescales, we can see that over a pointing jitter correlation time (milliseconds) the photon capture probability variation due to the distance change can be considered quasi-static. Furthermore, over each realization of the pointing jitter in the order of fractions of milliseconds, at least thousands of photons will be sent due to the single photon source rate. Hence, in each of this pointing jitter realizations, as the light beam and its position are fixed, the photon capture probability for these thousands of photons will be the same. Hence in a single realization of the pointing jitter that lasts for $\Delta\tau_R$, where $\tau_{SPS} \ll \Delta\tau_R \sim \tau_{PJ}$, the number of photons captured follows a binomial distribution $X \sim B(N, \eta)$ with $N = \Delta\tau_R\, \nu_{SPS}$ and η is the instantaneous photon capture probability given by the divergence of the light beam and the pointing error value at that realization.

5

ENTANGLED PAIR CAPTURE PROBABILITY UNDER POINTING JITTER

Due to the pointing jitter, the photon capture probability for *each* of the downlink channels varies over time. Lets consider the case in which we send a pair of entangle photons. The first photon travels through channel 1, while the second photon travels through channel 2. The photon capture probability η_1 in channel 1 considering pointing jitter is given by a probability density function $f_1(\eta_1)$. In the same way, the photon capture probability in channel 2 (η_2) is given by a probability density function $f_2(\eta_2)$. We will consider that these two stochastic processes are completely uncorrelated. This assumption comes from the fact that, in general, each of the two downlink beams will be controlled by a different fast steering assembly [16].

We will now try to calculate the probability of capturing both entangled photons in their respective stations. In a single realization of these two channels, the probability of the channel 1 being under the condition $\in (\eta_1, \eta_1 + d\eta_1)$ is $f_1(\eta_1)\, d\eta_1$. Hence, the probability of the photon being captured when the channel is in $\in (\eta_1, \eta_1 + d\eta_1)$ is $\eta_1 f_1(\eta_1)\, d\eta_1$. An analogous derivation for channel 2 yields $\eta_2 f_2(\eta_2)\, d\eta_2$. At a certain

realization of channels 1 and 2, the probability of capturing both entangled photons is given by $\eta_\infty = \eta_1 \cdot \eta_2$ (recalling that the pointing jitter in these channels are statistically independent). Hence, the probability density function of the probability of both photons being captured is given by [36]

$$f_\infty(\eta_\infty) = \int_{\eta_\infty}^{1} f_1(\eta_1) f_2\left(\frac{\eta_\infty}{\eta_1}\right) \frac{1}{\eta_1}\, d\eta_1, \qquad \eta_\infty \in (0,1] \tag{5.32}$$

And the average of this probability density function

$$\overline{\eta}_\infty = \overline{\eta}_1 \cdot \overline{\eta}_2 = \int_0^1 f_\infty(\eta_\infty) \cdot \eta_\infty \cdot d\eta_\infty \tag{5.33}$$

where the first equality is due to the statistical independence of the channels. As mentioned before, over each realization of the pointing jitter, there will be a huge number N of entangled-photon pairs send through the same channel. Furthermore, considering that each of these entangled pairs are uncorrelated from each other w.r.t. their spatial location, then the probability of capturing k pairs of entangled photons in the ground stations when a total of N are sent through the double downlink channel at condition η_∞ is given by a binomial distribution

$$f(k, N, \eta_\infty) = \binom{N}{k} \eta_\infty^k (1-\eta_\infty)^{(N-k)} \tag{5.34}$$

because each of the entangled-photon pair capture event is independent. This will be the statistics describing the number of photons captured over a specific instant in time. Over a time period Δt_P longer than the pointing jitter characteristic time $\Delta t_\mathrm{P} \gg \tau_\mathrm{PJ}$, the number of photons captured will be given by the weighted sum of binomial distributions. The weighting will be given by the density function $f_\infty(\eta_\infty)$. Hence if in this time period Δt_P the total number of photons emitted by the source is $N_\mathrm{P} = \nu_\mathrm{SPS} \cdot \Delta t_\mathrm{P}$, the probability of capturing k entangled photons is given by

$$f_\mathrm{P}[k, N_\mathrm{P}, f_\infty(\eta_\infty), \eta_\infty] = \int_0^1 f_\infty(\eta_\infty) f(k, N_\mathrm{P}, \eta_\infty)\, d\eta_\infty = \binom{N_\mathrm{P}}{k} \int_0^1 f_\infty(\eta_\infty)\, \eta_\infty^k (1-\eta_\infty)^{(N_\mathrm{P}-k)}\, d\eta_\infty \tag{5.35}$$

Hence, the number of entangled photons captured over a period Δt_P, does no longer follow a binominal distribution. It follows the weighted binomial distribution given in Eq. (5.35), the weighting being given by the statistics of the photon capture probability due to the pointing

jitter (and atmospheric effects in case they are considered). Hence, over a single pass of the satellite, the photon capture statistics can be computed by considering each time step t_i where $t_{i+1} - t_i = \Delta t_P$ (where Δt_P is in the timescale of the link distance variation $\sim \tau_D$). In each of this time steps the entangled-photon pair capture probability is given by η_∞^i, and hence described by the density function f_∞^i. The variation of this density function is due to the variation of the distance (and other considerations) in each of the elementary links.

According to the discussion above, we now have a model to exactly obtain the photon capture probability considering the stochastic disturbances impinging the channel (pointing jitter and atmospheric effects). The equations above can not be solved analytically, as already the density functions of the photon capture probability of each of the channels, i.e. $f_{1,2}(\eta_{1,2})$, do not have a closed form in the general case [39].

Our objective is to know if the *average entangled-photon capture probability* $\overline{\eta}_\infty$ is a good performance parameter for evaluating the performance of quantum entanglement distribution protocols. As this probability can be obtained by multiplying the average of each of the channels $\overline{\eta}_1$ and $\overline{\eta}_2$, this is very convenient. Remember that the entangled-photon capture probability is averaged out over the pointing jitter statistics in this case. We will consider photons in the spatial Gaussian fundamental mode, and pointing jitters given by Gaussian bi-variate density functions [40]. We will now numerically demonstrate the statistics obtained for Eq. 5.32 and 5.35.

In Fig. 5.4 the results for a Monte Carlo simulation over a second are shown when both satellites are at 500 km distance from both ground stations. The pointing jitter considered for all the simulations is the one reported in the Micius satellite [37], i.e. $\sigma_{PJ} = 0.47$ μrad. The entangled-photon pair source rate is the one also reported for this satellite 5.9 MHz. In this figure two scenarios are presented: non-optimized and optimized beams. The non-optimized beam (shown in red color in the figures), refers to a Gaussian beam with a 10 μrad full width divergence approximately equal to the one reported in Ref. [41]. On the other hand, the optimized beam (shown in green color in the figures), refers to a Gaussian beam with a beamwidth w_0 that is 80% of the transmitter's telescope radius of 15 cm, being the truncation effects of the transmitted beam negligible. This gives a divergence of approximately 4 μrad for the optimized beam. It can be seen in the figure that the fluctuations over the average are much higher in the optimized case than in the non-optimized case. Although this fluctuations around the average can be very detrimental in classical communication links [42], this is not the case for quantum entanglement distribution. Furthermore, in the bottom of Fig. 5.4 the cumulative number of entangled-photon pairs over time is shown, comparing it to

the linear fit given by the average entangled-photon capture probability $\overline{\eta}_\infty = \overline{\eta}_1\overline{\eta}_2$. It is shown that almost no difference can be found between the two of them in both the non-optimized and the optimized channels. It is important to mention that the density function shown for η_∞ in the Monte Carlo simulations, corresponds to Eq. (5.35) derived before.

To understand the behavior of the double downlink channel over a longer time period, the approximate time period of satellite pass is simulated. Maintaining the distance from the two ground stations to the satellite constant and equal, the distribution of the entangled-pairs per second is shown in Fig. 5.5. The binomial distribution with the same average entangled-photon capture rate are also shown. For a more realistic assessment, Fig. 5.6 shows the simulation considering the distance variation over time from each of the satellites. For this simulation a typical pass over a satellite at an altitude of 400 km passing over Madrid and Lisbon has been considered, considering at each time the distance from the satellite to the respective ground station (Madrid and Lisbon in this case).

By comparing the optimized beam presented is one that tries to maximize (up to the limit in which the truncation effect are negligible) the average photon capture probability for each of the channels. This is done for single photons in the spatial Gaussian mode by minimizing the width of the beam in the ground station. This maximization of the average however, comes at the cost of the fluctuations of the capture probability over this average being increased too. Although this last trade-off has to be considered in classical channels (captured power instead of capture probability for classical communications), it has been proven in this section that for the dynamical processes considered, the maximization of the average is to be pursued in quantum entanglement distribution channels. The latter should be done even when the fluctuations increase drastically in this optimization, as it results in a larger number of entangled photons captured in both ground stations over a satellite pass.

5.9.2. EFFECT OF CLIPPING AND POINTING JITTER

In the previous section, it has been proven that the maximization of the average capture photon probability for each channel should be pursued in satellite quantum entanglement distribution systems. However, and only for the sake of the demonstration, the single photon have been considered to be described by the spatial Gaussian fundamental mode. However, trying to maximize the average photon capture probability for each channel means making the spread of this spatial Gaussian mode as small as possible in the ground station. This in turn is achieved by collimating the beam as much as possible in the transmitter aperture plane. Hence, this means making the beamwaist w_0 as big as possible

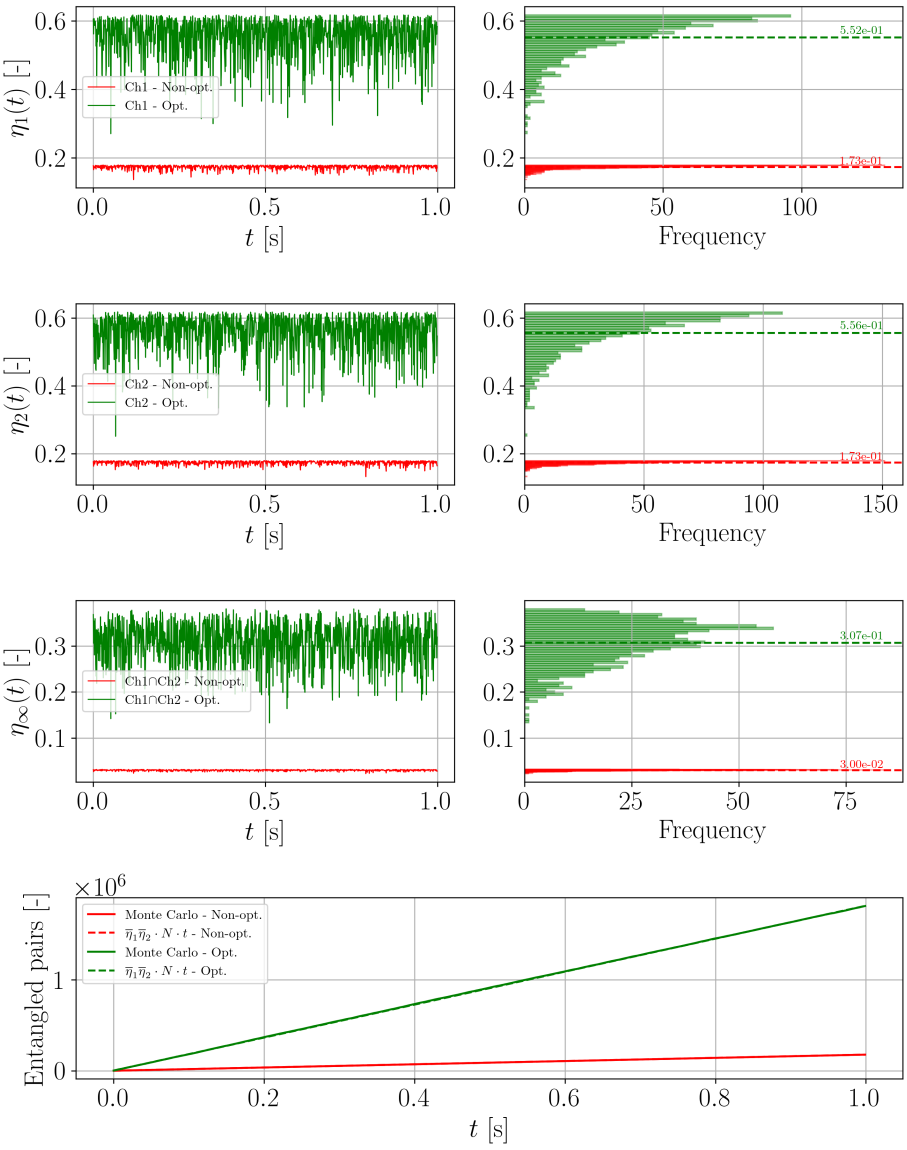

Figure 5.4: Monte Carlo simulation of the capture probabilities and the accumulated entangled-pair over a second. First three rows show the variation over time of the respective capture probabilities and the probability distributions associated. The bottom figure shows the cumulative entangled-photon pairs capture by both ground stations over time.

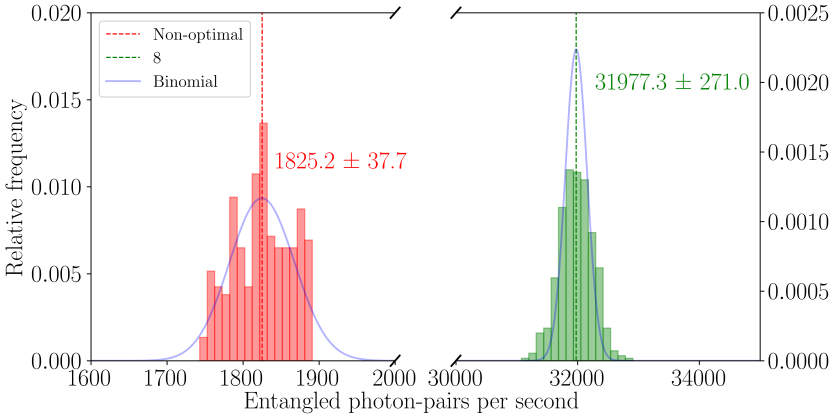

Figure 5.5: Probability distribution of the entangled-photon pair capture rate from the satellite to two ground stations at 500 km distance.

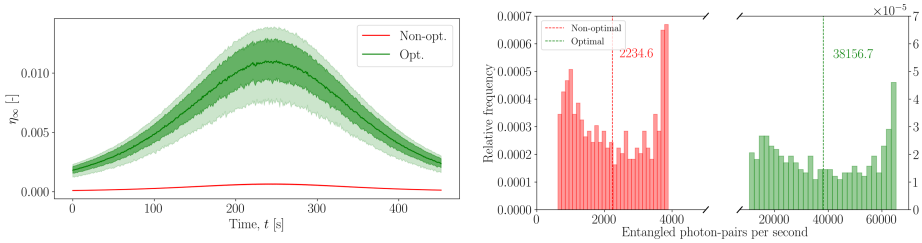

Figure 5.6: Entangled-photon pair capture statistics over a realistic satellite pass connecting Madrid and Lisbon. (Left) shows the variation of the entangled-photon pair capture probability over the satellite pass, where the filled areas delimit the 10%-90-% and the 25%-75% quantiles. (Right) shows the probability distribution of the entangled-photon pair capture rate over the pass.

in the transmitter aperture plane. It is however important to mention that this trend follows up to a certain w_0, as the beamwidth at distance z is given by $w_z = w_0\sqrt{1+z^2\lambda^2/(\pi^2 w_0^4)}$, where λ is the wavelength of the beam. This point is reached for beamwaists w_0 much higher than the apertures of the transmitters considered for the satellite terminal (e.g. the point is reached for $w_0 \approx 35$ cm for a distance of 500 km).

Hence, in principle making the beamwaist w_0 larger on the satellite aperture plane will create a smaller beamwidth in the ground station location, and therefore a higher average photon capture probability.

However, as the beamwaist of the spatial Gaussian mode is increased, the border effects due to the finite size of the transmitter's aperture will start to play a role. The truncation of the Gaussian mode due to the transmitter's aperture will create a loss on the probability of transmitting the single photon. Furthermore, the truncation of the Gaussian mode will induce a diffraction that will change the divergence of the transmitted mode. The latter will no longer be purely Gaussian due to this diffraction effect.

OPTIMIZATION OF THE TRANSMITTED BEAM

All considered, as the truncation of the Gaussian beam is relevant when aiming for beams that have a small far-field beamwidth, a complete optical propagation model is required to accurately calculate the spatial mode associated with the single photon on the receiver side. By using the model presented in [23], the average photon capture probability, accounting for truncation effects, can be obtained for a given pointing jitter, Gaussian beamwaist, and aperture sizes involved. This model propagates the spatial mode of the single photon from the transmitter plane to the receiver plane through Fourier optics. Then the the spatial mode of the single photon in the receiver aperture plane is combined with the pointing jitter statistics to obtain the probability density of the photon capture probability. From this density function, the average photon capture probability for the individual channel can be obtained.

Furthermore, by maximizing this average an optimization of the transmitted beam can be performed that optimizes the performance of the quantum entanglement distribution system according to Sec. 5.9.1. The results for such an optimization for a distance of 400 km and a ground station aperture radius of 60 cm are presented in Fig. 5.7, for different transmitter aperture radii a and transmitter angular pointing jitters. In this manner, the optimal transmitted beam for a given set of parameters is computed and the maximum average photon capture probability is assigned to the channel at each instant of time.

5.9.3. ATMOSPHERIC EFFECTS

As the single photon state propagates through the atmosphere there are several atmospheric effects that need to be assessed. Firstly, the atmospheric absorption and scattering reduce the probability of the photon being capture by the receiver. This is modeled in our analysis according to Ref. [44]. Secondly, there are several turbulence induced effects. The stochastic change of the index of refraction due to the atmospheric turbulence will mainly create: beam spread, beam wander and scintillation. Under the weak turbulence conditions considered in this paper the beam spread and wander effects are negligible in downlink channels [19]. The zenith angle of the downlink is limited

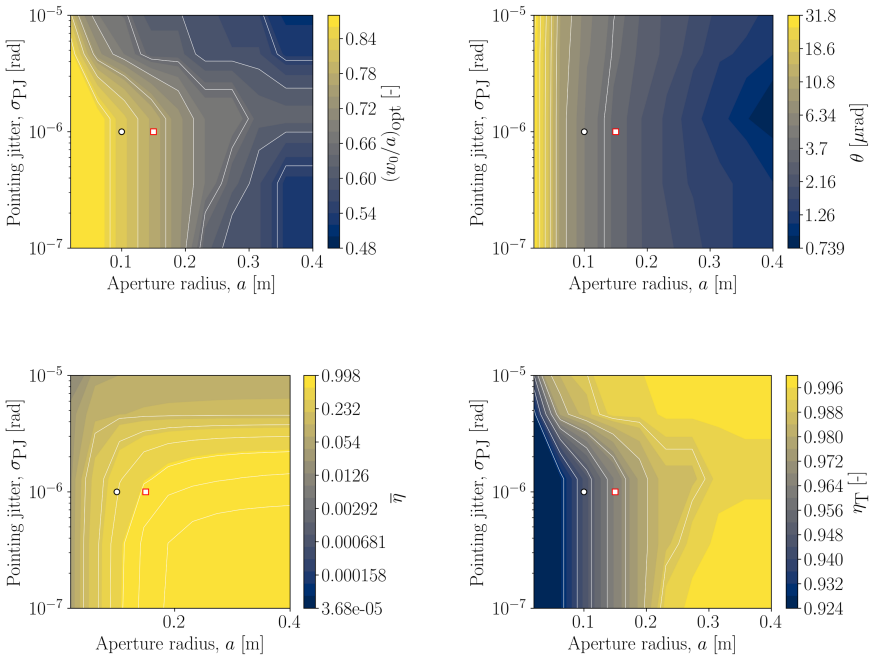

Figure 5.7: Optimization of the truncated Gaussian beam for different transmitter aperture sizes a and pointing jitters σ_{PJ} using the full numerical propagation model in [23]. Top-left is the optimum beam-waist to aperture ratio. Top-right is the divergence of the resulting optimum beam. Bottom-left is the optimum average photon capture probability (maximum obtainable). Bottom-right is the transmission efficiency of the telescope (i.e. the probability of losing the single photon on the transmitter's aperture). The circle and square points show the characteristics of the Jinan and Micius satellites respectively [16, 43].

to 70º for the simulations, where the effect of beam spread and other atmospheric effects is limited [45].

Concerning the scintillation there are several things that need to be considered. Assuming weak turbulence and large diameter of the ground station's telescope, the turbulence induced scintillation is already diminished [19]. Furthermore, for the results obtained the ground station is assumed to have an adaptive optics system that counteracts for the variations due to the scintillation on the fiber coupling. An overall detector coupling efficiency of $CL = 0.5$ is assumed, which is in agreement with simulations and experimental data in optical

downlink channels with adaptive optics and single mode fiber coupling [25–27]. This coupling efficiency could be increased by considering free space coupling into the single photon detectors [28], or multimode fiber coupling [29, 30] (maintaining the adaptive optics system). Finally, considering the specific application of QKD, previous studies have shown that scintillation has minimal impact on this quantum communication protocols [46].

REFERENCES

[1] C. H. Bennett and G. Brassard. “Quantum cryptography: Public key distribution and coin tossing”. In: *Theoretical Computer Science* 560 (2014). Theoretical Aspects of Quantum Cryptography – celebrating 30 years of BB84, pp. 7–11. issn: 0304-3975. doi: https://doi.org/10.1016/j.tcs.2014.05.025. url: https://www.sciencedirect.com/science/article/pii/S0304397514004241.

[2] A. K. Ekert. “Quantum cryptography based on Bell’s theorem”. In: *Phys. Rev. Lett.* 67 (6 Aug. 1991), pp. 661–663. doi: 10.1103/PhysRevLett.67.661. url: https://link.aps.org/doi/10.1103/PhysRevLett.67.661.

[3] S. Pirandola, U. L. Andersen, L. Banchi, M. Berta, D. Bunandar, R. Colbeck, D. Englund, T. Gehring, C. Lupo, C. Ottaviani, J. L. Pereira, M. Razavi, J. S. Shaari, M. Tomamichel, V. C. Usenko, G. Vallone, P. Villoresi, and P. Wallden. “Advances in quantum cryptography”. In: *Adv. Opt. Photon.* 12.4 (Dec. 2020), pp. 1012–1236. doi: 10.1364/AOP.361502. url: https://opg.optica.org/aop/abstract.cfm?URI=aop-12-4-1012.

[4] P. Kómár, E. M. Kessler, M. Bishof, L. Jiang, A. S. Sørensen, J. Ye, and M. D. Lukin. “A quantum network of clocks”. In: *Nature Physics* 10.8 (2014), pp. 582–587. doi: 10.1038/nphys3000. url: https://doi.org/10.1038/nphys3000.

[5] X. Guo, C. R. Breum, J. Borregaard, S. Izumi, M. V. Larsen, T. Gehring, M. Christandl, J. S. Neergaard-Nielsen, and U. L. Andersen. “Distributed quantum sensing in a continuous-variable entangled network”. In: *Nature Physics* 16.3 (2020), pp. 281–284. doi: 10.1038/s41567-019-0743-x. url: https://doi.org/10.1038/s41567-019-0743-x.

[6] L.-Z. Liu, Y.-Z. Zhang, Z.-D. Li, R. Zhang, X.-F. Yin, Y.-Y. Fei, L. Li, N.-L. Liu, F. Xu, Y.-A. Chen, and J.-W. Pan. “Distributed quantum phase estimation with entangled photons”. In: *Nature Photonics* 15.2 (2021), pp. 137–142. doi: 10.1038/s41566-020-00718-2. url: https://doi.org/10.1038/s41566-020-00718-2.

[7] H. Buhrman and H. Röhrig. “Distributed Quantum Computing”. In: *Mathematical Foundations of Computer Science 2003*. Ed. by B. Rovan and P. Vojtáš. Lecture Notes in Computer Science. Berlin, Heidelberg: Springer, 2003, pp. 1–20. isbn: 978-3-540-45138-9. doi: 10.1007/978-3-540-45138-9_1.

[8] W. K. Wootters and W. H. Zurek. “A single quantum cannot be cloned”. In: *Nature* 299.5886 (1982), pp. 802–803. doi: 10.1038/299802a0. url: https://doi.org/10.1038/299802a0.

[9] L. .-. Duan, M. D. Lukin, J. I. Cirac, and P. Zoller. “Long-distance quantum communication with atomic ensembles and linear optics”. In: *Nature* 414.6862 (2001), pp. 413–418. doi: 10.1038/35106500. url: https://doi.org/10.1038/35106500.

[10] N. Sangouard, C. Simon, H. de Riedmatten, and N. Gisin. “Quantum repeaters based on atomic ensembles and linear optics”. In: *Rev. Mod. Phys.* 83 (1 Mar. 2011), pp. 33–80. doi: 10.1103/RevModPhys.83.33. url: https://link.aps.org/doi/10.1103/RevModPhys.83.33.

[11] S. Muralidharan, J. Kim, N. Lütkenhaus, M. D. Lukin, and L. Jiang. “Ultrafast and Fault-Tolerant Quantum Communication across Long Distances”. In: *Phys. Rev. Lett.* 112 (25 June 2014), p. 250501. doi: 10.1103/PhysRevLett.112.250501. url: https://link.aps.org/doi/10.1103/PhysRevLett.112.250501.

[12] W. J. Munro, A. M. Stephens, S. J. Devitt, K. A. Harrison, and K. Nemoto. “Quantum communication without the necessity of quantum memories”. In: *Nature Photonics* 6.11 (2012), pp. 777–781. doi: 10.1038/nphoton.2012.243. url: https://doi.org/10.1038/nphoton.2012.243.

[13] J. Yin, Y. Cao, Y.-H. Li, J.-G. Ren, S.-K. Liao, L. Zhang, W.-Q. Cai, W.-Y. Liu, B. Li, H. Dai, M. Li, Y.-M. Huang, L. Deng, L. Li, Q. Zhang, N.-L. Liu, Y.-A. Chen, C.-Y. Lu, R. Shu, C.-Z. Peng, J.-Y. Wang, and J.-W. Pan. “Satellite-to-Ground Entanglement-Based Quantum Key Distribution”. In: *Phys. Rev. Lett.* 119 (20 Nov. 2017), p. 200501. doi: 10.1103/PhysRevLett.119.200501. url: https://link.aps.org/doi/10.1103/PhysRevLett.119.200501.

[14] S.-K. Liao, W.-Q. Cai, J. Handsteiner, B. Liu, J. Yin, L. Zhang, D. Rauch, M. Fink, J.-G. Ren, W.-Y. Liu, Y. Li, Q. Shen, Y. Cao, F.-Z. Li, J.-F. Wang, Y.-M. Huang, L. Deng, T. Xi, L. Ma, T. Hu, L. Li, N.-L. Liu, F. Koidl, P. Wang, Y.-A. Chen, X.-B. Wang, M. Steindorfer, G. Kirchner, C.-Y. Lu, R. Shu, R. Ursin, T. Scheidl, C.-Z.

Peng, J.-Y. Wang, A. Zeilinger, and J.-W. Pan. “Satellite-Relayed Intercontinental Quantum Network”. In: *Phys. Rev. Lett.* 120 (3 Jan. 2018), p. 030501. doi: 10.1103/PhysRevLett.120.030501. url: https://link.aps.org/doi/10.1103/PhysRevLett.120.030501.

[15] J. Yin, Y.-H. Li, S.-K. Liao, M. Yang, Y. Cao, L. Zhang, J.-G. Ren, W.-Q. Cai, W.-Y. Liu, S.-L. Li, R. Shu, Y.-M. Huang, L. Deng, L. Li, Q. Zhang, N.-L. Liu, Y.-A. Chen, C.-Y. Lu, X.-B. Wang, F. Xu, J.-Y. Wang, C.-Z. Peng, A. K. Ekert, and J.-W. Pan. “Entanglement-based secure quantum cryptography over 1,120 kilometres”. In: *Nature* 582.7813 (June 2020). Number: 7813 Publisher: Nature Publishing Group, pp. 501–505. issn: 1476-4687. doi: 10.1038/s41586-020-2401-y. url: https://www.nature.com/articles/s41586-020-2401-y (visited on 08/14/2023).

[16] J. Yin, Y. Cao, Y.-H. Li, S.-K. Liao, L. Zhang, J.-G. Ren, W.-Q. Cai, W.-Y. Liu, B. Li, H. Dai, G.-B. Li, Q.-M. Lu, Y.-H. Gong, Y. Xu, S.-L. Li, F.-Z. Li, Y.-Y. Yin, Z.-Q. Jiang, M. Li, J.-J. Jia, G. Ren, D. He, Y.-L. Zhou, X.-X. Zhang, N. Wang, X. Chang, Z.-C. Zhu, N.-L. Liu, Y.-A. Chen, C.-Y. Lu, R. Shu, C.-Z. Peng, J.-Y. Wang, and J.-W. Pan. “Satellite-based entanglement distribution over 1200 kilometers”. In: *Science* 356.6343 (June 2017), pp. 1140–1144. doi: 10.1126/science.aan3211. url: https://www.science.org/doi/10.1126/science.aan3211 (visited on 07/27/2023).

[17] O. Alia, A. Huang, H. Luo, O. Amer, M. Pistoia, and C. Lim. “Quantum-safe 10 Gbps Site-to-Site IPsec VPN Tunnel over 46 km Deployed Fibre”. In: *2024 Optical Fiber Communications Conference and Exhibition (OFC)*. 2024, pp. 1–3.

[18] Telefónica and Vithas. *Telefónica and Vithas test quantum-attack shielding in hospitals*. Telefónica, Press Room. Available at: telefonica.com/es/sala-comunicacion/prensa. Feb. 2025.

[19] L. C. Andrews and R. L. Phillips. *Laser Beam Propagation Through Random Media*. 1000 20th Street, Bellingham, WA 98227-0010 USA: SPIE, Sept. 2005. isbn: 978-0-8194-5948-0. doi: 10.1117/3.626196. url: http://link.aip.org/link/doi/10.1117/3.626196 (visited on 06/07/2022).

[20] M. Gündoğan, J. S. Sidhu, V. Henderson, L. Mazzarella, J. Wolters, D. K. L. Oi, and M. Krutzik. “Proposal for space-borne quantum memories for global quantum networking”. In: *npj Quantum Information* 7.1 (2021), p. 128. doi: 10.1038/s41534-021-00460-9. url: https://doi.org/10.1038/s41534-021-00460-9.

[21] X. Ma, C.-H. F. Fung, and H.-K. Lo. “Quantum key distribution with entangled photon sources”. In: *Phys. Rev. A* 76 (1 July 2007), p. 012307. doi: 10.1103/PhysRevA.76.012307. url: https://link.aps.org/doi/10.1103/PhysRevA.76.012307.

[22] V. D. Tubío, M. B. Aldecocea, J. van Dam, A. S. Sørensen, and J. Borregaard. *Satellite-assisted quantum communication with single photon sources and atomic memories*. 2024. arXiv: 2411.09533 [quant-ph]. url: https://arxiv.org/abs/2411.09533.

[23] M. Badas Aldecocea, J. Bouwmeester, P. Piron, and J. J. D. Loicq. “Impact of transmitter wavefront errors and pointing jitter on intersatellite free space optical communications”. In: *SPIE Optical System Design 2024: Computational Optics*. Ed. by D. G. Smith and A. Erdmann. Vol. 13023. Proceedings of SPIE – The International Society for Optical Engineering 1302302. Conference held April 7–12, 2024, Strasbourg, France. United States: SPIE, 2024. doi: 10.1117/12.3021617.

[24] D. L. Bakker, Y. Jong, B. P. F. Dirks, and G. C. Amaral. “A Best-Path Approach to the Design of a Hybrid Space–Ground Quantum Network with Dynamic Constraints”. In: *Photonics* 11.3 (2024). issn: 2304-6732. doi: 10.3390/photonics11030268. url: https://www.mdpi.com/2304-6732/11/3/268.

[25] M. Chen, C. Liu, and H. Xian. “Experimental demonstration of single-mode fiber coupling over relatively strong turbulence with adaptive optics”. en. In: *Applied Optics* 54.29 (Oct. 2015). Publisher: Optica Publishing Group, p. 8722. issn: 0003-6935, 1539-4522. doi: 10.1364/ao.54.008722. url: https://opg.optica.org/abstract.cfm?URI=ao-54-29-8722 (visited on 07/11/2025).

[26] V. Marulanda Acosta, D. Dequal, M. Schiavon, A. Montmerle-Bonnefois, C. B. Lim, J.-M. Conan, and E. Diamanti. “Analysis of satellite-to-ground quantum key distribution with adaptive optics”. en. In: *New Journal of Physics* 26.2 (Feb. 2024). Publisher: IOP Publishing, p. 023039. issn: 1367-2630. doi: 10.1088/1367-2630/ad231c. url: https://iopscience.iop.org/article/10.1088/1367-2630/ad231c (visited on 07/11/2025).

[27] M. T. Gruneisen, M. B. Flanagan, and B. A. Sickmiller. “Modeling satellite-Earth quantum channel downlinks with adaptive-optics coupling to single-mode fibers”. en. In: *Optical Engineering* 56.12 (Dec. 2017). Publisher: SPIE-Intl Soc Optical Eng, p. 1. issn: 0091-3286. doi: 10.1117/1.oe.56.12.126111. url: https://www.spiedigitallibrary.

org/journals/optical-engineering/volume-56/issue-12/126111/Modeling-satellite-Earth-quantum-channel-downlinks-with-adaptive-optics-coupling/10.1117/1.OE.56.12.126111.full (visited on 07/11/2025).

[28] A. S. Mueller, B. Korzh, M. Runyan, E. E. Wollman, A. D. Beyer, J. P. Allmaras, A. E. Velasco, I. Craiciu, B. Bumble, R. M. Briggs, L. Narvaez, C. Peña, M. Spiropulu, and M. D. Shaw. "Free-space coupled superconducting nanowire single-photon detector with low dark counts". EN. In: *Optica* 8.12 (Dec. 2021). Publisher: Optica Publishing Group, pp. 1586–1587. issn: 2334-2536. doi: 10.1364/OPTICA.444108. url: https://opg.optica.org/optica/abstract.cfm?uri=optica-8-12-1586 (visited on 07/11/2025).

[29] D. Zheng, Y. Li, E. Chen, B. Li, D. Kong, W. Li, and J. Wu. "Free-space to few-mode-fiber coupling under atmospheric turbulence". en. In: *Optics Express* 24.16 (Aug. 2016). Publisher: Optica Publishing Group, p. 18739. issn: 1094-4087. doi: 10.1364/oe.24.018739. url: https://opg.optica.org/abstract.cfm?URI=oe-24-16-18739 (visited on 07/11/2025).

[30] P. V. Trinh, D. R. Kolev, K. Shiratama, A. Carrasco-Casado, Y. Munemasa, H. Yamazoe, H. Komatsu, T. Kamata, T. Nakao, S. Ohta, K. Iwamoto, M. Fujiwara, H. Tsuji, and M. Toyoshima. "Experimental verification of fiber coupling characteristics for FSO downlinks from the International Space Station". en. In: *Optics Express* 31.5 (Feb. 2023). Publisher: Optica Publishing Group, p. 9081. issn: 1094-4087. doi: 10.1364/oe.484512. url: https://opg.optica.org/abstract.cfm?URI=oe-31-5-9081 (visited on 07/11/2025).

[31] J. Wallnöfer, F. Hahn, M. Gündoğan, J. S. Sidhu, F. Wiesner, N. Walk, J. Eisert, and J. Wolters. "Simulating quantum repeater strategies for multiple satellites". In: *Communications Physics* 5.1 (June 2022). doi: 10.1038/s42005-022-00945-9. url: https://doi.org/10.1038%2Fs42005-022-00945-9.

[32] C. Liorni, H. Kampermann, and D. Bruß. "Quantum repeaters in space". In: *New Journal of Physics* 23.5 (May 2021), p. 053021. doi: 10.1088/1367-2630/abfa63. url: https://doi.org/10.1088%2F1367-2630%2Fabfa63.

[33] J. F. Fitzsimons. "Private quantum computation: an introduction to blind quantum computing and related protocols". In: *npj Quantum Information* 3.1 (June 2017), pp. 1–11. issn: 20566387. doi: 10.1038/S41534-017-0025-3. url: https://www.nature.com/articles/s41534-017-0025-3.

[34] R. Van Meter and S. J. Devitt. “The Path to Scalable Distributed Quantum Computing”. In: *Computer* 49.9 (Sept. 2016), pp. 31–42. issn: 00189162. doi: 10.1109/MC.2016.291.

[35] J. W. Goodman. *Introduction to Fourier optics*. English. 3rd ed. Englewood, Colo.: Roberts & Co., 2005. isbn: 978-0-9747077-2-3. url: http://catdir.loc.gov/catdir/toc/ecip051/2004023213.html (visited on 03/09/2023).

[36] V. K. Rohatgi and A. K. M. E. Saleh. *An Introduction to Probability and Statistics*. en. 2nd ed. John Wiley & Sons, Incorporated, 2001.

[37] X. Wang, X. Wang, C. Li, J. Jia, J. Jia, J. Wu, R. Shu, R. Shu, L. Zhang, L. Zhang, L. Zhang, J. Wang, J. Wang, J. Wang, and J. Wang. “Angular micro-vibration of the Micius satellite measured by an optical sensor and the method for its suppression”. EN. In: *Applied Optics* 60.7 (Mar. 2021), pp. 1881–1887. issn: 2155-3165. doi: 10.1364/AO.416811. url: https://opg.optica.org/ao/abstract.cfm?uri=ao-60-7-1881 (visited on 10/25/2022).

[38] J.-M. Merolla, B. Pages, J. Cussey, R. Martinenghi, E. Fretel, J. Prieur, and J. Piris. “High-performance 1560 nm Entangled Photon Source for high secure key rates QKD satellite-based communications”. In: *ICSOS International Conference on Space Optics (ICSO 2022)*. Dubrovnik, Croatia, Oct. 2022, pp. 1–12. url: https://publiweb.femto-st.fr/tntnet/entries/19339/documents/author/data.

[39] M. Badás, P. Piron, J. Bouwmeester, and J. Loicq. “On the optimum far-field irradiance distribution using Laguerre-Gaussian beams for intersatellite free-space optical communications”. In: *Optics Express* 32.18 (Aug. 2024), pp. 31597–31620. issn: 1094-4087. doi: 10.1364/OE.533250. url: https://opg.optica.org/oe/abstract.cfm?uri=oe-32-18-31597 (visited on 08/16/2024).

[40] V. D. Tubío, M. B. Aldecocea, J. v. Dam, A. S. Sørensen, and J. Borregaard. *Satellite-assisted quantum communication with single photon sources and atomic memories*. arXiv:2411.09533 [quant-ph]. Nov. 2024. doi: 10.48550/arXiv.2411.09533. url: http://arxiv.org/abs/2411.09533 (visited on 07/08/2025).

[41] C.-Y. Lu, Y. Cao, C.-Z. Peng, and J.-W. Pan. “Micius quantum experiments in space”. en. In: *Reviews of Modern Physics* 94.3 (July 2022), p. 035001. issn: 0034-6861, 1539-0756. doi: 10.1103/RevModPhys.94.035001. url: https://link.aps.org/doi/10.1103/RevModPhys.94.035001 (visited on 05/31/2023).

[42] H. Hemmati. *Deep Space Optical Communications*. en. John Wiley & Sons, June 2006. isbn: 978-0-470-04240-3.

[43] Y. Li, W.-Q. Cai, J.-G. Ren, C.-Z. Wang, M. Yang, L. Zhang, H.-Y. Wu, L. Chang, J.-C. Wu, B. Jin, H.-J. Xue, X.-J. Li, H. Liu, G.-W. Yu, X.-Y. Tao, T. Chen, C.-F. Liu, W.-B. Luo, J. Zhou, H.-L. Yong, Y.-H. Li, F.-Z. Li, C. Jiang, H.-Z. Chen, C. Wu, X.-H. Tong, S.-J. Xie, F. Zhou, W.-Y. Liu, Y. Ismail, F. Petruccione, N.-L. Liu, L. Li, F. Xu, Y. Cao, J. Yin, R. Shu, X.-B. Wang, Q. Zhang, J.-Y. Wang, S.-K. Liao, C.-Z. Peng, and J.-W. Pan. "Microsatellite-based real-time quantum key distribution". en. In: *Nature* (Mar. 2025). Publisher: Nature Publishing Group, pp. 1–8. issn: 1476-4687. doi: 10.1038/s41586-025-08739-z. url: https://www.nature.com/articles/s41586-025-08739-z (visited on 03/21/2025).

[44] D. L. Bakker, Y. Jong, B. P. F. Dirks, and G. C. Amaral. "A Best-Path Approach to the Design of a Hybrid Space–Ground Quantum Network with Dynamic Constraints". en. In: *Photonics* 11.3 (Mar. 2024). Number: 3 Publisher: Multidisciplinary Digital Publishing Institute, p. 268. issn: 2304-6732. doi: 10.3390/photonics11030268. url: https://www.mdpi.com/2304-6732/11/3/268 (visited on 05/31/2025).

[45] D. Vasylyev, W. Vogel, and F. Moll. "Satellite-mediated quantum atmospheric links". en. In: *Physical Review A* 99.5 (May 2019), p. 053830. issn: 2469-9926, 2469-9934. doi: 10.1103/PhysRevA.99.053830. url: https://link.aps.org/doi/10.1103/PhysRevA.99.053830 (visited on 03/04/2025).

[46] J. H. Shapiro. "Scintillation has minimal impact on far-field Bennett-Brassard 1984 protocol quantum key distribution". In: *Physical Review A* 84.3 (Sept. 2011). Publisher: American Physical Society, p. 032340. doi: 10.1103/PhysRevA.84.032340. url: https://link.aps.org/doi/10.1103/PhysRevA.84.032340 (visited on 02/18/2025).

6

OUTLOOK

In this chapter we give a brief summary of results presented in this dissertation, as well as of possible challenges we face in the future implementation of a satellite-based quantum network.

6.1. SUMMARY OF RESULTS

We have shown that state-of-the-art satellites, such as Micius [1], can achieve higher entanglement rates and longer transmission distances by upgrading ground stations to support qudit encoding. The high-dimensional encoding allows for the simultaneous generation of multiple Bell pairs between the ground stations, which minimizes the effect of decoherence in the quantum memories. When more than a single, high-fidelity Bell pair is required, for applications such as entanglement distillation, this can result in several orders magnitude enhancement in distribution rate compared to photonic qubit based approached with memory cut-off strategies.

Satellite-based links have already enabled quantum key distribution (QKD) over distances up to 7000 km [2], far exceeding the range of fiber-based systems. To extend secure quantum communication to intercontinental distances without relying on trusted nodes, quantum repeaters in space are needed [3–5]. We propose using individually trapped alkali atoms as both single-photon sources and quantum memories. This approach eliminates the need for cryogenic systems in space and enables near-deterministic Bell state measurements using Rydberg-mediated two-qubit gates. As a result, it significantly reduces the multiplexing required for long-distance entanglement compared to schemes based on probabilistic linear-optics BSMs. We show that with five satellites equipped with 50 cm telescopes and fewer than 200 atoms per repeater station, entanglement distribution on distances of the order of 10000 km becomes feasible.

Furthermore, we have investigated the feasibility of employing a Micius like satellite to connect several major cities across the Iberian Peninsula. Our analysis realistic effects such as weather conditions, fly-over-time, pointing jitter, beam clipping and finite key effects. Through careful optimization of the optical link budget, we have shown that current QKD applications, already demonstrated over fiber [6, 7], can be extended to cover the Iberian Peninsula via a single satellite link. By employing an entanglement-based QKD protocol [1], we eliminate the need for trusted nodes, reducing vulnerability to eavesdropping.

In summary, we show that current QKD use cases can be implemented via satellites like Micius, extending beyond fiber's range. Moreover, by upgrading ground stations to support high-dimensional (qudit) encoding, we can achieve higher distribution rates of multiple entangled pairs over distances of 200–1200 km without altering existing satellite payloads—enabling future, more demanding quantum communication applications.

6.2. FUTURE WORK AND CHALLENGES

There are two main challenges for the implementation of a future global (satellite-based) quantum network: one is application-related, and the other is hardware-related.

On the application side, there is currently no clear use case where quantum networks provide a definitive advantage over classical networks. While it is true that the no-cloning theorem [8] guarantees that quantum information cannot be copied, forming the security basis of quantum key distribution (QKD) [9, 10], there are also post-quantum cryptography (PQC) algorithms [11, 12] designed to be secure against attacks by quantum computers. Although there is no guarantee that PQC algorithms could not eventually be broken by future powerful quantum computers and yet-to-be discovered algorithms, such attacks do not yet exist. Furthermore, a clear advantage of PQC algorithms is that they use the already implemented infrastructure of conventional networks, allowing to move all around the globe, while current QKD devices need specialized and costly environments and quantum compatible fiber connections are not implemented all over the world. On the other hand, the strongest advantages of quantum networks so far seem to rely on entanglement, whether for connecting quantum computers, enabling distributed quantum computation [13], or linking sensors to enhance sensitivity [14, 15].

To establish entanglement between two nodes, quantum memories are needed at the end nodes to store the quantum information sent from one to the other. This is where the hardware-related challenge comes in. There are several promising platforms for quantum memories. Rare-earth-doped crystals [16–18], for example, offer coherence times

of up to an hour [18] but require cryogenic temperatures. Cold atoms [19, 20], on the other hand, can provide coherence times less than one minute but without the use of cryogenics.

In satellite-based entanglement distribution, where bridging long distances comes into play and where the communication window is usually less than 24 hours (unless using geostationary satellites), having quantum memories with coherence times on the order of hours is necessary for on-demand access and continuous coverage of entangled pairs. This makes rare-earth-doped crystals a promising option. However, their efficiency drops significantly over time, making long-term storage with high performance still an open challenge.

Therefore, there are several challenges for the near future of satellite-based quantum networks: improving the efficiency of current quantum memories and commercializing them, and finding an application beyond the connection of several quantum computers.

REFERENCES

[1] J. Yin, Y.-H. Li, S.-K. Liao, M. Yang, Y. Cao, L. Zhang, J.-G. Ren, W.-Q. Cai, W.-Y. Liu, S.-L. Li, R. Shu, Y.-M. Huang, L. Deng, L. Li, Q. Zhang, N.-L. Liu, Y.-A. Chen, C.-Y. Lu, X.-B. Wang, F. Xu, J.-Y. Wang, C.-Z. Peng, A. K. Ekert, and J.-W. Pan. "Entanglement-based secure quantum cryptography over 1,120 kilometres". In: *Nature* 582.7813 (June 2020). Number: 7813 Publisher: Nature Publishing Group, pp. 501–505. issn: 1476-4687. doi: 10.1038/s41586-020-2401-y. url: https://www.nature.com/articles/s41586-020-2401-y (visited on 08/14/2023).

[2] S.-K. Liao, W.-Q. Cai, J. Handsteiner, B. Liu, J. Yin, L. Zhang, D. Rauch, M. Fink, J.-G. Ren, W.-Y. Liu, Y. Li, Q. Shen, Y. Cao, F.-Z. Li, J.-F. Wang, Y.-M. Huang, L. Deng, T. Xi, L. Ma, T. Hu, L. Li, N.-L. Liu, F. Koidl, P. Wang, Y.-A. Chen, X.-B. Wang, M. Steindorfer, G. Kirchner, C.-Y. Lu, R. Shu, R. Ursin, T. Scheidl, C.-Z. Peng, J.-Y. Wang, A. Zeilinger, and J.-W. Pan. "Satellite-Relayed Intercontinental Quantum Network". In: *Phys. Rev. Lett.* 120 (3 Jan. 2018), p. 030501. doi: 10.1103/PhysRevLett.120.030501. url: https://link.aps.org/doi/10.1103/PhysRevLett.120.030501.

[3] C. Liorni, H. Kampermann, and D. Bruß. "Quantum repeaters in space". In: *New Journal of Physics* 23.5 (May 2021), p. 053021. doi: 10.1088/1367-2630/abfa63. url: https://doi.org/10.1088%2F1367-2630%2Fabfa63.

[4] J. Wallnöfer, F. Hahn, M. Gündoğan, J. S. Sidhu, F. Wiesner, N. Walk, J. Eisert, and J. Wolters. "Simulating quantum repeater strategies for multiple satellites". In: *Communications Physics* 5.1 (June 2022). doi: 10.1038/s42005-022-00945-9. url: https://doi.org/10.1038%2Fs42005-022-00945-9.

[5] V. D. Tubío, M. B. Aldecocea, J. van Dam, A. S. Sørensen, and J. Borregaard. *Satellite-assisted quantum communication with single photon sources and atomic memories*. 2024. arXiv: 2411.09533 [quant-ph]. url: https://arxiv.org/abs/2411.09533.

[6] V. Martin, J. P. Brito, L. Ortíz, R. B. Méndez, J. S. Buruaga, R. J. Vicente, A. Sebastián-Lombraña, D. Rincón, F. Pérez, C. Sánchez, M. Peev, H. H. Brunner, F. Fung, A. Poppe, F. Fröwis, A. J. Shields, R. I. Woodward, H. Griesser, S. Roehrich, F. de la Iglesia, C. Abellán, M. Hentschel, J. M. Rivas-Moscoso, A. Pastor-Perales, J. Folgueira, and D. López. "MadQCI: a heterogeneous and scalable SDN-QKD network deployed in production facilities". In: *npj Quantum Information* 10.1 (Sept. 2024), p. 80. doi: 10.1038/s41534-024-00873-2. url: https://www.nature.com/articles/s41534-024-00873-2.

[7] O. Alia, A. Huang, H. Luo, O. Amer, M. Pistoia, and C. Lim. "Quantum-safe 10 Gbps Site-to-Site IPsec VPN Tunnel over 46 km Deployed Fibre". In: *2024 Optical Fiber Communications Conference and Exhibition (OFC)*. 2024, pp. 1–3.

[8] W. K. Wootters and W. H. Zurek. "A single quantum cannot be cloned". In: *Nature* 299.5886 (1982), pp. 802–803. doi: 10.1038/299802a0. url: https://doi.org/10.1038/299802a0.

[9] S. Pironio, A. Acin, N. Brunner, N. Gisin, S. Massar, and V. Scarani. "Device-independent quantum key distribution secure against collective attacks". In: *New Journal of Physics* 11 (Apr. 2009). issn: 13672630. doi: 10.1088/1367-2630/11/4/045021.

[10] V. Scarani, H. Bechmann-Pasquinucci, N. J. Cerf, M. Dušek, N. Lütkenhaus, and M. Peev. "The security of practical quantum key distribution". In: *Reviews of Modern Physics* 81.3 (Sept. 2009), pp. 1301–1350. issn: 00346861. doi: 10.1103/RevModPhys.81.1301. url: https://journals.aps.org/rmp/abstract/10.1103/RevModPhys.81.1301.

[11] J. W. Bos, L. Ducas, E. Kiltz, T. Lepoint, V. Lyubashevsky, J. Schanck, P. Schwabe, G. Seiler, and D. Stehlé. "CRYSTALS-Kyber: A CCA-Secure Module-Lattice-Based KEM". In: *2018 IEEE European Symposium on Security and Privacy (EuroS&P)*. 2018, pp. 353–367. doi: 10.1109/EuroSP.2018.00031. url: https://pq-crystals.org/kyber/.

[12] L. Ducas, E. Kiltz, T. Lepoint, V. Lyubashevsky, P. Schwabe, G. Seiler, and D. Stehlé. "CRYSTALS-Dilithium: Digital Signatures from Module Lattices". In: *2018 IEEE European Symposium on Security and Privacy (EuroS&P)*. 2018, pp. 356–373. doi: 10.1109/EuroSP.2018.00032. url: https://pq-crystals.org/dilithium/.

[13] H. Buhrman and H. Röhrig. “Distributed Quantum Computing”. In: *Mathematical Foundations of Computer Science 2003*. Ed. by B. Rovan and P. Vojtáš. Lecture Notes in Computer Science. Berlin, Heidelberg: Springer, 2003, pp. 1–20. isbn: 978-3-540-45138-9. doi: 10.1007/978-3-540-45138-9_1.

[14] P. Kómár, E. M. Kessler, M. Bishof, L. Jiang, A. S. Sørensen, J. Ye, and M. D. Lukin. “A quantum network of clocks”. In: *Nature Physics* 10.8 (2014), pp. 582–587. doi: 10.1038/nphys3000. url: https://doi.org/10.1038/nphys3000.

[15] X. Guo, C. R. Breum, J. Borregaard, S. Izumi, M. V. Larsen, T. Gehring, M. Christandl, J. S. Neergaard-Nielsen, and U. L. Andersen. “Distributed quantum sensing in a continuous-variable entangled network”. In: *Nature Physics* 16.3 (2020), pp. 281–284. doi: 10.1038/s41567-019-0743-x. url: https://doi.org/10.1038/s41567-019-0743-x.

[16] D. Lago-Rivera, J. V. Rakonjac, S. Grandi, and H. d. Riedmatten. “Long distance multiplexed quantum teleportation from a telecom photon to a solid-state qubit”. In: *Nature Communications* 14.1 (2023), p. 1889. doi: 10.1038/s41467-023-37518-5. url: https://doi.org/10.1038/s41467-023-37518-5.

[17] D. Lago-Rivera, S. Grandi, J. V. Rakonjac, A. Seri, and H. de Riedmatten. “Telecom-heralded entanglement between multimode solid-state quantum memories”. In: *Nature* 594.7861 (June 2021), pp. 37–40. doi: 10.1038/s41586-021-03481-8.

[18] Y. Ma, Y.-Z. Ma, Z.-Q. Zhou, C.-F. Li, and G.-C. Guo. “One-hour coherent optical storage in an atomic frequency comb memory”. In: *Nature Communications* 12 (Apr. 2021), p. 2381. doi: 10.1038/s41467-021-22706-y.

[19] D. Bluvstein, H. Levine, G. Semeghini, T. T. Wang, S. Ebadi, M. Kalinowski, A. Keesling, N. Maskara, H. Pichler, M. Greiner, V. Vuletić, and M. D. Lukin. “A quantum processor based on coherent transport of entangled atom arrays”. In: *Nature* 604.7906 (2022), pp. 451–456. doi: 10.1038/s41586-022-04592-6. url: https://doi.org/10.1038/s41586-022-04592-6.

[20] A. W. Young, W. J. Eckner, W. R. Milner, D. Kedar, M. A. Norcia, E. Oelker, N. Schine, J. Ye, and A. M. Kaufman. “Half-minute-scale atomic coherence and high relative stability in a tweezer clock”. In: *Nature* 588.7838 (Dec. 2020), pp. 408–413. doi: 10.1038/s41586-020-3009-y. url: https://doi.org/10.1038%2Fs41586-020-3009-y.

ACKNOWLEDGEMENTS

After four years of work culminating in this dissertation, I owe deep gratitude to the many people who have accompanied me along the way. I want to begin by thanking my supervisor, **Johannes Borregaard**. These four years have been eventful, beginning with your move to Boston and my final year in Madrid. Yet, throughout it all, you were always there — supporting me and inspiring me with your vision and knowledge of quantum technologies.

I would also like to extend my thanks to my committee members, who agreed to read my thesis and discuss my work with me for an hour: thank you **Stephanie Wehner**, **Carlos Errando Herranz**, **Micheal Wimmer**, **Tim Schröder**, **Ivana Dimitrova**, **Ryoichi Ishihara** and **Gary Steele**.

I cannot forget to thank my Telefónica supervisor, **Diego López**. Thank you for giving me the opportunity to collaborate with industry during the final year of my PhD. It offered me valuable insights into how the 'real world' operates outside of academia.

I spent a significant part of my PhD immersed in mathematics, coding, and attempting to grasp the mysteries of quantum physics, an impossible task, as Richard Feynman famously remarked. Much of this journey took place in office B007, which I had the pleasure of sharing with **Julius Fischer**. Julius, I truly admire your German punctuality and tireless work ethic, always arriving at 8:30 sharp and often being one of the last to leave. I hope to be like you when I grow old. I'm grateful for the good times and laughter we shared, both in B007 and at various social events.

Much of that time was also spent discussing satellite orbits and beam propagation with **Mario Badás Aldecocea**. Mario, this work owes a great deal to your collaboration, your expertise, and, above all, your emotional support. Thank you for being there during the tough times.

Many thanks to my master's student, **Calvin Dijksman**. Without your strong mathematical background, the project on high-dimensional encoding for space-based algorithms would not have been possible. Thank you for sharing your calm outlook on life and your constant optimism.

I would also like to thank my friend **Francisco Horta Ferreira da Silva**. Thanks for your valuable insight into quantum networks, your friendship, and for visiting me during my stay in Madrid.

To the friends I made along the way during my PhD — **Pablo Cova Fariña**, **Irene Fernández De Fuentes**, **Oriol Pietx i Casas**, **Nicolas Demetriou**, **Hanifa Tidjani**, **Davide Degli Esposti**, **Brennan Undseth**, **Matteo Passini**, **Julia Brevoord**, **Niv Bharos**, **Sjoerd Loenen**,

and **Guus Avis** — thank you. A special mention goes to **Llorenç Escolà Farràs**, who always thinks my plans are a good idea and whose place in Amsterdam has become home every time I visit. I also want to thank my dearest raver friends, **Alberto Gori** and **Smit Chaudhary**, and **Pol de Dalmau Huguet**, for making your home my own.

I cannot forget the first friends I made in the Netherlands during my master's. Thank you **Sergio Barquero Pierantoni**, **Gabriel Fuentes Jerez**, **Álvaro Donís Vela**, **Alina Melissaki**, **Maialen Ortego Larrazabal**, **Bernat Durà i Faulí**, and **Beatriz Orozco Monroy** for being my first home in a foreign country. You made the master's easier, funnier, and full of core memories.

Thank you to the friends I made during my time at Telefónica, who made me feel right at home: **Alejandro Muñiz Da Costa**, **María Ruiz Fernández de Arcaya**, **Vanessa Villegas Zannella**, **Marta Blanco Caamaño**, and **Jorge Brito**.

During the five years I spent studying for my bachelor's degree in Santiago de Compostela, I found the *family we choose*, the friends I know will always be there. Through the hard times in the library (*en la Conchi*), preparing for the finals, we joined forces to get through those endless and often incomprehensible exams, and in doing so, our paths became forever intertwined. The nights in Tarasca, at the Quantum Music Festival (QMF), and in *la Conchi* have become some of my happiest and most cherished core memories. Even though I often say that if I could go back in time I would have studied medicine, I can not regret choosing physics, because otherwise, I would not have met you. Without you, I would not be the woman I am today (at least the part I am proud of). I am so grateful to have you in my life. These heartfelt thanks go to **Ledicia Díaz Lago**, **Sergio Balboa Barreiro**, **Carolina Calvo Salgado**, **Emma Lorenzo Casas**, **Alejandro Carballosa Calleja**, **Pablo Boullosa González**, **Bastián Carnero Groba**, and **Alejandro Cajide Gómez**.

I also want to thank my childhood friends, the ones who have been part of my life long before physics and quantum physics entered the picture. Friends I met back in school and who continue to be a part of my everyday life, playing an indispensable role in it. Thank you for always being there and for listening patiently to my endless dramas. Special thanks to **Carlos Ferreiro Suárez**, **Cristina Muñiz Da Costa**, **Paula Pérez Vázquez**, **Carme Estévez Filgueira**, and **Ana Triñanes Muñiz**.

Last but not least, I want to thank my family, without their support, none of this would have been possible. To my father, **Perfecto Domínguez Riveiro**, for calling every Sunday evening to check if the Nobel Prize was getting any closer. To my mother, **Carmen Tubío Pose**, always making sure I had everything I needed. To my sister, **Valentina Domínguez Tubío**, constantly asking when I would be coming home for a visit. To my newborn niece, **Carmen López Domínguez**. And to my dogs, my

first dog, **Chío**, whom I miss every single day, and my current companion, **Pipo**, who stays by my side as I write whenever I am back at my parents' home.

To all of you, thank you, truly, from the bottom of my heart.

CURRICULUM VITæ

Victoria Dominguez Tubio

12-01-1996 Born in Boiro, Spain.

EDUCATION

2014–2019 Undergraduate in Physics
Universidade de Santiago de Comspotela (ES)
Thesis: SU(N) transformations with optical couplers and their applicability to quantum information.
Supervisor: Dr. Jesús Liñares Beiras

2019–2021 Master in Research in Physics,
Quantum Matter & Quantum Optics
Leiden Universiteit (NL)
Thesis: Beam splitter based scheme for the generation of displaced Fock states.
Supervisor: Dr. Wolfgang Löffler

2025 PhD. Physics
Technische Universiteit Delft (NL)
Thesis: Modelling of space-based quantum networks
Supervisor: Dr. Johannes Borregaard
Promotor: Prof. Dr. Stephanie D. C. Wehner

TEACHING EXPERIENCE

2022 Teacher Assistant for Quantum Hardware II,
MSc Quantum Information Science & Technology,
TU Delft (NL)

2023–2024 Supervision of Master Thesis,
MSc Quantum Information Science & Technology,
Thesis: Enhancing long-range satellite-based entanglement distribution through high-dimensional information encoding.
Student: Marc Calvin Dijksman

LIST OF PUBLICATIONS

3. V. D. Tubío, M. C. Dijksman, and J. Borregaard. *Satellite-assisted Entanglement Distribution with High-Dimensional Photonic Encoding*. 2025. arXiv: 2505.16751 [quant-ph]. url: https://arxiv.org/abs/2505.16751

2. V. Domínguez Tubío, M. Badás Aldecocea, J. van Dam, A. S. Sørensen, and J. Borregaard. "Satellite-assisted quantum communication with single photon sources and atomic memories". In: *Phys. Rev. Res.* 8 (1 Jan. 2026), p. 013099. doi: 10.1103/z1vn-11m5. url: https://link.aps.org/doi/10.1103/z1vn-11m5

1. V. D. Tubío, M. B. Aldecocea, D. L. Bakker, G. C. Amaral, D. López, and J. Borregaard. "Quantum key distribution in the Iberian Peninsula". In: *Optica Quantum* 4.1 (Feb. 2026), pp. 22–30. doi: 10.1364/OPTICAQ.581903. url: https://opg.optica.org/opticaq/abstract.cfm?URI=opticaq-4-1-22

The implementation of a quantum network opens up a range of new opportunities for secure communication and distributed quantum computing. In this thesis, we focus on the development and analysis of satellite-based quantum networks.

We begin by exploring how current satellite links can be made more efficient. To this end, we propose the use of high-dimensional encoding, showing an improvement in the rate of entanglement compared with conventional qubit encoding.

We then extend the analysis to a complete satellite-based quantum network employing multiple space-borne quantum repeaters. Using trapped atoms as both photon sources and quantum memories, we evaluate how hardware imperfections and transmission losses affect performance, and determine the requirements needed to generate high-fidelity entanglement at a chosen transmission rate.

Finally, we go to a more specific example of distributing quantum key (QKD) to different cities of the Iberian Peninsula. Taking into account real-time weather conditions, atmospheric effects, and propagating losses, we analyze the feasibility of deploying current use cases of satellite-based QKD.